AD-A163 735 THEORETICAL INVESTIGATION OF POINT DEFECTS OF MERCURY 1/2
CADMIUM TELLURIDE(U) CALIFORNIA UNIV LOS ANGELES SCHOOL
OF ENGINEERING AND APPLIED.. D PAN 01 NOV 85
UNCLASSIFIED ARO-17684.3-EL DAAG29-81-K-0054 F/G 20/2 NL

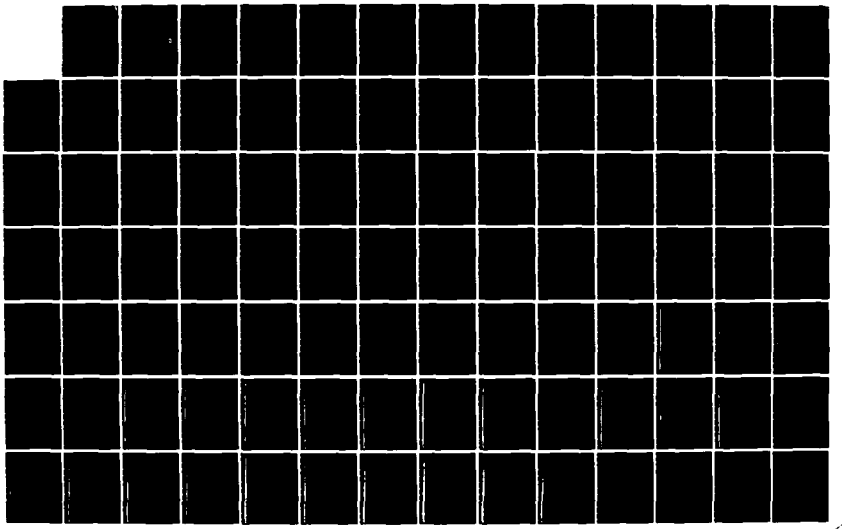

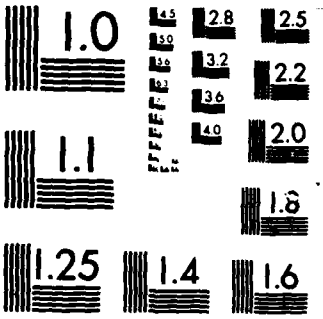

REPORT DOCUMENTATION PAGE

READ INSTRUCTIONS BEFORE COMPLETING FORM

1. REPORT NUMBER: ARO 17684.3-EL	2. GOVT ACCESSION NO.: N/A
3. RECIPIENT'S CATALOG NUMBER: N/A	
4. TITLE (and Subtitle): Theoretical Investigation of Point Defects of Mercury Cadmium Telluride	5. TYPE OF REPORT & PERIOD COVERED: 20 Mar 81 - 19 Sep 85 Final Report
	6. PERFORMING ORG. REPORT NUMBER:
7. AUTHOR(s): Dr. Dee-Son Pan	8. CONTRACT OR GRANT NUMBER(s): DAAG 29-81-K-0054
9. PERFORMING ORGANIZATION NAME AND ADDRESS: University of California, Los Angeles, Los Angeles, California 90024	10. PROGRAM ELEMENT, PROJECT, TASK AREA & WORK UNIT NUMBERS: N/A
CONTROLLING OFFICE NAME AND ADDRESS: U. S. Army Research Office, Post Office Box 12211, Research Triangle Park, NC 27709	12. REPORT DATE: November 1, 1985
	13. NUMBER OF PAGES: 178
MONITORING AGENCY NAME & ADDRESS (if different from Controlling Office)	15. SECURITY CLASS. (of this report): Unclassified
	15a. DECLASSIFICATION/DOWNGRADING SCHEDULE

DISTRIBUTION STATEMENT (of this Report)

Approved for public release; distribution unlimited.

DISTRIBUTION STATEMENT (of the abstract entered in Block 20, if different from Report)

NA

18. SUPPLEMENTARY NOTES

The view, opinions, and/or findings contained in this report are those of the author(s) and should not be construed as an official Department of the Army position, policy, or decision, unless so designated by other documentation.

19. KEY WORDS (Continue on reverse side if necessary and identify by block number)

Mercury cadmium telluride, point defects, alloy semiconductors, vacancy, alloy fluctuation potential, generalized effective mass theory, alloy boradening, band-gap bowing.

20. ABSTRACT (Continue on reverse side if necessary and identify by block number)

We have investigated a number of electronic properties related to point defects in the $Hg_{1-x}Cd_xTe$ alloy system. A detailed calculation for the electronic starter for mercury vacancies was carried out and we found those mercury vacancies are shallow double acceptors. Both the first and second ionization energies are calculated for the whole range of alloy composition. The theoretical results are consistent with current experimental data. But more conclusive and accurate data are required. We have investigated other

native point defects as well, interesting qualitative conclusions were reached. We have looked into the substitutional disorder in $Hg_{1-x}CdxTe$ alloy system.

An empirical pseudopotential theory for alloy fluctuation potential in this case was proposed. We have applied the theory to study the band gap bowing, and level broadening of shallow donors and acceptor, as well as bound excitons. The theoretical results agrees well with the only available data from bound exciton broadening and from band gap bowingin $Hg_{1-x}Cdx\ Te$. Nonparabolic effects in a narrow band gap $Hg_{1-x}Cdx\ Te$ were also investigated. Interesting results on energy level of shallow donors and transport properties are reported.

ARO 17684.3-EL

THEORETICAL INVESTIGATION OF POINT DEFECTS OF MERCURY CADMIUM TELLURIDE

FINAL REPORT

PRINCIPAL INVESTIGATOR: DEE-SON PAN

NOVEMBER 1, 1985

U. S. ARMY RESEARCH OFFICE

DAAG 29-81-K-0054

SCHOOL OF ENGINEERING AND APPLIED SCIENCE

UNIVERSITY OF CALIFORNIA,
LOS ANGELES, CA 90024

THE VIEW, OPINIONS, AND/OR FINDINGS CONTAINED IN THIS REPORT ARE THOSE OF THE AUTHOR(S) AND SHOULD NOT BE CONSIDERED AS AN OFFICIAL DEPARTMENT OF THE ARMY POSITION, POLICY, OR DECISION, UNLESS SO DESIGNATED BY OTHER DOCUMENTATION.

TABLE OF CONTENTS

		PAGE
I.	List of Appendixes.	2
II.	REPORT	
	A. Statement of the Problem Studied.	3
	B. Summary of the Most Important Results	4
	C. List of All Publications.	7
	D. List of all participating scientific personnel showing any advanced degree earned by them while employed on the Project	8
III.	BIBLIOGRAPHY.	9
IV.	APPENDIXES	
	Appendix A.	26
	Appendix B.	62
	Appendix C.	118
	Appendix D.	153

I. LIST OF APPENDIXES

1. Appendix A - Self-Consistent GEMT of Double Acceptors

2. Appendix B - Band Gap Bowing Due to Alloy Fluctuation Potential

3. Appendix C - Alloy Broadening of Localized States

4. Appendix D - Mobility of $Hg_{1-x}Cd_xTe$ Near Zero Band Gap

II. REPORT

A. Statement of the Problem Studied

The problem we proposed to investigate is about various electronic pro-properties related to point defects in the $Hg_{1-x}Cd_xTe$ alloy system. Since the $Hg_{1-x}Cd_xTe$ has substitutional randomness as an alloy crystal, the effects of the alloy fluctuational potential on the energy gaps and defect levels are investigated in detail. The conduction band edges for the $Hg_{1-x}Cd_xTe$ alloy are known to be nonparabolic. The effect of non-parabolicity on shallow donor levels, as well as on electronic transport are studied. We have also looked into the natures of electronic states associated with native defects in $Hg_{1-x}Cd_xTe$, especially those with Hg vacancies. An interesting phenomenon about the mobility of the $Hg_{1-x}Cd_xTe$ near zero band gap is also studies with experimental results.

B. SUMMARY OF THE MOST IMPORTANT RESULTS

a. Alloy effects in $Hg_{1-x}Cd_xTe$

A large number of investigations has been directed to alloy effect in solids. Most of them are still qualitative. Only a few of them are for the II-VI or III-V compound alloys. An important result from our study is that the alloy fluctuation potential in HgCdTe system (and in general for other semiconductor alloys) can be calculated from a superposition of pseudopotentials of each atomic species defined in the parent compounds. This approach is well known in regular crystals. However, the alloy fluctuation potential is the small differences between the pseudopotentials of each atomic species, which are usually not defined to great absolute accuracy. But it turns out that if a consistent procedure to obtain the pseudopotential parameters for parent compounts is adopted, the result is very satisfactory. Furthermore, the effect of alloy fluctuation potential can be calculated by a perturbation theory based on the virtual crystal approximation (VCA). It is known, especially for metal alloys, that for many alloy systems such a simple approach for alloy potential is not valid due to the self-consistent requirement on the potential. In that case, the coherent potential approximation (CPA) is claimed to be a better scheme. We found for $Hg_{1-x}Cd_xTe$, the usual perturbation theory is very good. This is attributed to the great band width of HgCdTe and the weak perturbation introduced by the substitutional disorder. A test of our theory has been carried out by computing the alloy broadening of the bound exciton lines in $Hg_{0.52}Cd_{0.48}Te$. Our theoretical value of broadening agrees quite well with

experimental results. In contrast, one recent CPA calculation on alloy broadening of exciton lines in alkali halides found line widths 10-20 times smaller than the experimental data. The details of this test will be published. The theory is applied to the alloy broadening of defect levels in $Hg_{1-x}Cd_xTe$ and band gap bowing in $Hg_{1-x}Cd_xTe$. These are published as listed in Section *III.C*

b. Native Defects in $Hg_{1-x}Cd_xTE$

Hg vacancies in $Hg_{1-x}Cd_xTe$ has long been suspected to be responsible for p-type behavior in some prepared material. Many detailed investigations have been carried out for the single vacancy in Si, some for vacancies in III-V compound, but few for the II-VI compound, the cation vacancy in II-VI compound is in fact simpler than that in Si or III-V compound, because the introduced perturbation is weaker.

We have carried out intensive calculation for the Hg vacancy and antisites based on the generalized effective mass approximation. The ideal vacancy has been treated by empirical tight binding method (Swartz, Daw and McGill, 1981). We approximate the ideal Hg vacancy in the VCA by the ionic model potential screened by the k-dependent dielectric function. A self-consistent interaction is carried out for the case of binding two holes. The hole-hole interaction between the s envelope functions (which are expanded in 21 Gaussian type orbitals) is screened by the k-dependent dielectric function. The other interactions with the d envelope functions (also in 21 GTOs) are screened only by the dielectric constant in order to make the calculation tractable. We find that the first and second hole ionization

energies are 20 and 35 meV respectively for X = 0.25, and 47 and 86 meV respectively for X = 0.48. The antisite double acceptor Ga_{As} has been observed recently in GaAs (K.R. Elliott, et al., 1982) with the first and second ionization energies being 77 meV and 230 meV, and our model obtains results within 60% accuracy. This agreement established the validity of the theory for double acceptor. Since the Jahn-Teller distortion will only further lower the level, we conclude that the Hg vacancies are shallow acceptors for X < 0.5. Self consistent calculations have also been carried out for the antisite Cd_{Te}. Our results indicate that the first hole ionization energy is 1.47 eV for X = 0.48 and 2.38 eV for X = 1. The results suggest that the acceptor levels of neutral Cd_{Te} antisite are inactive and also that the ideal anion vacancy is inactive. The Te_{Cd} antisite is currently speculated to be a major defect in nonstoichiometric p-type sample (C.D. Jones et. al., (1982). Our calculation using the Γ valley indicated that Te_{Cd} is a shallow double donor. However, states composed of L valleys may provide deep donor levels as suggested by our calculation of Cd_{Te}.

The details of these findings are presented in published papers. Some of the yet unpublished results are put in the appendixes.

C. LIST OF ALL PUBLICATIONS

1. "Pseudopotential Theory of the Alloy Broadening of Defect Levels", J. Vac. Sci. Technol. 21 (1), 195, (1982)

2. "The Effect of Nonparabolicity of the Conduction Band on Shallow Donors", Solid State Comm. 43, 287, (1982).

3. "The Energy Band Gap Bowing in Alloy Seminconductors", Bulletin of APS, 28, 418, (1983).

4. "The Alloy Broadening of Bound Exciton Spectral Lines", Bulletin of APS, 28, 542, (1983).

5. "Application of Generalized Effective Mass Theory to Some Native Point Defects in $Hg_{1-x}Cd_xTe$", J. Vac. Sci. Technol. A1(3), 1631, (1983).

6. "On the Energy Band Gap Bowing in $Hg_{1-x}Cd_xTe$", Solid State Comm. 48, 747 (1983).

D. LIST OF ALL PARTICIPATING SCIENTIFIC PERSONNEL SHOWING ANY ADVANCED DEGREES EARNED BY THEM WHILE EMPLOYED ON THE PROJECT

1. Chong-Lung Wang - received Ph.D degree in 1984
2. Sheldon Wu - received Ph.D degree in 1984
3. Ching-Yu Wang - received M.S. degree in 1984
4. Cheng-Chih Yang - received M.S. degree in 1983

III. BIBLIOGRAPHY

(i) References for Appendix A

(ii) References for Appendix B and C

(iii) References for Appendix D

(i) FOR APPENDIX A

REFERENCES

1. C. Kittel ,and A. H. Mitchel, Phys. Rev. 96(6), 1488 (1954).

2. J. M. Luttinger, and W. Kohn, Phys. Rev. 97 (4), 869 (1955).

3. J. M. Luttinger, Phy. Rev. 102 (4), 1030 (1956).

4. D. Schechter, J. Phys. Chem. Solids 23, 237 (1962)

5. K. S. Mendelson, and H. M. James, J. phys. Chem. Solids 25, 729 (1964).

6. K. S. Mendelson, and D. R. Schultz, Phys. Status Solidi 31, 59 (1969).

7. A. Baldereschi, and N. O. Lipari, Phys. Rev. B 8(6), 2697 (1973).

8. A. Baldereschi, and N. O. Lipari, Phys. Rev. B 9(4), 1525 (1974).

9. J. Bernholc, and S. T. Pantelides, Phys. Rev. B 15(10), 4935 (1977).

10. S. T. Pantelides, and C. T. Sah, Phys. Rev. B 10(2), 621 (1974).

11. H. Ehrenreich, and M. H. Cohen, Phys. Rev. 115(4), 786 (1959).

12. J. P. Walter, and M. L. Cohen, Phys. Rev. B 2(6), 1821 (1970).

13. J. Callaway, Phys. Rev. 3 (8), 2556 (1970).

14. G.A.Baraff, and M. Schluter, Phys. Rev. Lett. 41 (13), 892 (1978).

15. J. Bernholc, N. O. Lipari, and S. T. Pantelides, Phys. Rev. Lett. 41 (13), 895 (1978)

16. A. T. Hunter, and T. C. McGill, J. Appl. Phys. 52 (9), 5779 (1981).

17. C. T. Elliot, I. Meingailis, T. C. Hartman, and A. G. Foyt, J. Phys. Chem. Solids 33, 1527 (1972).

18. W. Scott, E. L. Steltzer, and R. J. Hager, J. Appl. Phys. 47(4), 1408 (1976).

19. M. H. Weiler, Semiconductors and Semimetals, editted by R. K. Willardson and A. C. Beer (Academic, New York, 1981), Vol. 16, P.119.

20. C. A. Swarts, M. S. Daw, and J. Dow, J. Vac. Sci. Tech. 21, 198 (1982).

21. A. Kobayashi, O. Sankey, and J. Dow, Phys. Rev. B25, 6367 (1982).

22. I. V. Abarenkov, and V. Heine, Philosophical Magazine 12, 1249 (1965).

23. Animalu, and V. Heine, Philosophical Magazine 12, 1249 (1965).

24. M. Tinkham, Group Theory and Quantum Mechanics (McGraw Hill, 1964).

25. G. M. Martin, A. Mitonneau, and A. Mircea, Electron Lett. 13, 192(1977).

26. D. E. Holmes, R. T. Chen, K. R. Elliott, C. G. Kirkpatrick, and P. W. Yu, IEEE Trans. MMT-30, 949 (1982).

27. D. E. Holmes, R. T. Chen, and J. Yang, Appl. Phys. Lett. 42(5), 419 (1983).

28. P. W. Yu, and D. C. Reynolds, J. Appl. Phys. 53(2), 1263 (1982).

29. P. W. Yu, W. C. Mitchel, M. G. Meier, S. S. Li, and W. W. Wang, Appl. Phys. Lett. 41(6), 532 (1982).

30. S. R. Morrison, R. C. Newman, and F. Thomson, J. Phys. C 7, 633 (1974)

31. E. Louis, and J. A. Verges, Phys. Rev. B24, 6020 (1981).

32. N. O. Lipari, A. L. Baldereschi, and M. L. W. Thewalt, Solid State Comm. 33, 277 (1980).

33. C. L. Wang, S. Wu, and D. S. Pan, J. Vac. Sci. Tech. A1(3), 1631 (1983).

34. B. Stebe, and G. Munschy, Solid State Comm. 35, 557 (1980).

35. B. Stebe, and G. Munschy, Phys. Stat. Sol.(B) 88, 713 (1978).

36. D. S. Pan, D. L. Smith, and T. C. McGill, Solid State Comm. 18, 1557 (1976).

37. Y. C. Chang, and T. C. McGill, Solid State Comm. 30, 187 (1979).

38. D. S. Pan, Solid State Comm. 37, 375 (1981).

39. M. Taniguchi, M. Hirano, and S. Narita, Phys. Rev. Lett. 35(16), 1095 (1975).

40. V. V. Alexandrov, E. M. Gershenzon, A. P. Mel'nikov, and N. A. Serebryakova, Sov. Phys.-JETP 43(2), 305 (1976).

41. M. H. Cohen, and V. Heine, Phys. Rev. 122, 1821 (1961).

42. B. J. Austin, V. Heiné, and L. J. Sham, Phys. Rev. 127, 276 (1962).

43. Gideon Weisz, Phys. Rev. 149(2), 504 (1966).

44. S. Bloom, and T. K. Bergstresser, Solid State Comm. 6, 465 (1968).

45. D. J. Chadi, and M. L. Cohen, Phys. Rev. B7(2), 692 (1973).

46. F. Herman, and S. Skillman, Atomic Structure Calculations (Prentice Hall, Inc.)

47. Per-Olov Lowdin, J. Chem. Phys. 19(11), 1396 (1951).

48. D. Brust, Phys. Rev. 134 no.5A, A1337 (1964).

49. S. Wu, C. L. Wang, and D. S. Pan, J.Vac. Sci. Tech. 21(1), 195 (1982).

50. A. Morita, and H. Nara, J. Phys. Soc. Jap. Suppl. 21, 234, (1966).

51. A. Glodeanu, Phys. Stat. Solidi 35, 481 (1969).

52. J. R. Haynes, Phys. Rev. Lett. 4, 361 (1960).

53. R. E. Halsted, and M. Avens, Phys. Rev. Lett. 14, 64 (1965).

54. C. Kittel, Quantum Theory of Solid, (John Wiley & Sons, 1963).

55. E. H. Bogardus, and H. B. Rebb, Phys. Rev. 176, 993 (1968).

56. M. A. Lampert, Phys. Rev. Lett. 1, 450 (1958).

57. E. M. Gershenzon, G. N. Gol'tsman, and A. P. Mel'nikov, Sov. Phys.-JETP Lett. 14, 185 (1971).

58. M. A. Gilleo, P. J. Bailey, and D. E. Hill, J. Luminescence 1/2, 562 (1970).

59. M. Tinkham, Group Theory and Quantum Mechanics (McGraw-Hill, 1964).

60. L. Nordheim, Ann. Physik 9, 607 and 641 (1931).

61. T. Muto, Sci. Papers Inst. Phys. Chem. Research (Tokyo) 34, 377 (1938).

62. R. H. Parmenter, Phys. Rev. 97, 587 (1955).

63. M. Weissbluth, Atoms and Molecules (Academic Press, 1978).

64. R. Dornhaus, and G. Nimtz, 'The Properties and Applications of the Hg Cd Te Alloy System' in Springer Tracts in Modern Physics, edited by G. Hohler (Springer, Berlin, 1976), Vol. 78.

65. S. T. Pantelides, Rev. mod. Phys. 50(4), 797 (1978).

66. G. F. Koster, J. O. Dimmock, R. G. Wheeler, and H. Statz, Properties of the Thirty-two Point Groups (M.I.T., Cambridge, Mass., 1963).

67. G. Wannier, Phys. Rev. 52, 191 (1937).

68. J. A. Verges, and E. louis, Phys. Rev. B23, 6676 (1981).

69. A. Baldereschi, Phys. Rev. B1(12), 4673 (1970).

70. D. S. Pan, Solid State Comm. 37, 953 (1981).

71. D. J. Wilford, B. G. Streetman, S. Lai, and M. V. Klein, Solid State Comm. 32, 51 (1979).

72. C. A. Swarts, M. S. Daw, and T. C. McGill, J. Vac. Sci. & Tech. 21, 198 (1982).

(ii) FOR APPENDIX B and C

REFERENCES

1.D. Stroud and H. Ehrenreich, "Band structure of SiGe; Coherent-potential approximation," Phys. Rev. B2, 3197(1970).

2.H.C. Casey,Jr. and M.B. Panish, Heterostructure Lasers, Academic Press, New York, 1978.

3.R. Dornhaus and G. Nimtz, "The properties and applications of the (Hg,Cd)Te alloy systems," in Springer Tracks in Modern Physics, volume 78, Springer-Verlag, Berlin, 1976.

4.S.Uthanna and P. Jayarama Reddy, "Structure and electrical properties of Cd(Se,Te) thin films," Solid State Commun. 45, 979(1983).

5.J.A. Van Vechten and T.K. Bergstresser, "Electronic structures of semiconductor alloys," Phys. Rev. B1, 3351(1970).

6.S.M. Sze, Physics of Semiconductor Devices, 2nd edition, John Wiley and Sons, N.Y., 1981.

7.C Kittel, Introduction to Solid State Physics, 5th edition, John Wiley and Sons, N.Y., 1976.

8.B.R. Nag, Electron Transport in Compound Semiconductors, Springer Series in Solid State Science, volume 11, Springer-Verlag, Berlin, 1980.

8a.H. Temkin and V.G. Keramidas, "Room-temperature conductivity and the band structure of n-(Al,Ga)As," J. Appl. Phys. 51, 3269(1980).

9.H.C. Casey,Jr., "Room-temperature threshlod-current dependence of GaAs-(Al,Ga)As double-heterostructure laser on x and active layer thickness," J. Appl. Phys. 49, 3684(1978).

10.G.B. Stringfellow and R. Linnebach, "Photoluminescence of shallow acceptors in epitaxial (Al,Ga)As," J. Appl. Phys. 51, 2212(1980).

11.G.L. Hansen, J.L. Schmit, and T.N. Casselman, "Energy gap versus alloy composition and temperature in (Hg,Cd)Te," J. Appl. Phys. 53, 7099(1982).

12.W.A. Harrison, Solid State Theory, McGraw-Hill, N.Y., 1970.

13.L. Nordheim, Ann. Physik 9, 607 and 641(1931).

14.T. Muto, Sci. Papers Inst. Phys. Chem. Research (Tokyo) 34, 377(1938).

15.R.H. Parmenter, "Energy levels of a disordered alloy," Phys. Rev. 97, 587(1955).

16.R. Braunstein, A. Moore, and F. Herman, Phys. Rev. 109, 695(1958).

17.S.S. Vishnubhatla, B. Eyglunent, and J.C. Woolley, "Electroreflectance measurements in mixed III-V alloy," Can. J. Phys. 47, 1661(1969).

18.P. Soven, "Coherent-potential model of substitutional disordered alloys," Phys. Rev. 156, 809(1967).

19.B. Velicky, S. Kirkpatrick, and H. Ehrenreich, "Single-site approximations in the electronic theory of simple binary alloys," Phys. Rev. 175, 747(1968).

20.R.J. Elliott, J.A. Krumhansl, and P.L. Leatha, "The theory and properties of randomly disordered crystals and related physical systems," Rev. Mod. Phys. 46, 465(1974).

21.H. Ehrenreich and L.M. Schwartz, "The electronic structure of alloys," in Solid State Physics, volume 31, Academic Press, N.Y., 1976.

22.F. Yonezawa, "Coherent potential approximation," in The Structure and Properties of Matter, (Springer Series in Solid State Science, volume 28), Springer-Verlag, Berlin, 1982.

23.J.S. Faulkner, "The modern theory of alloys," Prog. Mater. Scien. 27, 1(1982).

24.J.A. Van Vechten, O. Berolo, and J.C. Woolley, "Spin-orbit splitting in compositionally disordered semiconductors," Phys. Rev. Lett. 29, 1400(1972).

25.D.J. Chadi, "Spin-orbit splitting in crystalline and compositionally disordered semiconductors," Phys. Rev. B16, 790(1977).

26.R. Dingle, R.A. Logan, and R.J. Nelson, "Exciton-phonon coupling in indirect (Al,Ga)As," Solid State Commun. 29, 171(1981).

27.A.T. Hunter and T.C. McGill, "Luminescence from (Hg,Cd)Te alloys," J. Appl. Phys. 52, 5779(1981).

28.H. Mariette, J. Chevallier, and P. Leroux-Hugon, "Local-environment effect on the nitrogen bound state in Ga(As,P) alloys; experiments and coherent-potential approximation theory," Phys. Rev. B21, 5706(1980).

29.H. Ehrenreich, "Electron mobility of In(As,P)," J. Phys. Chem. Solids 12, 97(1959).

30.M.A. Littlejohn, J.R. Hauser, and T.H. Glisson, "Alloy scattering and high-field transport in ternary and quaternary III-V semiconductors," Solid State Elect. 21, 107(1978).

31.H. Brooks, Unpublished results.

32.J.W. Harrison and J.R. Hauser, "Alloy scattering in ternary III-V compounds," Phys. Rev. B13, 5347(1976).

33.A. Baldereschi and K. Maschke, "Band structure of semiconductor alloys beyond the virtual crystal approximation; effect of compositional disorder on the energy gaps in Ga(As,P)," Solid State Commun. 16, 99(1975).

34.M.L. Cohen and V. Heine, "The fitting of pseudopotential to experimental data and their subsequent application," in Solid State Physics, volume 24, Academic Press, N.Y., 1976.

35.K.-R. Schulze, H. Neumann, and K. Unger, "Band structure of (Ga,In)As," Phys. Stat. Sol. (b)75, 493(1976).

36.K.C. Hass, H. Ehrenreich, and B. Velicky, "Electronic structure of (Hg,Cd)Te," Phys. Rev. B27, 1088(1983).

37.A. Baldereschi, E. Hess, K. Maschke, H. Neumann, K.-R. Schulze, and K. Unger, "Energy band structure of (Al,Ga)As," J. Phys. C; Solid State Phys., 10, 4709(1977).

38.A.O.E. Animalu and V. Heine, "The screened model potential for 25 elements," Phil. Mag. 12, 1249(1965), and references therein.

39.W. Kohn, "Shallow impurity states in silicon and germanium," in Solid State Physics, volume 5, Acamedic Press, N.Y., 1957.

40.A. Baldereschi and N.O. Lipari, "Spherical model of shallow acceptor states in semiconductors," Phys. Rev. B8, 2697(1973).

41.C.L. Wang, Ph,D. dissertation, University of California at Los Angeles, 1984.

42.D.S. Pan, D.L. Smith, and T.C. McGill, "Concentration broadening of bound-exciton spectral lines," Phys. Rev. B21, 3581(1980).

43.A. Zunger, "Contemporary pseudopotentials -simple reliability criteria," J. Vac. Scien. Technol. 16, 1337(1979).

44.M.L. Cohen and J.R. Chelikowsky, "Pseudopotentials for semiconductors," in Handbook on Semiconductors, volume 1, North-Holland Publishing Co., Amsterdam, 1982.

45.J.C. Phillips and L. Kleinman, Phys. Rev. 116, 287(1959).

46.B.J. Austin, V. Heine, and L.J. Sham, "General theory of pseudopotentials," Phys, Rev. 127, 276(1962).

47.J. Ziman, Principles of the Theory of Solids, Cambridge Univ. Press, London, 1964.

48.W.A. Harrison, Pseudopotentials in the Theory of Metals, W. A. Benjamin, Inc. N.Y., 1966.

49.J.R. Chelikowsky and M.L. Cohen, "Electronic structure of silicon," Phys. Rev. B10, 5095(1974).

50.N.J. Sherchik, J. Tejeda, M. Cardona, and D.W. Langer, "Photoemission and density of valence states of the II-VI compounds," Phys. Stat. Sol. (b)59, 87(1973).

51.L. Ley, R.A. Pollak, F.R. McFeely, S.P. Kowalczyk, and D.A. Shirley, "Total valence-band densities of states of III-V and II-VI compounds from X-ray photoemission spectroscopy," Phys. Rev. B9, 600,(1974).

52.D.E. Eastman and W.D. Grobman, "Photoemission spectroscopy using synchrotron radiation. I.Overview of valence-band structure for Ge, GaAs, GaP, InSb, ZnSe, CdTe, and AgI," Phys, Rev. B9, 3473(1974).

53.J.R. Chelikowsky and M.L. Cohen, "Nonlocal pseudopotential calculations for the electronic structure of eleven diamond and zinc-blende semiconductors," Phys. Rev. B14, 556(1976).

54.L.M. Falicov and S. Golin, "Electronic band structure of Arsenic. I.Pseudopotential approach," Phys. Rev. 137, A871(1965).

55.M. Schluter, R. Chelikowsky, S.G. Louie, and M.L. Cohen, "Self-consistent pseudopotential calculations for Si(111) surfaces," Phys. Rev. B12, 4200(1975).

56.O.V. Konstantinov, Sh.K. Nasibullaev, and M.M. Panakhov, "Analytic expression for the pseudopotential form factor," Sov. Phys. Semicond. 11, 519(1977).

57.A.E.O. Animalu, "The total electronic band structure energy for 29 elements," Proc. Roy. Soc.(London) 294, 376(1966).

58.D.R. Penn, "Wave-number-dependent dielectric function of semiconductors," Phys. Rev. 128, 2093(1962).

59.J.C. Phillips, "Covalent bond in crystal. I.Elements of a structure theory," Phys. Rev. 166, 832(1968).

60.G. Srinivasan, "Microscopic dielectric function of a model simiconductor," Phys. Rev. 178, 1244(1969).

61.M.L. Cohen and T.K. Bergstresser, "Band structure and pseudopotential form factors for fourteen semiconductors of the diamond and zinc-blende structure," Phys. Rev. 141, 789(1966).

62.L.I. Schiff, Quantum Mechanics, 3rd edition, McGraw-Hill, Inc. N.Y., 1971.

63.E. Merzbacher, Quantum Mechanics, 2nd edition, John Wiley and Sons, M.Y., 1970.

64.E.O. Kane, "The k.p method," in Semiconductors and Semimetals, volume 1, Academic Press, N.Y., 1966.

65.J. Mathews and R.L. Walker, Mathematical Methods of Physics, 2nd edition, Academic Press, N.Y., 1973.

66.L. Esaki and R. Tsu, "Superlattice and negative conductivity in semiconductors," IBM Res., Internal Rep. RC2418, March 26, 1969.

67.R. Dingle, H.L. Stormer, A.C. Gossard, and W. Wiegmann, "Electron mobilities in modulation-doped semiconductor heterojunction superlattice," Appl. Phys. Lett. 33, 665(1978).

68.A.-B. Chen and A. Sher, "Electronic structure of pseudobinary semiconductor alloys (Al,Ga)As, Ga(P,As), and (Ga,In)P," Phys. Rev. B23, 5360(1981).

69.E. Hess, I. Topol, K.-R. Schulze, H. Neumann, and K. Unger, "Band structure and pseudopotential form factors for AlAs," Phys. Stat. Sol. (b)55, 187(1973).

70.K. Unger, Wiss. Z. Karl-Marx-Universitat, Leipzig, Math.-Naturw. Reihe 20, 13(1971).

71. J.P. Walter and M.L. Cohen, "Calculation of the reflectivity, modulated reflectivity, and band structure of GaAs, GaP, ZnSe, and ZnS," Phys. Rev. 183, 763(1969).

72. G.C. Osbourn and D.L. Smith, "Transmission and reflection coefficients of carriers at an abrupt GaAs-(Al,Ga)As (100) interface," Phys. Rev. B19, 2124(1979).

73. E. Caruthers and P.J. Lin-Chung, "Pseudopotential calculations for (GaAs)1-(AlAs)1 and related monolayer hetero-structures," Phys. Rev. B17, 2705(1978).

74. H.C. Casey,Jr. and M.B. Panish, "(Al,Ga)As direct and indirect energy bandgap," J. Appl. Phys. 40, 4910(1969).

75. O. Berolo and J.C. Woolley, Can. J. Phys. 49, 1335(1971).

76. A. Onton, M.R. Lorenz, and J.M. Woodall, Bull. Am. Phys. Soc. 16, 371(1971).

77. W.M. Yim, J. Appl. Phys. 42, 2854(1971).

78. H.P. Klug and H. Neumann, EXp. Techn. Phys. 23, 605(1975).

79. M.B. Panish, J. Appl. Phys. 44, 2667(1973).

80. B. Monemar, K.K. Shih, and G.D. Pettit, "Some optical properties of the (Al,Ga)As alloy system," J. Appl. Phys. 47, 2604(1976).

81. R. Dingle, R.A. Logan, and J.R. Arthur,Jr., "The lower conduction band structure of (Al,Ga)As," Inst. Phys. Conf. Ser. No. 33a, 210(1977).

82. M.H. Weiler, "Magnetooptical properties of (Hg,Cd)Te alloys," in Semiconductors and Semimetals, volume 16, Academic Press, N.Y., 1981.

83. Proceeding of the First Workshop on the Physics and Chemistry of (Hg,Cd)Te, Minneapolis, Minnesota, 1981. (Published in J. Vac. Sci. Technol. 21, May/June 1982).

84. Proceeding of the Second Workshop on the Physics and Chemistry of (Hg,Cd)Te, Dallas, Texas, 1983. (Published in J. Vac. Sci. Technol. A1, July-sept. 1983).

85. Semiconductors and Semimetals, volume 18, ed. R.K. Willardson and A.C. Beer, Acamedic Press, N.Y., 1981.

86. H. Overhof, "A model calculation for the energy bands in the (Hg,Cd)Te mixed crystal system," Phys. Stat. Sol. (b)45, 315(1971).

87. S. Katsuki and M. Kunimune, "The band structures of alloy system (Hg,Cd)Te calculated by the pseudopotential method," J. Phys. Soc. Japan 31, 415(1971).

88. D.J. Chadi and M.L. Cohen, "Electronic structure of (Hg,Cd)Te alloys and charge-density calculations using representative k points," Phys. Rev. B7, 692(1973).

89. S. Bloom and T.K. Bergstresser, Phys. Stat. Sol. 42, 191(1970).

90. D.J. Chadi, J.P. Walter, M.L. Cohen, Y. Petroff, and M. Balkanski, "Reflectivities and electronic band structure of CdTe and HgTe," Phys. Rev. B5, 3058(1972).

91. M.T. Czyzyk and M. Podgorny, "Energy bands and optical properties of HgTe and CdTe calculated on the basis of the tight-binding model with spin-orbit interaction," Phys. Stat. Sol. (b)98, 507(1980).

92. A. Kobayashi, O.F. Sankey, and J.D. Dow, "Chemical trends for defect energy levels in (Hg,Cd)Te," Phys. Rev. B25, 6367(1982).

93. O. Berolo, J.C. Woolley, and J.A. Van Vechten, "Effects of disorder on the conduction-band effective-mass, valence-band spin-orbit splitting, and the direct bandgap in III-V alloys," Phys. Rev. B8, 3794(1973).

94. D. Stroud, "Band gaps of semiconductor alloys," Phys. Rev. B5, 3366(1972).

95. M. Altarelli, "Effect of disorder on direct and indirect bandgaps of semiconductor alloys," Solid State Commun. 15, 1607(1974).

96. J.P. Walter and M.L. Cohen, "Pseudopotential calculations of electronic charge densities in seven semiconductors," Phys. Rev. B4, 1877(1971).

97. J.C. Phillips, Bonds and Bands in Semiconductors, Academic Press, N.Y. 1973.

98. L. Pauling, The Nature of Chemical Bond, Cornell U. P., Ithaca, N.Y. 1939.

99. G.F. Koster, J.O. Dimmock, R.G. Wheder, and H. Statz, Properties of the Thirty-two Point Groups, MIT Press, Cambridge, Mass. 1963.

100. U. Kaufmann and J. Schneider, "Point defects in GaP, GaAs, and InP," in Advances in Electronics and Electron Physics, volume 58, (ed. C. Marton) Academic Press, N.Y. 1982. (and references therein.)

101. N. Lifshitz, A. Jayaraman, and R.A. Logan, "Pressure and compositional dependences of the Hall coefficient in (Al,Ga)As and their significance," Phys. Rev. B21, 670(1980).

102. V. Swaminathan, M.D. Sturge, and J.L. Zilko, "Free-to-bound transitions in Si-doped epitaxial (Al,Ga)As," J. Appl. Phys. 52, 6306(1981).

103. W. Scott, E.L. Stelzer, and R.J. Hager, "Electrical and far-infrared optical properties of p-type (Hg,Cd)Te," J. Appl. Phys. 47, 1408(1976).

104. G.C. Osbourn and D.L. Smith, "Auger and radiative transition for acceptor bound-excitons in direct-gap semiconsuctors," Phys. Rev. B20, 1556(1979).

105. P. Lowdin, J. Chem. Phys. 19, 1396(1951).

106. D. Brust, "Electronic spectra of crystalline germanium and silicon," Phys. Rev. 134, A1337(1964).

107. Excitons, ed. K. Cho, (Topics in Current Physics, volume 14),Springer-Verlag, Berlin, 1979.

108. D.C. Reynolds and T.C. Collins, Excitons: Their Properties and Uses, Academic Press, N.Y. 1981.

109. Excitons, ed. E.I. Rashba and M.D. Sturge, North-Holland Publishing Co., Amsterdam, 1982.

110. R.J. Nelson, N. Holonyak,Jr. and W.O. Groves, Phys. Rev. B13, 5415(1976).

111. R.J. Nelson and N. Holonyak,Jr., J. Phys. Chem. Solids 37, 629(1976).

112. D.J. Wolford, B.G. Streetman, S. Lai, and M.V. Klein, "Resonant excitation of bound-exciton luminescence in Ga(As,P) alloys," Solid State Commun. 32, 51(1979).

113. P.N. Sen, "Excitonic doublets in mixed crystals of alkali and cuprous halides; coherent-potential approximation," Phys. Rev. Lett. 30, 553(1973).

114. D.J. Wolford, B.G. Streetman, and J. Thompson, "Zero-phonon structure of N trap states in Ga(As,P) alloys," J. Phys. Soc. Japan 49, Suppl. A. 223(1980).

115. D.S. Pan, "The j-j coupling in bound excitons in the effective mass approximation," Solid State Commun. 37, 375(1981). (and references therein.)

116. C.R. Whitsett, J.G. Broerman, and C.J. Summers, in Semimetals and Semiconductors, volume 16, (Ed. R.K. Willardson and A.C. Beer), Acdemic Press, N.Y., 1981.

117. S.T. Pantelides, "The electronic structure of impurities and other point defects in semiconductors," Rev. Mod. Phys. 50, 707(1978).

118. N.O. Lipari, A. Baldereschi, and M.L.W. Thewalt, "Central cell effects on acceptor spectra in Si and Ge," Solid State Commun. 33, 277(1980).

(iii) FOR APPENDIX D

REFERENCES

1. D.L. Smith, T.C. McGill and J.N. Schulman, Appl. Phys. Lett. 43(2), p.180, July 1983,

2. D. Long and L. Smith, in Semimetals and Semiconductors, V. 5, edited by R.K. Willarson and A.C. Beer, Academic Press, p.175, N.Y. (1970).

3. W.W. Anderson, Appl. Phys. Lett. 41(11), p.1080, December 1982.

4. R.S. Putnam and M.M. Salour, Appl. Phys. Lett, V.43, No.5, p.408, Sept. 1983.

5. G. Weil, A. Kozachi and C. Verie, Proc. III International Conf. Phys. 'Narrow-Gap Semiconductor', Warsaw 1977.

6. T.C. Harman and I. Melngailis, Narrow Gap Semiconductors, Appl. Solid State Sci. 4. (1974)

7. R. Dornhaus and G. Nimtz, in Springer Tracts in Modern Physics, V.78, edited by Hohler (Springer-Berlin, 1976).

8. 'Semiconductors and Semimetals', V.18, edited by R.K. Willardson and A.C. Beer, (1981).

9. D. Chattopadhyay and B.R. Nag, Phys. Rev. B. V.12, p.5676, (1975).

10. E.T. Whittaker and G.N. Watson, 'A Course of Modern Analysis', 4th ed. Cambridge, Cambridge University Press, (1927).

11. W. Szymanska and T. Dietl, J. Phys. Chem. Solids 39, p.1025, (1978).

12. W. Szymanska, P. Boguslawski and W. Zawadzki, Phys. Status Solidi (b) 65, p.641, (1974).

13. W. Zawadzki and W. Szymanska, Phys. Status Solidi (b) 45, p.415, (1971).

14. D.L. Rode and J.D. Wiley, Phys. Status Solidi (b)56, p.699, (1973).

15. S.T. Pantelides, Rev. Mod. Phys. 50, p.797, (1978).

16. D.M. Larsen, J. Phys. Chem. Solids V.29, p.271, (1968).

17. R. Bowers and Y. Yafet, Phys. Rev. 115, p.1165, (1959).

18. J.M. Luttinger and W. Kohn, Phys. Rev. 97, p.869, (1955).

19. W. Kohn, Solid State Phys. 5, p.258, 1957, edited by F. Sietz and D. Turnbull.

20. H.A. Bethe and E.E. Salpeter, 'Quantum Mechanics of one and two-electron atoms', Academic Press, N.Y. (1957).

21. H. Ehrenreich, J. Phys. Chem. Solids 2, p.131, (1957).

22. E.O. Kane, J. Phys. Chem. Solids 1, p.249, (1957).

23. E.O. Kane, in Semiconductors and Semimetals, edited by R.K. Willardson and A.C. Beer, V.1, p.75, Academic Press, N.Y. (1966).

24. L. Liu and E. Tosatti, Phys. Rev. Letters 23, p.772, (1969); Phys. Rev. B2, p.1926, (1970).

25. J.G. Broerman, L. Liu and K.N. Pathak, Phys. Rev. B4, p.664, (1971).

26. D.J. Howarth and E.H. Sondheimer, Proc. Soc. A219, p.53, (1957).

27. J. Kolodziejczak, Acta Phys. Polon. 20, p.379, (1961).

28. C. Erginsoy, Phys. Rev. 79, p.1013, (1950).

29. W.A. Harrison, Phys. Rev. 101, p.903, (1956).

30. P. Boguslawski, Phys. Status Solidi (b) 70, p.53, (1975).

31. J.J. Dubowski, T.Dietl, W. Szymanska and R.R. Galazka, J. Phys. Chem. Solids, V.42, p.351, (1980).

32. R.J. Iwanowski, T. Dietl and W. Szymanska, J. Phys. Chem. Solids, V.39, p.1059, (1978).

33. T. Dietl and W. Szymanska, J. Phys. Chem. Solids, V.39, p.1041, (1978).

34. J. Bajaj, S.H. Shin, G. Bostrup and D.T. Cheung, J. Vac. Sci. & Tech., V.21, No.1, p.244, (1982).

35. Y. Guldner, C. Rigaux, A. Mycielski and Y. Couder, Phys. Status Solidi (b)82, p.149, (1977).

36. G.L. Hansen, J.L. Schmit and T.N. Casselman, J. Appl. Phys. 53(10), October 1982.

37. J.D. Wiley and R.N. Dexter, Phys. Rev. 181, p.1181, (1969).

38. M.W. Scott, J. Appl. Phys. 40, p.4077, (1969).

39. J.L. Schmit and E.L. Stelzer, J. Appl. Phys. V.40, p.4865, (1969).

40. J.L. Schmit, J. Appl. Phys. V.41, No.7, p.2876, (1970).

41. A. Mauger and J. Friedel, Phys. Rev. B. V.12, No.6, p.2412, (1975).

42. C. Finck, S. Otmezguine, G.Weill and C. Verie, in Proc. of the 11th International Conf. on the Phys. of Semi. V.2, p.944, (1972).

APPENDIX A

Chapter III

SELF-CONSISTENT GEMT OF DOUBLE ACCEPTORS

3.1 THE CATIONIC VACANCIES IN MERCURY CADMIUM TELLURIDE

3.1.1 Introduction and Experimental Data

HgCdTe is an important II-VI compound alloy, and has been known as a good candidate for far-infrared detectors. The usefulness comes from the linear variability of the bandgap E_g with x, which is the molar concentration of CdTe in the alloy. The bandgap varies from -0.3 eV (semi-metal) for HgTe to 1.6 eV for CdTe. The bandstructure for each x can be calculated from pseudopotential method based on the Virtual Crystal Approximation (VCA)[60,61,62]. As an example, the band structures of CdTe and HgTe are shown in Fig. 3.1.

Elliot, et al[17], reported electrical transport and photoluminescence (PL) measurements for uncompensated p-type HgCdTe. In the electrical measurement, the acceptor ionization energy E_A ranged from 15 to 22 meV for x in the range 0.26 to 0.34; and from the PL measurement, E_A ranged 10~16 meV for x=0.30~0.34 and 25 meV for x=0.50. Scott, Stelzer and Hager[18] measured a p-type compensated $Hg_{0.6}Cd_{0.4}Te$ and obtained the acceptor level to be 14±1 meV. They did not give the nature and source of this p-type properties. Hunter and McGill did luminenscence measurements on HgCdTe alloys[16], and estimated that

the acceptor binding energies in x=0.32 and x=0.48 materials are 14.0 ±1.0 and 15.5±2.0 meV. This impurity was thought to be the Hg vacancy. However, during sample preparation, the sample was gold plated and annealed in Hg vapor. This process could dope the crystals with Au and reduce the number of Hg vacancies. Therefore, the acceptor for this p-type sample is either substitutional Au or Hg vacancies.

All the above experimental results seem to be in good agreement. Our task is to do a theoretical study on p-type HgCdTe so as to get a better understandings of the source of the defect states of these acceptors.

3.1.2 General theoretical model

We will apply the shallow level approach for this HgCdTe acceptor problem. We will calculate two possible cases: 1. A simple acceptor (A^- ,h^+) which exists when an Au atom occupies the cationic site. 2. A double acceptor in the neutral (A^{-2};h^+ ,h^+) state, and its ionized states (A^{-2},h^+), which can occur due to a cationic vacancy.

In the first case, the Au atom has only one valence electron, while the Hg and Cd atoms have 2 (The $_{79}$Au is isocoric with Hg). The impurity potential is well represented by a -1 point charge center, screened by the dielectric response of the surrounding valence electrons. This is a simple acceptor problem, the calculation method has been described in Chapter 2.

The Luttinger parameters for $Hg_{1-x}Cd_xTe$ are functions of x. Some empirical formulae for these parameters are available in Weiler's article[19]. We first determine the band gap by:

$$E_g = -304 + \frac{0.63T^2}{11+T}(1-2x) + 1858x + 54x^2 \qquad (3.1.1)$$

where T is the temperature in °K, and E_g is in meV. The Luttinger parameters are functions of E_g :

$$\gamma_1 = 3.3 + 6333/E_g$$
$$\gamma_2 = 0.1 + 3167/E_g$$
$$\gamma_3 = 0.9 + 3167/E_g \qquad (3.1.2)$$

The temperature T is set to be 0 since we are interested in low temperature acceptor levels. The dielectric coefficient ϵ is also a fuction of x, and the curve of ϵ vs. x is available from Fig. 85, P.93 in Dornhaus and Nimtz's article[60]. All the necessary parameters ϵ, γ_1, γ_2, γ_3, E_g, effective Rydberg R_* and effective Bohr radius a^* are then calculated and listed in Table 3.1.

For the 2nd case, the cationic vacancy problem is a many body problem. During the crystal growth of HgCdTe alloy, Hg or Cd vacancies can be formed in the lattice. Hg and Cd atoms are randomly distributed in the cationic sites but with Cd molar concentration equal to x. A schematic representation of such a cationic vacancy is shown in Fig. 3.2

This vacancy problem has been treated by Swarts et al[20] using a tight binding Green's function method. We would like to point out that

in this case, the cationic vacancy introduces a -2e defect charge center, which is much weaker than the perfect crystal potential. The defect state wavefunction is very spread out (not localized enough to have a tight binding treatment). A shallow level method of GEMT is more suitable. However, the deep level method is good for a Si vacancy in Si, in which the defect charge center, -4e, is strong and comparable to the crystal field potential. This Si vacancy problem has been treated in several papers both with and without the Jahn-Teller effect (lattice relaxation). The II-VI vacancy is a simpler problem than the Si vacancy.

Another way to justify that the perturbing potential can be described by a -2e point charge is to look at the the model potential plot of Hg and Cd ions (Fig. 3.3). A model potential is a potential which divide the lattice ion potential into two regions: the core region and the region outside the core. Inside the core, the lattice potential is replaced with the square well potentials; outside the core, the potential varies like the Coulomb potential. The model potential can give the correct eigenvalues and wavefunctions in certain energy range. The model potential we used in our plot is the Heine-Abarenkov model potential which is defined by:

$$V_{model} = \begin{cases} \sum B_\ell P_\ell \quad \ell = 0, 1, 2 & \text{for } r < R_M \\ \dfrac{Z}{r} & \text{for } r > R_M \end{cases} \qquad (3.1.3)$$

The radii of the sphere of the core region R_M are less than $3a_B$ (a_B =0.53 Å---Bohr radius), and are smaller than the lattice constant of HgCdTe. It is seen from this model potential viewpoint that except for this small central cell region, the defect potential of the cationic vacancy can be well described as the absence of this point charge potential. However, in the central cell region, the point charge Coulomb potential is apparently deeper than the model potential and will result in an overestimate of the binding energy. Due to the smallness of this central cell region, and A_2, A_1, A_0 are not too different from the Coulomb potential at R_M, the overestimate is small.

For the double acceptor, Z_A=-2, we will carry out the calculation for $(A^{-2};h^+,h^+)$ and $(A^{-2};h^+)$. For $(A^{-2};h^+)$, the singly charged ionized state can be treated exactly like a simple acceptor problem except the defect potential should be $-2\cdot\frac{2}{\epsilon r}$. For the neutral double acceptor $(A^{-2};h^+,h^+)$, the total Hamiltonian has to include the Coulomb interaction:

$$H(\vec{r}_1,\vec{r}_2) = H_0(\vec{r}_1) + H_0(\vec{r}_2) + \frac{2}{|\vec{r}_2-\vec{r}_1|} \qquad (3.1.4)$$

where $H_0(\vec{r}_1)$ and $H_0(\vec{r}_2)$ are the single hole Hamiltonian operators. We know from Chapter 2 that $H_0(\vec{r})$ is reducible to a radial coupling equation of GEMT. To solve eq. (3.1.4), we reduce it to the single hole Hartree-Fock operator through the standard variational principle:

$$H^{HF}(\vec{r}) = H_0(\vec{r}) + \int \phi'^{+}(\vec{r}')\frac{2}{|\vec{r}-\vec{r}'|}\phi'(\vec{r}')\,d^3r'$$

and

$$H^{HF}\phi(\vec{r}) = E^{HF}\phi(\vec{r}) \qquad (3.1.5)$$

where $\phi'(\vec{r}')$ is the known orbital. Then, the solution are iterated for a self-consistent $\phi(r)$.

The Hartree-Fock equation still needs to be simplified. First, we can simplify the Coulomb interaction matrix element, which will be described in the coming subsection.

3.1.3 The Coulomb matrix element

Both holes in the double acceptor at ground state have Γ_8 symmetry, and angular quantum number F=3/2. Because of Pauli exclusion rule, these two holes can not occupy the same quantum state, i.e. their F_z's ought to be different (F_z can be one of 3/2, 1/2, -1/2, -3/2). The Coulomb matrix element:

$$\langle \phi_{F_{z_1}}(\vec{r}_1)\,\phi_{F_{z_2}}(\vec{r}_2)\left|\frac{2}{|\vec{r}_2-\vec{r}_1|}\right|\phi_{F_{z_1}}(\vec{r}_1)\,\phi_{F_{z_2}}(\vec{r}_2)\rangle$$

$$= \iint \phi^*_{F_{z_1}}(\vec{r}_1)\,\phi^*_{F_{z_2}}(\vec{r}_2)\,\frac{2}{|\vec{r}_2-\vec{r}_1|}\,\phi_{F_{z_1}}(\vec{r}_1)\,\phi_{F_{z_2}}(\vec{r}_2)\,d^3r_1\,d^3r_2 \qquad (3.1.6)$$

will be different for different choices of F_{z_1} and F_{z_2}. But the difference will be small and unimportant when we perform the Hartree-Fock iteration. We will fix the small differences in the later section as we discuss the j-j coupling and the exchange term. For convenience, we select F_{z_1}=3/2 and F_{z_2}=-3/2 to find the Coulomb matrix element. Our goal is to find a radial form for the double integral of eq.(3.1.6), so as to make it compatible with the radial operator in the simple acceptor GEMT equation.

The Γ_8 symmetry hole states, as mentioned in Chapter 3, is expressable in the s-like and d-like radial envelope functions multiplied by their angular quantum states (which is a coupling of the orbital angular momentum and the Bloch states effective 'spin'), i.e.

$$\phi^{8}_{\pm 3/2} = f(r)\,|L=0, J=\tfrac{3}{2}, F=\tfrac{3}{2}, F_z=\pm\tfrac{3}{2}\rangle + g(r)\,|L=2, J=\tfrac{3}{2}, F=\tfrac{3}{2}, F_z=\pm\tfrac{3}{2}\rangle. \qquad (3.1.7)$$

Our first step is to decouple the angular kets. By refering to the Clebsch-Gordan coefficient table, the angular kets are decomposed into the spherical harmonic Y_{lm} space and the effective spin J=3/2 functional space:

$$|L=0\ J=\tfrac{3}{2}\ F=\tfrac{3}{2}\ F_z=\pm\tfrac{3}{2}\rangle = Y_{00}\chi_{\pm\frac{3}{2}}$$

$$|L=2\ J=\tfrac{3}{2}\ F=\tfrac{3}{2}\ F_z=\pm\tfrac{3}{2}\rangle = \sqrt{\tfrac{1}{5}}\,Y_{20}\chi_{\pm\frac{3}{2}} \pm\sqrt{\tfrac{2}{5}}\,Y_{2\pm1}\chi_{\pm\frac{1}{2}} - \sqrt{\tfrac{2}{5}}\,Y_{2\pm2}\chi_{\mp\frac{1}{2}} \qquad (3.1.8)$$

where $\chi_{J_z}(J_z = 3/2,\ 1/2)$ represents the spinor 3/2 states. We will assume an approximation that the spin states χ are orthogonal to each other, and χ are independent of the radial part and the Y_{lm} space. This approximation is very good for the spread out defect states of shallow acceptors, but not for the localized state of deep levels. The Coulomb interaction integral should not only be integrated over the spatial variable $\vec{r}_1$, $\vec{r}_2$, but also be intergrated over the spin part χ_1 and χ_2.

We use $\hat{g}$ to denote the Coulomb operator $\frac{2}{|\vec{r}_2-\vec{r}_1|}$. In our approximation, $\hat{g}$ has nothing to do with the spinor states. Thus, we can se-

parate out the spin functions in the ϕ_{F_2} and carry out the spin integrations on particle 1 and particle 2 based on their orthogonal property. This step can greatly reduce the number of terms in the final expansion of the matrix element.

We use a simple table to indicate the result after the integration of the spin states of the first particle $\phi^*_{1/2}\phi_{1/2}$,where f,, g, are radial envelope functions of $\phi^{(\vec{r}_1)}_{1/2}$:

Spin integration	$f_1Y_{00}\chi_{1/2}$	$\sqrt{\frac{1}{3}}g_1Y_{10}\chi_{1/2}$	$\sqrt{\frac{2}{3}}g_1Y_{21}\chi_{1/2}$	$-\sqrt{\frac{2}{3}}g_1Y_{22}\chi_{-1/2}$
$f_1Y^*_{00}\chi^\dagger_{1/2}$	$f_1f_1Y^*_{00}Y_{00}$	$\sqrt{\frac{1}{3}}f_1g_1Y^*_{00}Y_{10}$	0	0
$\frac{1}{\sqrt{3}}g_1Y^*_{10}\chi^\dagger_{1/2}$	$\sqrt{\frac{1}{3}}g_1f_1Y^*_{10}Y_{00}$	$\frac{1}{3}g_1g_1Y^*_{10}Y_{10}$	0	0
$\sqrt{\frac{2}{3}}g_1Y^*_{21}\chi^\dagger_{1/2}$	0	0	$\frac{2}{5}g_1g_1Y^*_{21}Y_{21}$	0
$-\sqrt{\frac{2}{3}}g_1Y^*_{21}\chi^\dagger_{-1/2}$	0	0	0	$\frac{2}{5}g_1g_1Y^*_{22}Y_{22}$

(3.1.9)

6 terms are left for the first particle $\vec{r}_1$. Similarly, spin integration of the second particle $\vec{r}_2$ also leaves 6 terms, where f_2, g_2 are radial envelope functions of $\phi^{(\vec{r}_2)}_{1/2}$:

Spin integration	$f_2Y_{00}\chi_{-1/2}$	$\sqrt{\frac{1}{3}}g_2Y_{10}\chi_{-1/2}$	$-\sqrt{\frac{2}{3}}g_2Y_{2-1}\chi_{-1/2}$	$-\sqrt{\frac{2}{3}}g_2Y_{2-2}\chi_{1/2}$
$f_2Y^*_{00}\chi^\dagger_{-1/2}$	$f_2f_2Y^*_{00}Y_{00}$	$\sqrt{\frac{1}{3}}f_2g_2Y^*_{00}Y_{10}$	0	0
$\sqrt{\frac{1}{3}}g_2Y^*_{10}\chi^\dagger_{-1/2}$	$\sqrt{\frac{1}{3}}g_2f_2Y^*_{10}Y_{00}$	$\frac{1}{3}g_2g_2Y^*_{10}Y_{10}$	0	0

$$\begin{array}{|cccc|} -\sqrt{\frac{1}{5}}\, g_1 Y_{1-1}^{*} \chi_{-\frac{1}{2}}^{\dagger} & 0 & 0 & \frac{2}{5} g_1 g_2 Y_{1-1}^{*} Y_{21} & 0 \\ -\sqrt{\frac{1}{5}}\, g_1 Y_{1-1}^{*} \chi_{\frac{1}{2}}^{\dagger} & 0 & 0 & 0 & \frac{2}{5} g_1 g_2 Y_{1-1}^{*} Y_{20} \end{array}$$

(3.1.10)

Picking any one term in the first table, multiplying it with the Coulomb operator $\hat{g}$ and any one term in the 2nd table, then integrate over $\vec{r}_1$ and $\vec{r}_2$ will give us one term in the final expansion. Therefore, we have 6 x 6 = 36 terms to evaluate. For example,

$$\langle f_1 Y_{00}^{*} f_2 Y_{00} | \hat{g} | f_1 Y_{00} f_2 Y_{00} \rangle$$

$$= \int d^3 r_1 \int d^3 r_2 \, f_1(r_1) Y_{00}^{*}(\Omega_1) f_2(r_2) Y_{00}^{*}(\Omega_2) \frac{2}{|\vec{r}_2 - \vec{r}_1|} f_1(r_1) Y_{00}(\Omega_1) f_2(r_2) Y_{00}(\Omega_2)$$

is the first term.

We treat the general term

$$\langle h_1(r_1) Y_{l_1 m_1}(\Omega_1) h_2(r_2) Y_{l_2 m_2}(\Omega_2) | \hat{g} | h_3(r_1) Y_{l_3 m_3}(\Omega_1) h_4(r_2) Y_{l_4 m_4}(\Omega_2) \rangle$$

like in the atomic physics. The operator $\hat{g}$ is expandable into the Y_{lm} space of $\vec{r}_1$ and $\vec{r}_2$ through the addition theorem:

$$\hat{g} = \frac{2}{|\vec{r}_2 - \vec{r}_1|} = 2 \sum_{L=0}^{\infty} \frac{2L+1}{4\pi} \sum_{M=-L}^{L} \frac{r_<^L}{r_>^{L+1}} Y_{LM}^{*}(\theta_1, \phi_1) Y_{LM}(\theta_2, \phi_2) \tag{3.1.11}$$

where $r_<$ means the smaller one, $r_>$ the larger one of r_1 and r_2.

With eq. (3.1.11) , eq. (3.1.6) is further separable into the product of a radial integral and two angular integrals, summed over all 36 terms:

$$\langle h_1(r_1) Y_{l_1 m_1}(\Omega_1) h_2(r_2) Y_{l_2 m_2}(\Omega_2) | \hat{g} | h_3(r_1) Y_{l_3 m_3}(\Omega_1) h_4(r_2) Y_{l_4 m_4}(\Omega_2) \rangle$$

$$= 2 \sum_{k=0}^{\infty} C_k(l_1 m_1, l_3 m_3) C_k(l_2 m_2, l_4 m_4) R^{(k)}(h_1, h_2, h_3, h_4) \tag{3.1.12}$$

where

$$R^{(k)}(l_1 l_2 l_3 l_4) = \int_0^\infty \int_0^\infty l_1(r_1) l_2(r_2) \frac{r_<^k}{r_>^{k+1}} l_3(r_1) l_4(r_2) r_1^2 r_2^2 dr_1 dr_2 \qquad (3.1.13)$$

is an radial integral.

$$c_k(l_i m_i, l_j m_j) = \iint \sin\theta d\theta d\phi \, Y^*_{l_i m_i}(\theta,\phi) Y^*_{k M}(\theta,\phi) Y_{l_j m_j}(\theta,\phi)$$

$$M = m_j - m_i \qquad (3.1.14)$$

is called the Gaunt's coefficient, and is equal to

$$(-1)^{m_i} \sqrt{\frac{(2l_i+1)(2k+1)(2l_j+1)}{4\pi}} \begin{pmatrix} l_i & k & l_j \\ m_i & M & m_j \end{pmatrix} \begin{pmatrix} l_i & k & l_j \\ 0 & 0 & 0 \end{pmatrix}$$

where the parentheses $\begin{pmatrix} a & b & c \\ d & e & f \end{pmatrix}$ are 3-j symbols. Gaunt's coefficients are tabulated in some books[39,63].

These 36 terms can be calculated one by one with the help of Gaunt's coefficients. For example, the first term

$$\begin{aligned} &\langle f_1 Y_{00} f_2 Y_{00} | \hat{g} | f_1 Y_{00} f_2 Y_{00} \rangle \\ &= \sum_k c_k(0\,0, 0\,0)\, c_k(0\,0, 0\,0)\, R^{(k)}(f_1, f_2, f_1, f_2) \\ &= 1 \cdot 1 \cdot R^{(0)}(f_1 f_2 f_1 f_2) \\ &= R^{(0)}(f_1 f_2 f_1 f_2) \end{aligned} \qquad (3.1.15)$$

because only $c_0(0,0,0,0)=1$ and all other $c_k=0$.

After we calculate each of the 36 terms, the total sum for the Coulomb interaction matrix element is found to be:

$$\begin{aligned} &\langle \phi_{3/2} \phi_{-3/2} | \hat{g} | \phi_{3/2} \phi_{-3/2} \rangle \\ &= R^{(0)}(f_1 f_2 f_1 f_2) + R^{(0)}(f_1 g_2 f_1 g_2) + R^{(0)}(g_1 f_2 g_1 f_2) \end{aligned}$$

$$+\frac{4}{25} R^{(4)}(f_1 g_1 f_2 g_2) \qquad (3.1.16)$$

All terms are radial integrals.

The $R^{(4)}$ term is very small compared to the other terms and can be neglected in our calculation.

3.1.4 Derivation of the radial Hartree-Fock operator

The double acceptor wavefunction can be written as an anti-symmetrized product of the two individual hole wavefunctions (In our calculation, we have assumed one hole with $F_{z_1}=3/2$, the other with $F_{z_2}=-3/2$):

$$\psi(\vec{r}_1,\vec{r}_2) = \mathcal{A}\left\{\phi_{3/2}(\vec{r}_1)\phi_{-3/2}(\vec{r}_2)\right\} = \frac{1}{\sqrt{2}}\begin{vmatrix} \phi_{3/2}(\vec{r}_1) & \phi_{-3/2}(\vec{r}_1) \\ \phi_{3/2}(\vec{r}_2) & \phi_{-3/2}(\vec{r}_2) \end{vmatrix} \qquad (3.1.17)$$

The binding energy E is given by the matrix element of the total Hamiltonian

$$\begin{aligned} E &= \langle \psi(r_1,r_2) | H_{tot}(\vec{r}_1,\vec{r}_2) | \psi(r_1,r_2)\rangle \\ &= \langle \phi_1(\vec{r}_1)|H_0(\vec{r}_1)|\phi_1(\vec{r}_1)\rangle + \langle \phi_2(\vec{r}_2)|H_0(\vec{r}_2)|\phi_2(\vec{r}_2)\rangle \\ &\quad + \iint \phi_1^*(\vec{r}_1)\phi_2^*(\vec{r}_2)\frac{2}{|\vec{r}_2-\vec{r}_1|}\phi_1(\vec{r}_1)\phi_2(\vec{r}_2)\,d^3r_1\,d^3r_2 \\ &\quad - \iint \phi_1^*(\vec{r}_1)\phi_2^*(\vec{r}_2)\frac{2}{|\vec{r}_2-\vec{r}_1|}\phi_2(\vec{r}_1)\phi_1(\vec{r}_2)\,d^3r_1\,d^3r_2 \end{aligned} \qquad (3.1.18)$$

The first two terms in (3.1.18) are the single hole Hamiltonian, the third term is the Coulomb interaction and the fourth term is the exchange interaction.

We know from the simple acceptor EMT, the $H_o(r)$ can be approximated by the spherical model H_{sph} and the angular integration can be performed by the reduced matrix element method and 6j symbols. The single hole part is reduced to the radial integral bracket:

$$\langle \phi | H_{sph} | \phi \rangle = \langle f | \Omega_{11} | f \rangle + \langle f | \Omega_{12} | g \rangle + \langle g | \Omega_{21} | f \rangle + \langle g | \Omega_{22} | g \rangle \qquad (3.1.19)$$

where Ω_{11}, Ω_{12}, Ω_{21}, Ω_{22} are radial operators defined in eq.(2.3.2) of Chapter 2. The Coulomb matrix element are known to have a radial form derived in section 3.1.4, and the exchange term has a similar form, but with a smaller value.

The $\langle \psi | H_{eff} | \psi \rangle$ term can then be expressed in the radial form:

$$\begin{aligned}\langle \psi | H_{eff} | \psi \rangle = {} & \langle f_1 | \Omega_{11} | f_1 \rangle + \langle f_1 | \Omega_{12} | g_1 \rangle + \langle g_1 | \Omega_{21} | f_1 \rangle + \langle g_1 | \Omega_{22} | g_1 \rangle \\ & + \langle f_2 | \Omega_{11} | f_2 \rangle + \langle f_2 | \Omega_{12} | g_2 \rangle + \langle g_2 | \Omega_{21} | f_2 \rangle + \langle g_2 | \Omega_{22} | g_2 \rangle \\ & + R^{(0)}(f_1 f_2, f_1 f_2) + R^{(0)}(f_1, g_2, f_1, g_2) + R^{(0)}(g_1, f_2, g_1, f_2) \\ & + \tfrac{4}{25} R^{(2)}(f_1, g_1, f_2, g_2) \qquad (3.1.20)\end{aligned}$$

It is understood that the above brackets notation only means the radial integrals. The normalization of wavefunctions then require that

$$\langle \phi_1 | \phi_1 \rangle = \langle f_1 | f_1 \rangle + \langle g_1 | g_1 \rangle = 1,$$

and

$$\langle \phi_2 | \phi_2 \rangle = \langle f_2 | f_2 \rangle + \langle g_2 | g_2 \rangle = 1 \qquad (3.1.21)$$

and the orthogonality $\langle \phi_1 | \phi_2 \rangle = 0$

The variational principle requires to minimize $\langle \psi | H_{eff} | \psi \rangle$ under the normalization constraints: $\langle \phi_i | \phi_j \rangle = \delta_{ij}$

It is natural to use the Lagrangian multiplier method for minimization

$$\delta\left[\langle\psi|H_{tot}|\psi\rangle-\lambda_1\langle\phi_1|\phi_1\rangle-\lambda_2\langle\phi_2|\phi_2\rangle-\lambda_{12}\langle\phi_1|\phi_2\rangle\right]=0 \qquad (3.1.22)$$

We know there exists a set ϕ_1' and ϕ_2' by finding the appropriate linear combination of ϕ_1 and ϕ_2. This linear combination will not change $\langle\psi|H_{tot}|\psi\rangle$, but will make $\lambda_{12}=0$ (no off-diagonal eigenvalue term). This diagonalized λ_1, λ_2 and ϕ_1', ϕ_2' are what we are seeking. Let us for simplicity drop the primes of ϕ_1' and ϕ_2'. we can simply make

$$\delta\left[\langle\psi|H_{tot}|\psi\rangle-\lambda_1\langle\phi_1|\phi_1\rangle-\lambda_2\langle\phi_2|\phi_2\rangle\right]=0 \qquad (3.1.23)$$

From eq.(3.1.20), $\langle\psi|H_{tot}|\psi\rangle$ is reduced to the radial form having 4 variable functions f_1, f_2, g_1 and g_2. The variation operator then is equivalent to the infinitesimal variations of δf_1, δf_2, δg_1, δg_2 respectively.

We leave out the exchange terms in eq.(3.1.20) because they are small compared to the Coulomb terms. As a standard procedure, we can vary f_1 and g_1 from the left while treating f_2 and g_2 as known functions. Varying f_1, we obtain

$$\langle\delta f_1|\Omega_{11}|f_1\rangle+\langle\delta f_1|\Omega_{12}|g_1\rangle+\iint(\delta f_1)f_2\frac{2}{r_>}f_1f_2r_1^2r_2^2dr_1dr_2$$
$$+\iint(\delta f_1)f_2\frac{4}{25}\frac{2r_<^2}{r_>^3}g_1g_2r_1^2r_2^2dr_1dr_2-\lambda_1\langle\delta f_1|f_1\rangle=0 \qquad (3.1.24)$$

Eq.(3.1.24) can be expressed as

$$\langle\delta f_1|\Omega_{11}|f_1\rangle+\langle\delta f_1|\Omega_{12}|g_1\rangle+\langle\delta f_1|H_{int,11}|f_1\rangle+\langle\delta f_1|H_{int,12}|g_1\rangle$$
$$-\lambda_1\langle\delta f_1|f_1\rangle=0 \qquad (3.1.25)$$

where $H_{int_{11}}$, $H_{int_{12}}$ are implicit Coulomb field integrals of f_2 and g_2 defined by

$$H_{int_{11}}(r_1, f_2, g_2) = \int_0^\infty f_2(r_2) \frac{2}{r_>} f_2(r_2)\, r_2^2\, dr_2$$

$$H_{int_{22}}(r_1, f_2, g_2) = \frac{4}{25} \int_0^\infty f_2(r_2) \frac{2 r_<^2}{r_>^3} g_2(r_2)\, r_2^2\, dr_2 \qquad (3.1.26)$$

In a similar fashion, the variation of δg_1 from left reduces to

$$\langle \delta g_1 | \Omega_{21} | f_1 \rangle + \langle \delta g_1 | \Omega_{22} | g_1 \rangle + \langle \delta g_1 | H_{int_{22}} | g_1 \rangle - \lambda_1 \langle \delta g_1 | g_1 \rangle = 0 \qquad (3.1.27)$$

Coupling eq. (3.1.26) and eq. (3.1.27), and writing them in a matrix equation form, (the unknowns are f_1, g_1, and δf_1, δg_1 are arbitrary infinitesimal functions, we obtain:

$$\begin{bmatrix} \Omega_{11} + H_{int_{11}} & \Omega_{12} + H_{int_{12}} \\ \Omega_{21} & \Omega_{22} + H_{int_{22}} \end{bmatrix} \begin{bmatrix} f_1 \\ g_1 \end{bmatrix} = E^{HF} \begin{bmatrix} f_1 \\ g_1 \end{bmatrix} \qquad (3.1.28)$$

In the above equation, we replaced λ by the Hartree-Fock eigenenergy E^{HF}. Therefore, we have derived the Hartree-Fock equation for the double acceptor problem.

3.1.5 The screened Coulomb interaction

The Coulomb interaction between holes is screened by the valence electrons. We use the linear response theory to consider the electron redistribution at the presence of a hole charge. This linear theory approximates the dielectric wavefunction with $\epsilon(\vec{q})$, $\vec{q}$ is the wave vector. It is known in the 2nd chapter that $\epsilon(q)$ can be fitted to be:

$$\epsilon(q) = \epsilon_\infty \frac{q^2+\beta^2}{\epsilon_\infty q^2+\beta^2} \qquad (3.1.29)$$

The screened Coulomb potential due to one hole is

$$\int \frac{e^{-i\vec{q}\cdot\vec{r}}}{\epsilon(q)\,q^2} d^3q = \frac{2}{\epsilon(r)\,r} \qquad (3.1.30)$$

and $\epsilon(r)$ is found to be

$$\epsilon(r) = \left[1+(\epsilon_\infty-1)\,e^{-\beta r}\right]^{-1} \qquad (3.1.31)$$

With the dielectric function $\epsilon(r)$ in real space, the screened Coulomb interaction between two holes is

$$V_{ss} = \iint \rho_1(\vec{r}_1)\,\frac{2}{|\vec{r}_2-\vec{r}_1|\,\epsilon(|\vec{r}_2-\vec{r}_1|)}\,\rho_2(\vec{r}_2)\,d^3r_1\,d^3r_2 \qquad (3.1.32)$$

where $\rho(\vec{r}) = \phi^*(\vec{r})\phi(\vec{r})$ is the charge density.

Eq.(3.1.32) is a very complicated integral. To simplify it, we use the Fourier transform technique. The theorem we apply is

$$\iint u_1(\vec{r}_1)\,w(\vec{r}_2-\vec{r}_1)\,u_2(\vec{r}_2)\,d^3r_1\,d^3r_2$$
$$= \int u_{1k}(-\vec{k})\,w_k(|\vec{k}|)\,u_{2k}(\vec{k})\,d^3k \qquad (3.1.33)$$

where the functions with k sub-index means the Fourier transformed functions.

The screened Coulomb operator part $w(\vec{r}_2 - \vec{r}_1)$ obviously has the Fourier transform

$$w_k(|\vec{k}|) = \frac{2}{k^2 \epsilon(k)} = \frac{2(\epsilon_\infty k^2 + \beta^2)}{\epsilon_\infty k^2 (k^2 + \beta^2)} \qquad (3.1.34)$$

We know the hole wavefunction $\phi(\vec{r})$ has the form

$$\phi(\vec{r}) = f(r)|L=0, J=\tfrac{3}{2}, F=\tfrac{3}{2}, F_z\rangle + g(r)|L=2, J=\tfrac{3}{2}, F=\tfrac{3}{2}, F_z\rangle \qquad (3.1.35)$$

Let us use the abbreviated notation $|1\rangle$, $|2\rangle$ to denote the angular kets,

$$\phi_1(\vec{r}) = f_1(r)|1\rangle + g_1(r)|2\rangle$$

$$\phi_2(\vec{r}) = f_2(r)|1'\rangle + g_2(r)|2'\rangle \qquad (3.1.36)$$

The Fourier transform of the probability density of one hole is

$$\rho_{1k}(\vec{k}) = \int (f_1^2(r)\langle 1|1\rangle + g_1^2(r)\langle 2|2\rangle + f_1 g_1 \langle 1|2\rangle + g_1 f_1 \langle 2|1\rangle) e^{-i\vec{k}\cdot\vec{r}} d^3r$$

($\langle 1|2\rangle$ here does not imply integration) (3.1.37)

We will simply do the transform for f part only. The g part has a complicated angular part, and would be more complicated when integrated with the Coulomb operator. It is easier for the f part to be Fourier transformed because its angular integration part $\langle 1|1\rangle = \frac{1}{4\pi}$ is a constant, and f(r) is expanded in Gaussian basis functions. It can be easily verified that the Fourier transform of a Gaussian function remains a Gaussian function. The final result of the screened V_{hh} due to the f part of ϕ_1 and ϕ_2 is found to be

$$\sum_i \sum_j \sum_k \sum_l a_i a_j a_k a_l \left(\frac{1}{4\pi}\right)^2 \int c e^{-(d_i + d_j + d_k + d_l)k^2} w_k(|\vec{k}|) d^3k \qquad (3.1.37)$$

where a_i's are expansion coefficients of ϕ_1; a_k, a_l are coefficients of ϕ_2; and c is a constant.

The screening for the rest terms of f, g or g, g interaction are not considered for mathematical and programming simplicity. These terms simply preserve their unscreened form:

$$R^{(0)}(f_1, g_2; f_1, g_2) + R^{(0)}(f_1, f_2; g_1, f_2) + \frac{4}{25} R^{(2)}(f_1, f_2; g_1, g_2) \tag{3.1.38}$$

Therefore the only screened term we have included is the f, f interaction. This is none-the-less a good approximation. As we will see from our computer result, g amplitude is much smaller than the f amplitude, and $R^{(0)}(f_1, f_2, f_1, f_2)$ is the dominant term (usually of 2 orders larger than the other terms) in the unscreened Coulomb integral. We have seen that in the GaAs double acceptor, the screening of f, f interaction increases by about 10% from the bare Coulomb potential.

3.1.6 numerical methods and results

With the radial Hartree-Fock equation obtained in eq.(3.1.28), we can go through a similar formulation as for the simple acceptor. First, a pair of known envelope functions f', g' must be assumed. We expand all known and unknown f, g's in the Gaussian-type basis functions. The Hartree-Fock equation can be converted into matrix equations:

$$(\underline{\underline{A}}_0 + \underline{\underline{A}}_{int})\,\underline{c} = E^{HF}\,\underline{c} \tag{3.1.39}$$

where $\underline{\underline{A}}_0$ is a simple acceptor spherical matrix as given in eq.(2.3.19) $\underline{c}$ is the column matrix of the unknown expansion coefficients of f, g. $\underline{\underline{A}}_{int}$ is the extra matrix due to the Coulomb interaction, and

$$\underline{\underline{A}}_{int} = \begin{bmatrix} \langle \gamma_i | H_{int,11} | \gamma_j \rangle & \langle \gamma_i | H_{int,12} | \beta_j \rangle \\ i,j = 1,2,\cdots,2l & \\ 0 & \langle \beta_i | H_{int,22} | \beta_j \rangle \end{bmatrix} \tag{3.1.40}$$

The matrix elements have been found to be:

$$\langle \gamma_i | H_{int,11} | \gamma_j \rangle = \sum_{k=1}^{2l} \sum_{\ell=1}^{2l} \left\{ a'_k a'_\ell \frac{\sqrt{\pi}}{4} \frac{1}{\alpha_T^{5/2}} \left(\frac{1}{\alpha_{ij}} + \frac{1}{\alpha_{k\ell}} \right) + b'_k b'_\ell \left[\frac{3\sqrt{\pi}}{8} \frac{1}{\alpha_T^{5/2}} \left(\frac{1}{\alpha_{ij}} + \frac{1}{\alpha_{k\ell}} \right) + \frac{\sqrt{\pi}}{4} \frac{1}{\alpha_{k\ell}^2 \alpha_T^{1/2}} \right] \right\}$$

$$\langle \gamma_i | H_{int,12} | \beta_j \rangle = \sum_{k=1}^{2l} \sum_{\ell=1}^{2l} a'_k b'_\ell \frac{8\sqrt{\pi}}{25} \left[-\frac{3}{16} \frac{1}{\alpha_T^{5/2}} \left(\frac{1}{\alpha_{ij}} + \frac{1}{\alpha_{k\ell}} \right) - \frac{1}{4} \frac{1}{\alpha_T^{3/2}} \left(\frac{1}{\alpha_{ij}^2} + \frac{1}{\alpha_{k\ell}^2} \right) - \frac{1}{2\alpha_T^{1/2}} \left(\frac{1}{\alpha_{ij}^3} + \frac{1}{\alpha_{k\ell}^3} \right) + \frac{1}{2\alpha_{k\ell}^3 \alpha_{ij}^{1/2}} + \frac{1}{2\alpha_{ij}^3 \alpha_{k\ell}^{1/2}} \right]$$

$$\langle \beta_i | H_{int,22} | \beta_j \rangle = \sum_{k=1}^{2l} \sum_{\ell=1}^{2l} a'_k a'_\ell \sqrt{\pi} \left[\frac{3}{8} \frac{1}{\alpha_T^{5/2}} \left(\frac{1}{\alpha_{ij}} + \frac{1}{\alpha_{k\ell}} \right) + \frac{1}{4\alpha_{ij}^2 \alpha_T^{1/2}} \right] \tag{3.1.41}$$

where a'_k, a'_ℓ, b'_k, b'_ℓ are the expansion coefficients of the known radial envelope functions f' and g'. $\alpha_{ij} = \alpha_i + \alpha_j$, $\alpha_{k\ell} = \alpha_k + \alpha_\ell$, $\alpha_T = \alpha_i + \alpha_j + \alpha_k + \alpha_\ell$.

To include the valence electron screening due to the f, f interaction, the matrix block of $\langle \gamma_i | H_{int,11} | \gamma_j \rangle$ is replaced by

$$\sum_{k=1}^{2l} \sum_{\ell=1}^{2l} a'_k a'_\ell \left(C_1 - C_2 e^t \operatorname{erfc}(t) \right) \times 0.25 \epsilon_\infty \left(\frac{1}{\alpha_{ij} \alpha_{k\ell}} \right)^{3/2}$$

where $t = \beta \cdot \frac{1}{2} \left(\frac{1}{\alpha_{ij}} + \frac{1}{\alpha_{k\ell}} \right)^{\frac{1}{2}}$, $C_1 = \frac{1}{2}\sqrt{\frac{\pi}{t}}$,

and $C_2 = \frac{1}{2} \beta \pi / \epsilon_\infty$ (3.1.42)

In the iteration process, we use the known coefficients a_i', b_i''s of f', g' of one hole, and generate f, g of the unknown hole. At ground state, both holes have symmetry of Γ_8, and have identical radial parts. We iterate until f=f' and g=g', we know this is the self-consistent solution. An antisymmetric product of these two individual hole orbitals gives the double acceptor wavefunction. The binding energy E_B of the $(A^{-2}; h^+, h^+)$ system can be found by comparing the total double acceptor Hamiltonian and the one particle Hartree-Fock Hamiltonian, the relation is

$$E_B = 2E^{HF} - V_{hh} \qquad (3.1.43)$$

where V_{hh} is the hole-hole screened Coulomb interaction as defined earlier.

In experiments, what can be observed are the 1st ionization energy $\Delta E_1 = E_{(A^{-2};h^+)} - E_{(A^-;h^+,h^+)}$ and the 2nd ionization energy $\Delta E_2 = |E_{(A^{-2};h^+)}|$

For the simple acceptor (A^-, h^+), we have calculated the envelope functions at several x values, and the binding energies vs. x are:

x	0.2	0.4	0.6	0.8	1.0
$E_{(A^-,h^+)}$ (in meV)	9.7	14	20	27	33

Comparing the magnitude of the binding energies with Hunter and McGill's[16] photoluminescence data, we suggest the levels they observed were the simple acceptor levels from Au impurity.

For the double acceptor, we calculated $(A^{-3}; h^{+})$ and $(A^{-2}; h^{+}, h^{+})$ at x= 0.25, 0.48, 1.0. The ΔE_1, ΔE_2 are (Fig. 3.4) plotted to compare with the variation of bandgap E_g. It is seen that ΔE_1 and ΔE_2 are much smaller than E_g for $x \gtrsim 0.20$. These levels are indeed shallow levels. We also obtain the f, g envelope function plots, for example, f,g for x=0.25 are shown in Fig.3.5. It is seen from this plot that the amplitude of g is much smaller than that of f, indicating that this is a f-dominating (or S-like) state. The average radius can also be calculated for $(A^{-3}; h^{+})$ and $(A^{-2}; h^{+}, h^{+})$ by using the formula:

$$\langle r \rangle = \int_0^\infty r\,(f^2(r) + g^2(r)) \cdot r^2\,dr \qquad (3.1.44)$$

the results for $(A^{-}; h^{+})$ are 58Å, 46Å and 33Å at x= 0.4, 0.6 and 0.8. Average radius of $(A^{-3}; h^{+})$ are 79Å, 18Å and 10Å at x= 0.25, 0.48 and 1.0. The $\langle r \rangle$'s of $(A^{-2}; h^{+}, h^{+})$ are larger than the corresponding $(A^{-2}; h^{+})$ states. All these $\langle r \rangle$'s are several times larger than the central cell radius of just a few Angstroms. Thus, help to confirm the validity of using the point charge approximation as the defect potential.

The same Hartree-Fock scheme can also be extended to the Z_A=-3 and Z_A=-4 cases for qualitative purposes. These are strong defect centers, the defect states are expected to be localized, and the point charge approximation is no longer appropriate. However, the GEMT still works as an effective method for qualitative results. The modifications we need to make from the double acceptor SC-GEMT scheme

are: 1. The defect charge center should be replaced by -3 and -4. 2. At the ground state, the Hartree-Fock operator is replaced by:

$$H^{HF}(\vec{r}) = H_{spin}(\vec{r}) - (n-1)\int \phi^*(\vec{r}') \frac{2}{|\vec{r}-\vec{r}'|} \phi(\vec{r}')\, d^3r' \qquad (3.1.45)$$

where n (≤ 4) is the number of holes in the system (The Γ_8 symmetry can hold up to 4 holes with different F_z). 3. The equation for binding energy is

$$E_{is} = nE_a^{HF} - \frac{n(n-1)}{2} V_{ab} \qquad (3.1.46)$$

For our interest, we calculated the Z_A=-3 case (which has not yet been related to some kind of defect or defect complex), the levels are deeper and the wavefunctions are more localized than the Z_A=-2 case. The result for ionization energies is

x	ΔE_1 (meV)	ΔE_2 (meV)	ΔE_3 (meV)
0.25	43	72	110
0.48	287	523	878
1.0	489	990	1717

We also did a qualitative study on Z_A=-4 at x=1.0, this can be associated with the Cd_{Te} antisite in CdTe, the result based on point charge approximation (which is crude for this case) is $E_{(A^{-4};4h^+)} - E_{(A^{-4};3h^+)}$ = 2.4 eV, which lies within the conduction bands. This result can be

interpreted as that this level is either a deep level or is a resonant state (lying in the conduction band). This interpretation is in agreement with Swarts, Daw and McGill's[25] Green's function tight binding calculation.

3.2 DOUBLE ACCEPTOR IN GALLIUM ARSENIDE

GaAs is a semiconductor material of great interest because of its high mobility, Gunn Effect and usefulness for making high speed microwave devices and light emitting diodes.

Some intrinsic defect levels have been observed by photoluminescence, Hall measurement and DLTS, ... For example, a main electron trap level located at about 0.75 meV below the conduction band edge is suspected to be coming from the As anion antisite (this level is commonly referred to as the EL level) . This is a deep level double donor problem. In this section, we will discuss another type of intrinsic defect: Ga_{As} cationic antisite, which is a shallow level double acceptor problem.

Yu et al[28,29] identified an acceptor level located at 77 meV from the valence band edge in their liquid encapsulated Czochralski (LEC) grown GaAs sample with photoluminescence experiment. This level has been seen by other authors with different experimental techniques. A sketch of Yu's PL data is shown in Fig. 3.6. This level was present in both p-type conducting and n-type semi-insulating crystals grown on the Ga-rich melts. The main background impurities are C and B. The impurity level of C_{As} is a simple acceptor, is located at

1.493 eV, and is considerably different from the 77 meV (1.441 eV form the conduction band edge) level. On the other hand, the B impurity can also be a double acceptor by sitting at an As site. However, local mode spectroscopy shows that the Boron atom is mostly substitutional in Ga sites and B_{As} does not occur in p-type material. The PL spectrum also shows an emission at 1.284 eV with a very small intensity compared to 1.441 eV level. This 1.284 eV level (230 meV from the valence band edge) corresponds to the 2nd ionization energy of the double acceptor, which is consistent with the value determined by Hall measurement.

Theoretical calculations by Louis and Verges[31] shows that possible bound states of cationic antisites in GaAs are A_1 and T_2 states. The T_2 state has three fold orbital degereracy and two fold spin degeneracy. The neutral state Ga^{o}_{As} is the T_2 state occupied by four electrons. Three possible states: neutral, singly charged and doubly charged states (Ga^{+}_{As}, Ga^{-}_{As} and $Ga^{=}_{As}$) can exist for Ga_{As} antisites. The method they use is the tight-binding calculation based on the cluster Bethe-lattice with some fitting parameters. The same method was used in the study of vacancies in Si surface[67,68].

Our approach to this problem is the Hartree-Fock self-consistent GEMT we use in Section 3.1. When a Ga atom (atomic number 31) occupies an As (atomic number 33) site, this isocoric impurity has a charge deficiency of 2e, and becomes an A^{-2} acceptor center. The binding energies of two cases: 1. neutral Ga^{o}_{As} case 2. singly ionized Ga^{-}_{As} (A^{-2}; h^{+}), are calculated with the established scheme. As usual,

the perturbing (defect) potential is a valence electron screened -2e point charge:

$$U(r) = -2 \cdot \frac{2}{\epsilon r} \qquad (3.1.47)$$

The parameters we use in this calculation are μ= 0.767, ϵ_0=12.56, and β=0.93 a.u..

The binding energy of the one hole (A^{-2}; h^+) system is -290 meV according calculation. Thus, 290 meV is our theoretical value of the 2nd ionization energy. Compared to Yu's data, the deviation is 26%. The 2 hole system (A^{-2}; h^+, h^+) with screened hole-hole Coulomb interaction is found to have the theoretical binding energy of -415 meV, thus we deduce the first ionization to be 125 meV ($|\bar{E}_{(A^{-2};h^+)} - \bar{E}_{(A^-;h^+,h^+)}|$). Compared to Yu's experimental result of 77 meV, the deviation is 62%.

The over-estimate of our theoretical result comes mostly from the over-estimate of the perturbing potential in the central cell region by the point charge model. There are two practical ways to look into this discrepancy. The first way looks at this discrepancy through an empirical interpretation. The overestimate of energy with the point charge potential is obtained by taking the difference between the theoretical value and the experimental value, δE = 290 - 230 = 60 meV. With a rather crude assumption, we assume that in the 2 hole system, The overestimate δE stays the same for each hole (Apparently this is not true, since the average hole orbital radius $\langle r \rangle$ in (A^{-2}; h^+, h^+) is larger than (A^{-2}; h^+). The holes in $Ga^{\bullet}_{As}$ are farther away

from the central cell region, the overestimate in binding energy should be smaller than the single hole case), then the binding energy of $(A^{-2};\ h^{+},\ h^{+})$ is overestimated by $2\delta E$ = 120 meV (this is an upper bound for the overestimate). Therefore we obtain an underestimate for the $E_{(A^{-2};h^{+},h^{+})}$ which is (-415) - (-120) = -295 meV. This implies $\Delta E_{1}'$ = 295-230 = 65 meV, which is a lower bound to the ΔE_{1}, and is within -15% accuracy to the 77 meV experimental value.

The 2nd way to deal with the central call discrepancy is through a semi-empirical adjustment. This method has been suggested by Lipari et al[32] and applied to the Si and Ge spectral. The idea is to add a semi-empirical short range potential $V_{sr}(r)$ to the screened point charge potential. This short range correction potential accounts for the difference in the volume of the ionic core of the impurity atom, as well as for differences in lattice relaxation around it. A phenomenological approach is adopted to assume $V_{sr}(r)$ to be in this form:

$$V_{sr}(r) = 2(\epsilon_{\infty}-1)\frac{1}{r}\left[e^{-\beta r} - e^{-\beta' r}\right] \qquad (3.1.48)$$

where β' is selected to fit the ground state energy of $(A^{-2};\ h^{+})$. We found that β'=1.005 a.u. (slightly different from β=0.93 a.u.) could fit the binding energy $E_{(A^{-2},h^{+})}$ to the experimental value. The defect potential V_{def} and V_{sr} are plotted in Fig. 3.7. It can be seen that V_{sr} (r) is small and is important only in the central cell region. With this V_{sr}, we recalculate the $(A^{-2};\ h^{+},\ h^{+})$ system, and obtain the first ionization energy ΔE_{1} = 105 meV, which is within 30% accuracy with ex-

perimental result. The envelope functions f, g for the one hole and the two hole systems are shown in Fig. 3.8.

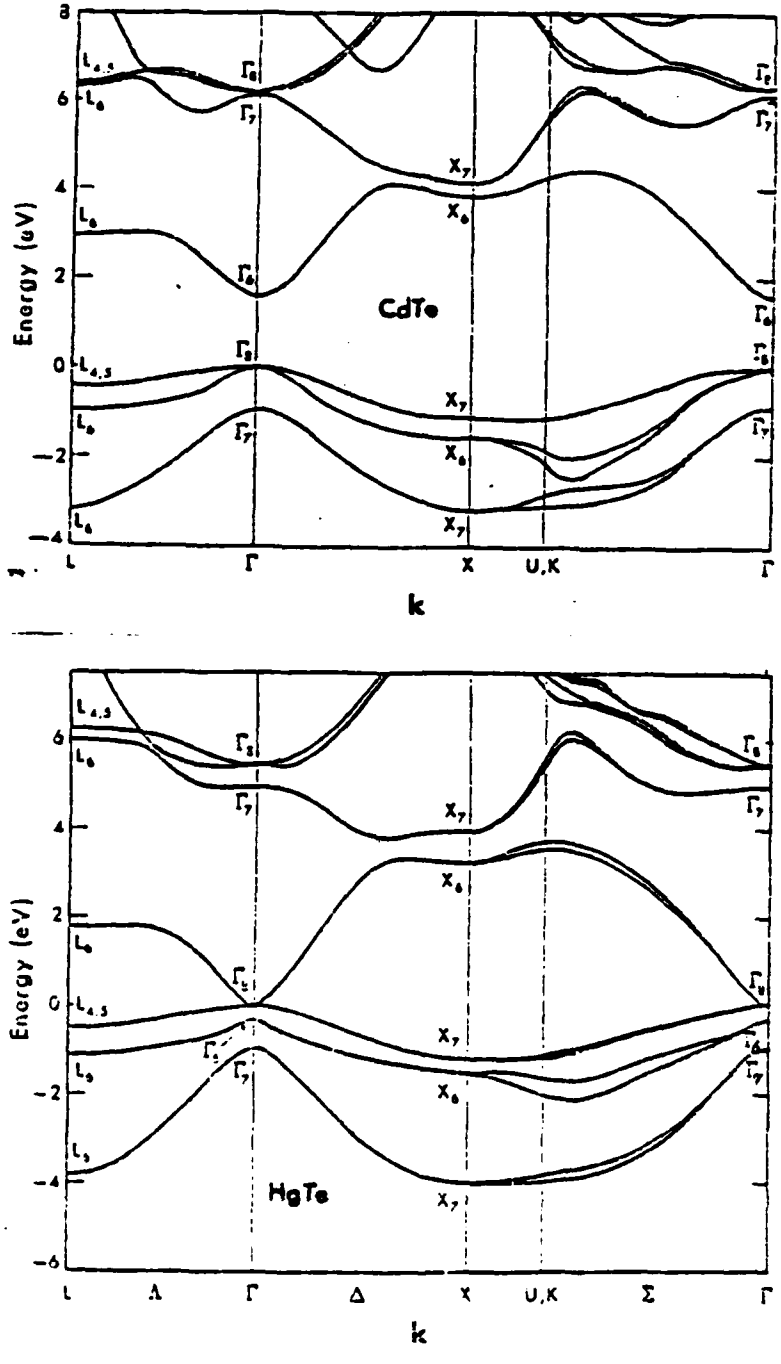

Fig. 3.1. Band structure of CdTe and HgTe

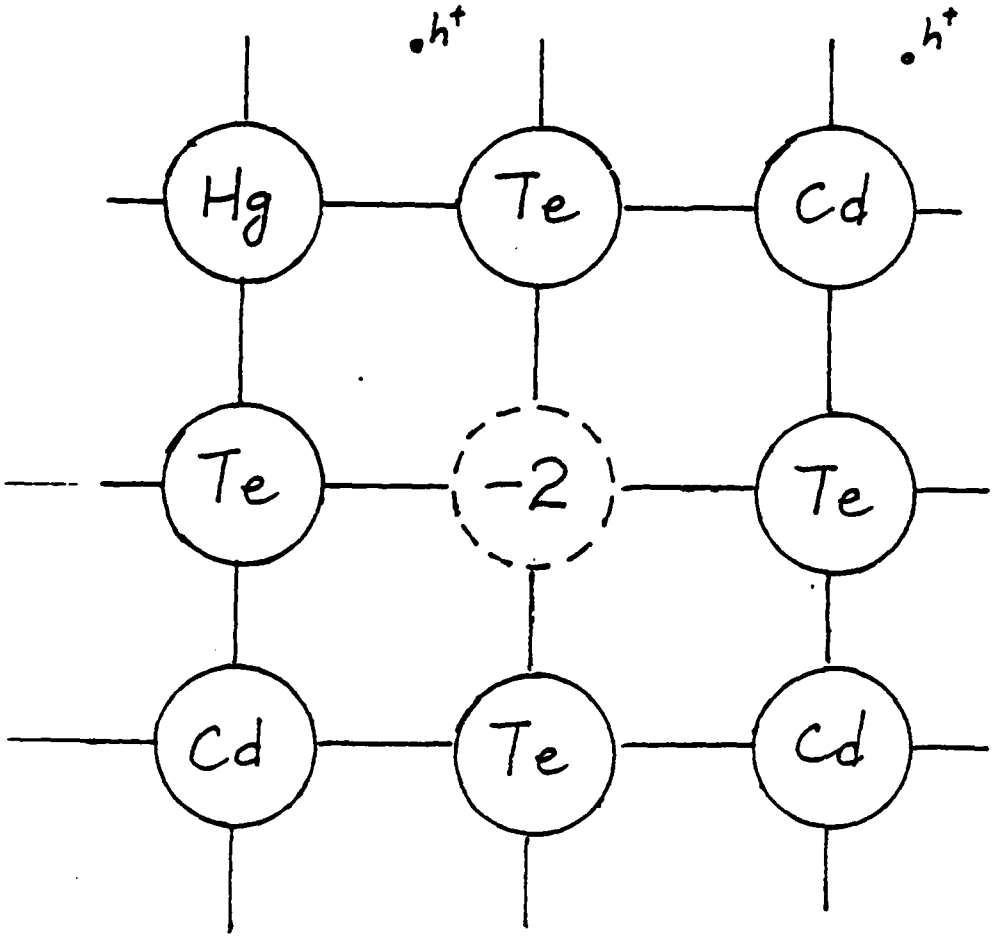

$$H = H_{\substack{\text{perfect} \\ \text{crystal}}} + U$$

$$U(r) \simeq Z_A e^2 \int \frac{e^{i\vec{q}\cdot\vec{r}}}{\epsilon(q) q^2} d^3q$$

Fig. 3.2. A cationic vacancy in HgCdTe

X	Eg (meV)	μ	ϵ_0	R (meV)	a^* (Å)
0.18	32	0.989	17.6	0.220	1861
0.20	70	0.976	17.4	0.479	865
0.25	164	0.95	16.7	1.25	357
0.30	258	0.923	16.2	1.875	238
✓0.32	296	0.913	16.1	2.423	197
✓0.40	448	0.877	15.3	3.34	141
✓0.48	600	0.845	14.2	4.88	103
0.50	638	0.835	14.1	5.19	98.5
✓0.60	830	0.804	13.2	7.12	76.5
0.70	1023	0.775	12.3	9.42	61.9
✓0.80	1217	0.748	11.8	11.6	52.9
0.90	1412	0.725	11.0	14.4	45.4
✓1.00	1608	0.704	10.8	16.2	41.3

Table 3.1. Parameters of $Hg_{1-x}Cd_xTe$

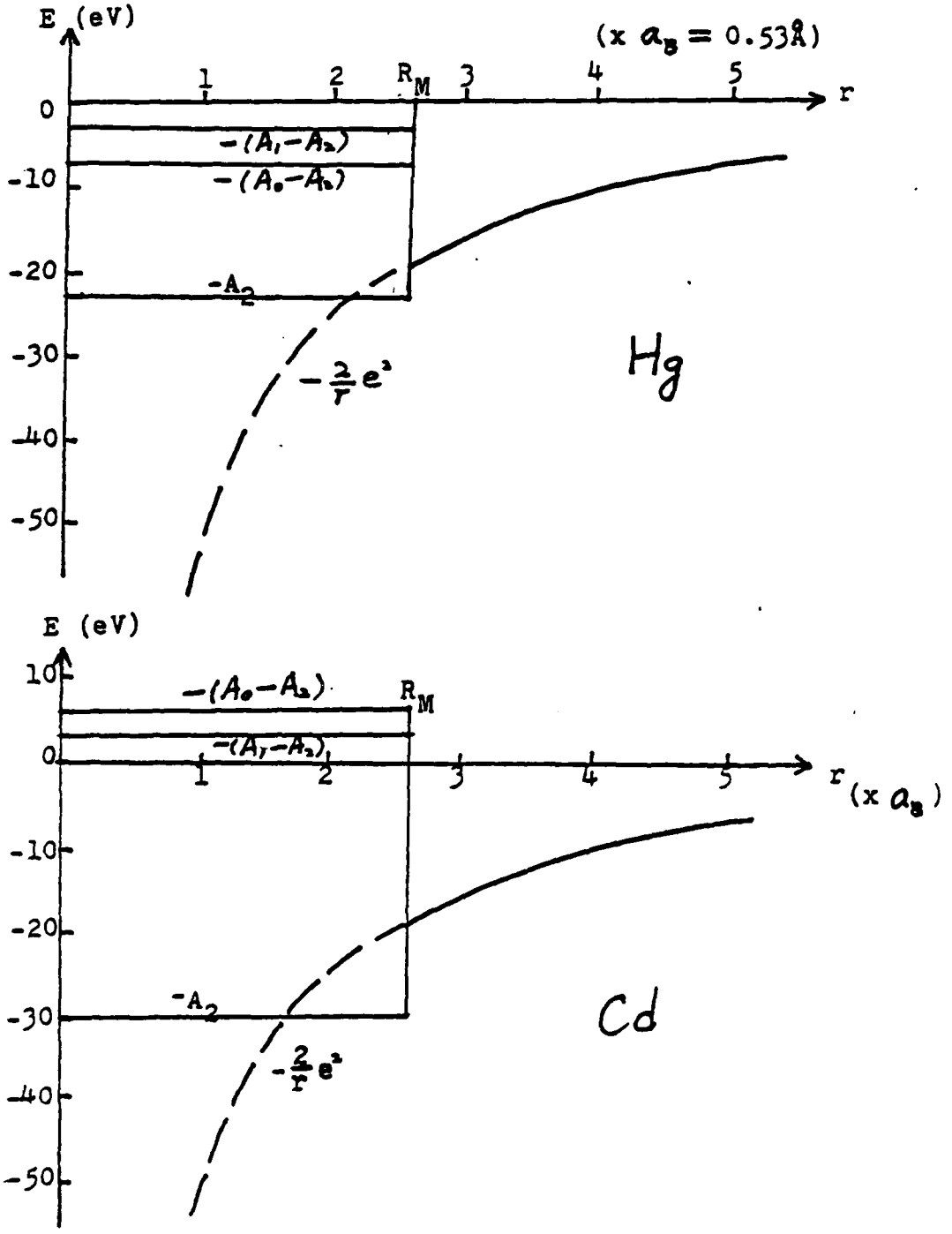

Fig. 3.3. Model potentials of Hg and Cd

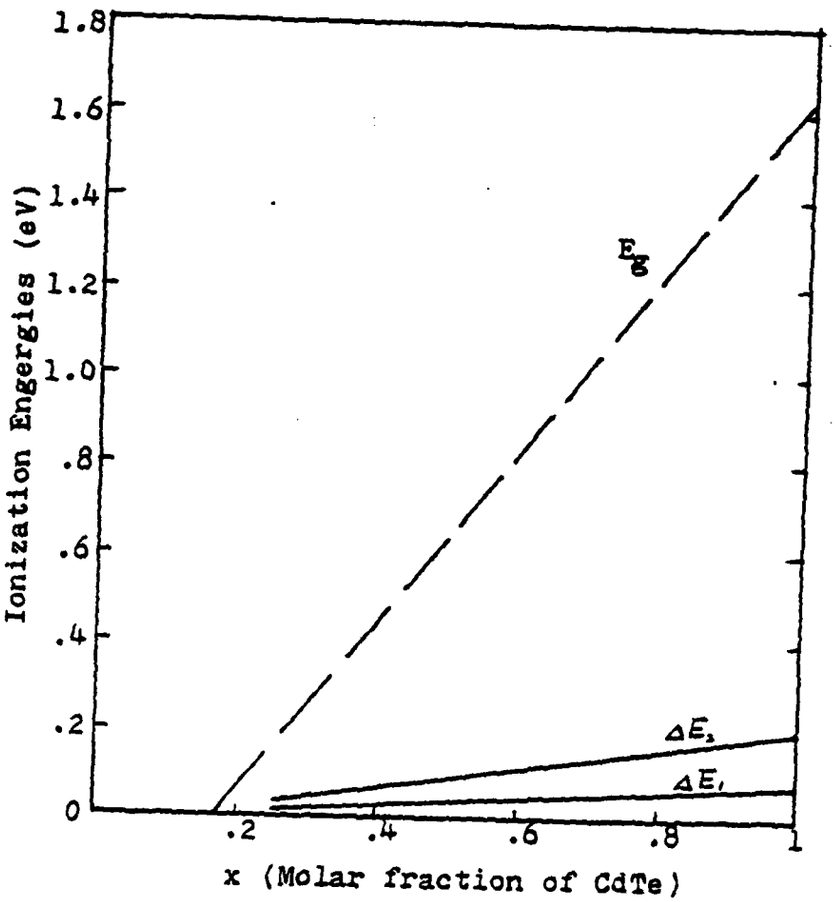

Fig. 3.4. Ionization energies of the double acceptor in $Hg_{1-x}Cd_xTe$.

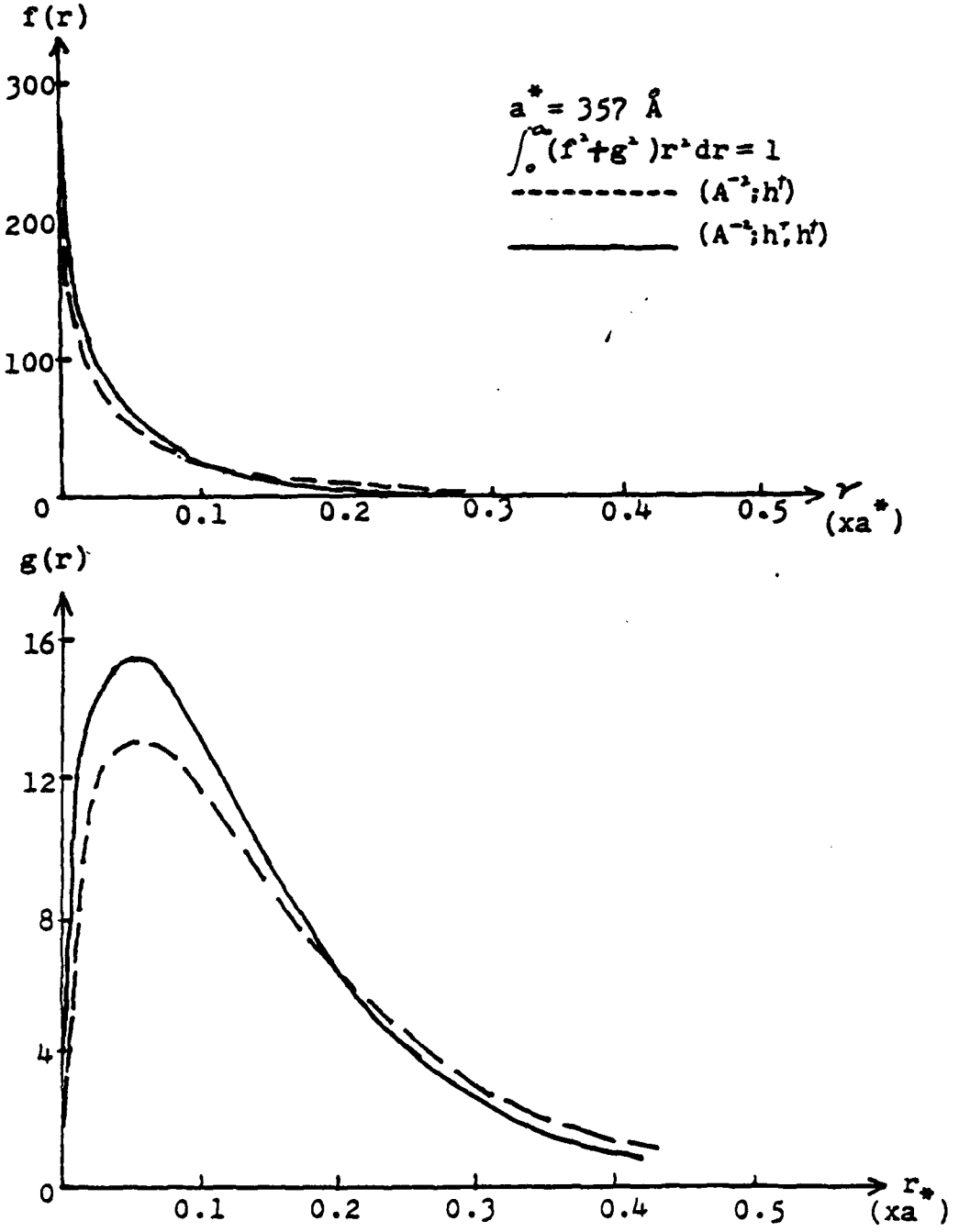

Fig. 3.5. Envelope functions of $(A^{-2};h^2,h^1)$ and $(A^{-2};h^1)$ in $Hg_{0.75}Cd_{0.25}Te$.

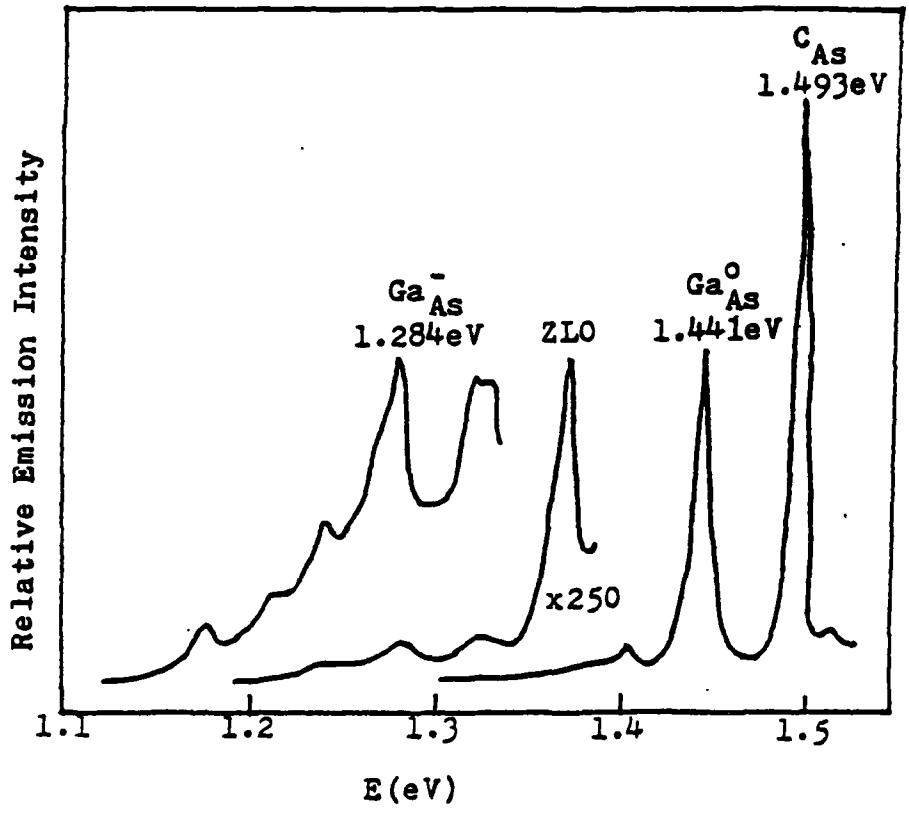

Fig. 3.6. Photoluminescence characteristics of a p-type GaAs sample.

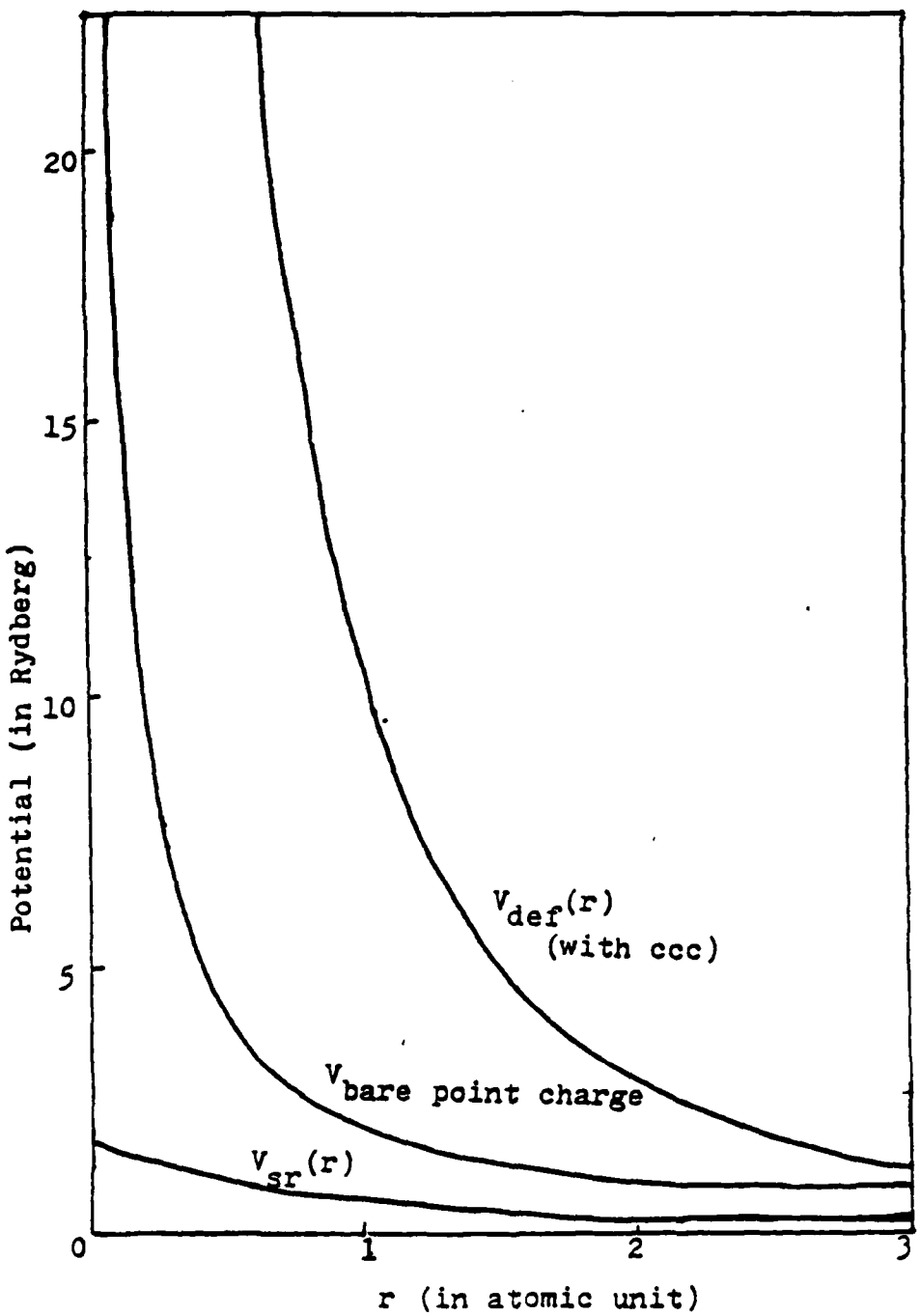

Fig. 3.7. The defect potential and the short range correction $V_{sr}(r)$.

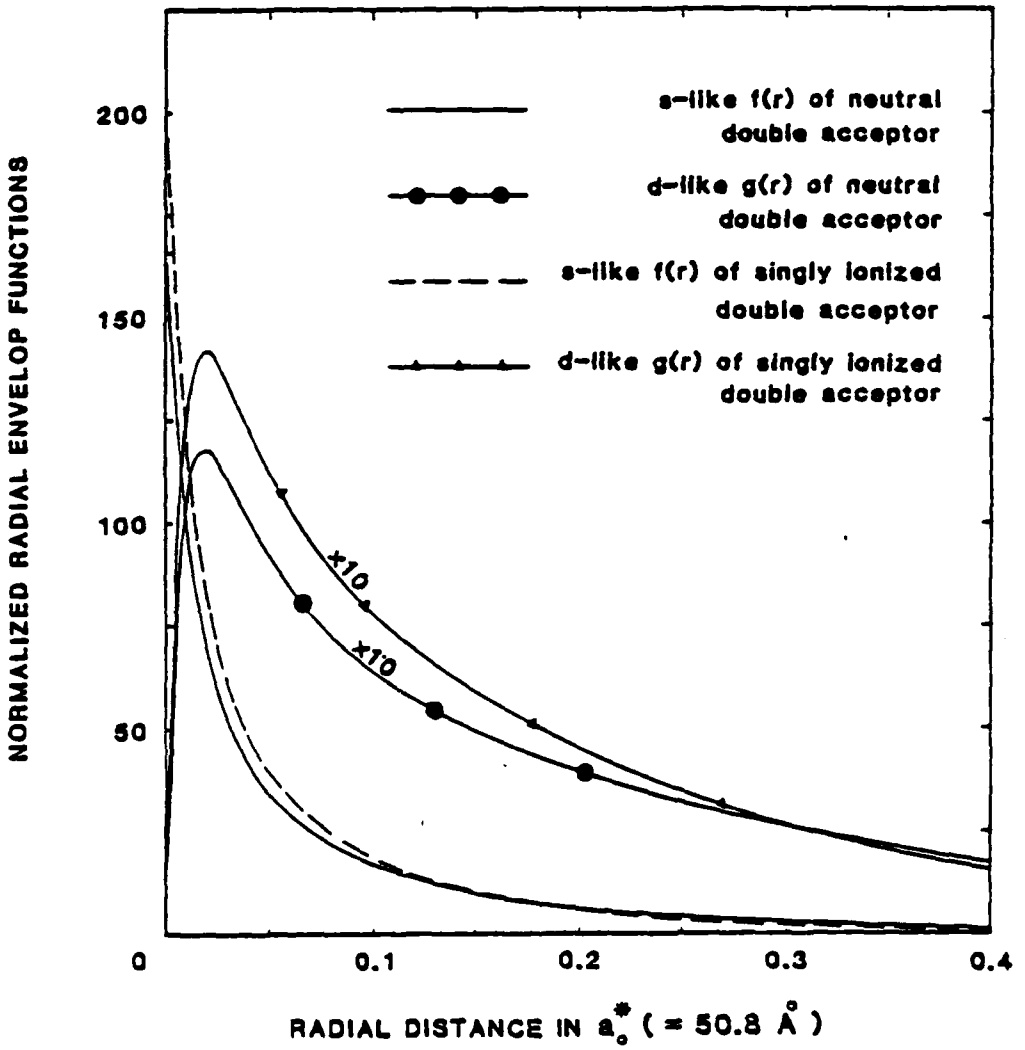

Fig.3.8. Envelope functions of Ga^{o}_{As} and Ga^{-}_{As}.

Chapter IV

SELF-CONSISTENT GEMT OF ACCEPTOR BOUND EXCITONS

4.1 INTRODUCTION

Since the first observations by Haynes[52], the radiative transitions due to the recombination of an exciton bound to a neutral impurity have become more and more important for the understanding of the low temperature emission spectra in a wide range of semiconductors. The double acceptor iteration method can be further extended to solve the acceptor bound exciton (A^0, X) problem. A neutral acceptor bound exciton is a system composed of a neutral acceptor $A^0 = (A^-, h^+)$ binding a free exciton $X=(e^-, h^+)$ (electron-hole pair). (A^0, X) is a 3-body problem with two kinds of moving charged particles.

For years, people have been studying the binding energies of the bound exciton complexes (D^0, X) and (A^0, X), where (D^0, X) is the neutral donor bound exciton. Plenty of accurate experimental results from photo-luminescence and other methods are available. It remains a theoretical problem to interpret the experimental results.

Most of the theoretical work has been done with a model Hamiltonian with a simple spherical valence band and conduction band. The Hamitonian commonly applied to (A^0, X) is[34,35,36]

$$H = -\nabla_1^2 - \nabla_2^2 - \sigma^{-1}\nabla_e^2 - 2\left(\frac{1}{r_1} + \frac{1}{r_2} - \frac{1}{r_e}\right) + 2\left(\frac{1}{r_{12}} - \frac{1}{r_{1e}} - \frac{1}{r_{2e}}\right) \qquad (4.1.1)$$

APPENDIX B

Chapter III

BANDGAP BOWING

3.1 PERTURBATION THEORY

The effect of alloy fluctuation potential on the compositional dependence of energy bandgap is discussed in two alloys, (Al,Ga)As and(Hg,Cd)Te, in order to examine our model of V_f. The former is an important material for semiconductor light source and the latter is the most widely used material for far-infrared detector. The investigation is carried out through a second-order perturbative calculation beyond the VCA. Perturbation theory is an important approximation method in quantum mechanics.[62,63] It was first used in an extensive calculation for bandgap bowing in reference 33, although it had been discussed much earlier in reference 15. In spite of the degenerate nature of every band structure, the time-independent nondegenerate perturbation scheme was used in practical calculations without any explanation. We shall also apply the nondegenerate perturbation equation to obtain second-order corrections to the VCA bandgap but we will discuss the effect of degenerate states.

Up to second-order the alloy energy level is in the form

$$E_n(\bar{k}x) = E_n^{(0)}(\bar{k}x) + E_n^{(2)}(\bar{k}x), \qquad (3.1a)$$

$$E_n^{(2)}(\bar{k}x) = x(1-x)N \cdot \qquad (3.1b)$$

$$\sum_{n',\bar{k}'} \frac{|\langle n\bar{k}x|dV_C|n'\bar{k}'x\rangle|^2 + \frac{1}{4}|\langle n\bar{k}x|dV_A|n'\bar{k}'x\rangle|^2}{E_n^{(0)}(\bar{k}x) - E_{n'}^{(0)}(\bar{k}'x)},$$

where the first order correction due to V_f is zero. $E_n^{(0)}(\bar{k}x)$ and $|n\bar{k}x)$ are the VCA band structure and Bloch states obtained from the EP band calculations without spin-orbit interaction. The Bloch state $|n\bar{k}x)$ is normalized to unity over the volume of whole cryatal. N is the number of unit cells in the cryatal The dV_C and dV_A are defined cation and anion disorder potentials.

Figure 3-1 shows the calculated EP band structure of AlAs along symmetry directions (100) and (111). During the calculation each Bloch function is expanded by 65 plane waves, so the energy bands and expansion coefficents are the eigenvalues and eigenfunctions of the 65 by 65 complex Hermitian matrix. The numerical number assigned to each band is to specify the band index n in equation 3.1. Higher conduction bands not shown in the figure have successive number up to 65 and only the lowest 15 bands will be used in folling calculations. Because we are onterested only in the lowest direct bandgap, the conduction band minimum and valence band maximum are referred to the states |50) and |40) at k=0. And their second-order shifts due to V_f are to be found by using equation 3.1. It is evident from Figure 3-1 that the energy denominator in the equation will be zero for certain degenerate k points in the Brillouin zone. If degen-

erate perturbation scheme is to be used, all degenerate states of the unperturbed system have to be known exactly. It is not possible in practical calculations because all the k points of degenerate states can not be known. However even with the nondegenerate scheme mathematical singularities may not appear in the calculation that will be explained in the following.

For states near |40) and |50) the discrete summation over k states can be transformed into an integration

$$\sum_{\bar{k}'} = \frac{N \int d^3k'}{4\left(\frac{2\pi}{a}\right)^3} = \frac{N\Omega}{(2\pi)^3} \int d^3k' \ , \qquad (3.2)$$

where a is the lattice constant and Ω is the volume of a unit cell. The energy levels near k=0 are expanded as polynomials in k according to the k.p theory.[66]

$$E_n(\bar{k}) = E_n(0) + \frac{\hbar^2 k^2}{2m} + \frac{\hbar^2}{m^2} \sum_{n'} \frac{|\bar{k} \cdot \bar{P}_{nn'}|^2}{E_n(0) - E_{n'}(0)}$$

$$\doteq E_n(0) + \frac{\hbar^2 k^2}{2m^*} \ , \qquad (3.3)$$

$$\bar{P}_{nn'} = \int u^*_{no}(\bar{r})\, \bar{p}\, u_{n'o}(\bar{r})\, d^3r \ , \qquad (3.4)$$

where m is the mass of a free electron, m^* is the band edge effective mass, $\hbar$ is the Planck constant devided by 2π, $\bar{p}$ is the momentum operator, and u(r) is the periodic part of band edge Bloch states.

The second-order energy correction due to states near k=0 is then

$$\Delta E_n^{(2)} = \sum_{\bar{k}'} \frac{|\langle n0|dV|n\bar{k}'\rangle|^2}{E_n^{(0)}(0) - E_n^{(0)}(\bar{k}')}$$

$$\doteq -\frac{N\Omega}{(2\pi)^3} \int |\langle n0|dV|n\bar{k}'\rangle|^2 \frac{2m^*}{\hbar^2} \sin\theta \, dk' \, d\theta \, d\phi \,, \qquad (3.5)$$

where $|n0)$ is the state at k=0 and $|n\bar{k}')$ is a state near k=0. If the quantity $|(n0|dV|n\bar{k}')|^2$ is a slowly varying function near k=0, the result of equation 3.5 can be further approximated as

$$\Delta E_n^{(2)} \doteq -\frac{2N\Omega m^*}{(2\pi)^3 \hbar^2} (4\pi)(\Delta k')|\langle n0|dV|n\bar{k}'\rangle|^2 . \qquad (3.6)$$

$N \to \infty$, $\Delta k' \to 0$

It is obvious that the second-order correction is finite for states near k=0 instead of being divergent. The assumption of nearly canstant matrix elements is checked allright in AlAs.

Similar procedure can be taken for degenerate states within the conduction bands.

$$E_n(\bar{k}) = E_n(\bar{k}_0) + \frac{\hbar}{m}(\bar{k}-\bar{k}_0)\cdot\bar{P}_{nn'} + \frac{\hbar^2}{2m}(\bar{k}^2-\bar{k}_0^2)$$

$$+ \frac{\hbar^2}{m^2}\sum_{n'} \frac{|(\bar{k}-\bar{k}_0)\cdot\bar{P}_{nn'}|^2}{E_n(\bar{k}_0) - E_{n'}(\bar{k}_0)}$$

$$\doteqdot E_n(\bar{k}_0) + \frac{\hbar}{m}(\bar{k}-\bar{k}_0)\cdot\bar{P}_{nn'} \qquad (3.7)$$

The summation over k states is again transformed into an integration over a small sphere centered at the degenerate k state. The matrix elements of dV are assumed to be slowly varying in the integration volume.

$$\sum_{\bar{k}'} \frac{|\langle n\bar{k}|dV|n'\bar{k}'\rangle|^2}{E_n^{(0)}(\bar{k}) - E_{n'}^{(0)}(\bar{k}')} \doteqdot -\frac{N\Omega\hbar}{(2\pi)^3 m}|\langle n\bar{k}|dV|n'\bar{k}'\rangle|^2$$

$$\cdot \int \frac{k''^2\, dk''\, d(\cos\theta)\, d\phi}{P_{nn'}\, k''\cos\theta}$$

$$\doteqdot -\frac{N\Omega\hbar}{(2\pi)^3 m}|\langle n\bar{k}|dV|n'\bar{k}'\rangle|^2 \; \mathcal{P}\left\{\int_0^{k_0'}\int_{-1}^{1} \frac{2\pi\, dx}{P_{nn'}\, x} k''\, dk''\right\}, \qquad (3.8)$$

where k_0' is the radius of the sphere and $\mathcal{P}$ stands for the principle value of the integration.[65] The result of second-order correction is again proved to be finite for degenerate states.

With the assurance that degenerate states do not cause any singularity in numerical method. The summation in equation 3.1 is carried out over the lowest 15 bands at 88 points in the irreducible (1/48) part of the Brillouin zone (BZ). The BZ of a face-center-cubic lattice is shown in Figure 3-2. Due to its symmetry properties, the summation over the whole BZ can be reduced to the smallest repeatable part which is denoted as the shaded region. The summation should in principle evaluated as a function of composition x. Because of the elaborate computations involved, we calculate it in the limits x=0 and x=1 only. In most cases the results of the summation term do not vary drastically between two parent compounds, therefore, a linear interpolation for it at intermediate x values serves as a good approximation.

3.2 (AL,GA)AS ALLOY SYSTEM

(Al,Ga)As is the most intensively studied alloy semiconductor for hetero-structure laser and photodiode. The application of it is based upon the close lattice match between GaAs and AlAs. Recently it is used to construct a hetero-structure type field-effect transistor in which a high mobility two-dimensional electron gas is separated from their parent donors.[66,67] Higher electron mobility is achieved because the scattering from ionized donor impurities is reduced and it is useful for high-speed and high-frequency devices.

There have been several determinations of the compositional dependence of the energy bandgap in (Al,Ga)As. And the largest uncer-

tainty in the assignment of bandgap versus composition is generally the determination of the composition of the sample. The experimental data will be examined more carefully when they are compared with the calculated results. Previous studies on the energy bandgap is reviewed here. The first theoretical calculation of bandgap bowing in (Al,Ga)As was carried out in the electronegativity model.[5] The intrinsic bowing in the VCA was zero and the extrinsic bowing -0.03 eV was much less than the experimental bowing -0.2eV. The difference in electronegativity of Al and Ga atoms and a semi-empirical second-order perturbative approach was used for obtaining the extrinsic bowing.

With an EP model for the cation disorder potential, the extrinsic bowing was evaluated by an extensive second-order perturbation calculation over the VCA.[37] A bowing parameter +0.04 eV with a wrong sign with respect to the downward bowing was obtained. It was suggested taht the EP model be not suitable for the bowing in this alloy which will be disproved by us later. The CPA was also applied to calculate the alloy band structure and scattering rates by Chen and Sher.[68] The Tight-Binding (TB) Hamiltonian was expanded by Gaussian-type atomic orbitals and the TB parameters were found by fitting band structure to pseudopotential results. The fluctuation potential was characterized not by the TB parameters but by bonding and antibonding energies of which the physical meaning is not clear. However a bowing parameter of about -0.17 eV was obtained without giving any interpretation.

In order to use equation 3.1, dV_C and dV_A in our model have to be defined first. Properties of published EP form factors are examined before they are applied to set up a suitable model of V_f. Tables 3-1 and 3-2 summarize the atomic local EP form factors fitted in GaAs and AlAs respectively.[37,61,69,70,71] The values of cation and anion disorder potentials are listed in Table 3-3. For the most important form factors at first two reciprocal G vectors, the magnitude of disorders are only 7% and 2% of the cation and anion atomic form factors respectively. They are one evidence of the smallness of the alloy fluctuation potential. However the anion disorder potential is large at high q values which corresponds to a not negligible effect of valence charge transfer mentioned in section 2.3. Supportive information of these different As atomic pseudopotentials can be found in the empirical tight-binding parameters shown in Table 3-4.[72] The site-diagonal parameters of As atom are fitted differently in two parent compounds in order to generate realistic band structures in each parent compound respectively.

Linear interpolation and extrapolation are used to approximate the continuous curves of disorder potentials as functions of wave number q. The procedure follows exactly discussed in section 2.4. The atomic MP parameters of Al and Ga are listed in Table 3-5 for the value of dV(q=0).[38] The radius R_M will be set equal for both atoms such that two Coulombic tails cancel each other exactly. The Fourier transform of the difference of constant potential wells inside R_M is expressed as

$$dV_{ion}(0) = -\frac{8\pi (R_M)^3}{\Omega}\left\{\frac{\Delta A_2}{3}\right. \qquad (3.9)$$

$$+\frac{\Delta(A_0-A_2)}{2}\left[\frac{1}{(k_F R_M)^2}-\frac{\sin(2k_F R_M)}{2(k_F R_M)^3}\right]$$

$$\left.+\frac{3\cdot\Delta(A_1-A_2)}{2}\left[\frac{1}{(k_F R_M)^2}+\frac{\sin(2k_F R_M)}{2(k_F R_M)^3}-\frac{2\sin^2(k_F R_M)}{(k_F R_M)^4}\right]\right\},$$

$$dV(0) = dV_{ion}(0)/\epsilon_0 . \qquad (3.10)$$

The second and third terms in the braces in equation 3.9 are less than 20% of the first term. They exhibit explicitly the nonlical properties of the ionic core in the MP formulations used here. Their small contribution in equation 3.9 makes the nonlocal MP compatible to the local EP model.

Because the perturbation calculations are performed upon parent compounds, the unit volumes and static dielectric constants of them are used for the screened atomic form factor at q=0. The numerical value of -0.002 Rydberg is obtained from equation 3.10. The form factor $dV_C(q=0)$ used in reference 37 for substituing Ga and Al atoms is exactly zero without any explanation. Another set of form factors for (Al,Ga)As can be found in the study of hetero-structures.[73] Their value of $dV_C(q=0)$ was -0.0058 Rydberg. All these choices of form factor at q=0 are comparable but our adaption of the MP is more clear in physical interpretation. Piecewise linear disorder potentials are plotted in Figure 3-3 with respect to q^2. The $dV_C(q)$ used in

reference 37 is linearized and plotted in the same figure. Its effect on bandgap bowing is also calculated in our program in order to make comparison between different models of V_f.

3.3 BANDGAP BOWING IN (AL,GA)AS

As shown in Figure 3-1 the valence band maximum at k=0 is three-fold degenerate without the spin-orbit interaction. State |40) is taken as the unperturbed level for valence band and |50) represents the unperturbed conduction level. The intrinsic bowing obtained in the VCA with our choice of EP form factors is zero. The extrinsic effect of disorder potentials is carried out as described in section 3.1 with the dV(q) curves shown in Figure 3-3. The calculated second-order bandgap shrinkages beyond the VCA in GaAs and AlAs are summarized in Table 3-6 without the x(1-x) factor in equation 3.1. The bowing parameter with a wrong sign in reference 37 is reproduced in our calculation with an approximated dV_C Although our value of +0.004 eV is ten times less than theirs, it is clear that further comparisons between these two model of dV_C are meaningful. The discripancy may come from the differences in Bloch states, disorder potentials, and sampling k points. The calculated bowing parameter in our model is -0.01 eV with only dV_C which is close to the -0.03 eV obtained in reference 5. But with both disorder potentials our calculated bowing parameter is -0.125 eV. The good agreement with exprimental bowing -0.1$\sim$ -0.2 eV proves the significance of the dV_A in a cationically disordered system.

The energy shifts of |40) and |50) states are listed in Table 3-7. Because of the band structure associated with the indirect bandgap of AlAs, detail contributions of each energy band are listed in Table 3-8. According to the perturbation theory, the specified state is pushed upward by all states below it and pushed downward by all states above it. |40) and |50) states are always pushed up by bands 2, 3, and 4 and pushed down by bands higher than 5. |40) has negligible interaction with band 5 under all three cation disorder potentials. The test cation disorder potential has a large form factor at q=0 as shown in Figure 3-4. |50) is pushed downward as a net result from all states within band 5. The calculated bandgap shrinkage in AlAs in twice as large as in GaAs. The same trend was observed in the CPA calculation of (Al,Ga)As[68] and in the perturbation calculation of Ga(P,As).[33] One reason may be related to this is that the energy bandgap of GaAs is about one half of those AlAs and GaP.

The effects of form factor at q=0 on bandgap bowing are summarized in Table 3-9. The very large q=0 value of the test potential does not change the total bowing much because the bowing is mainly controlled by the anion disorder potential. The determination of the high q tail in EP form factor is discussed in section 2.4. Monotonically decreasing tails are chosen for our disorder potentials as shown in Figure 3-3. If the high q tail ia an abrupt one as shown in Figure 3-4, its effect on the bandgap bowing is listed in Tables 3-10 and 3-11. The high q tail has little effect on the test potential but large effect on the anion disorder potential. The choice of a decreasing

tail is reflected in the better agreement of final bowing with experimental value. The overall result of our model shown in Table 3-7 is meaningful with respect to small variations in the dV(q) curves. Its comparison with experimental data is discussed in the following paragraphs.

The scatter in experimental data for the bandgap versus composition in (Al,Ga)As is substantial from earlier investigations[74,75,76,77,78] and an average curve computed from some scattered data has frequently been used for practical purposes.[79] One reason for this spread in data was the use of a variety of experimental methods such as Schottky-barrier photo-current[74], electroreflectance[75], and luminescence[76] in measuring the bandgap. The second reason was the control of composition in sample growth and the evaluation of alloy composition. More recent experimental measurements by means of low temperature photo-luminescence technique showed a consistent trend in bandgap variation.[10,80,81] As listed in Table 1-4 the bandgap varies linearly for $0.5>x>0$ and parabolically for $1.0>x>0.5$.

The determination of alloy composition in reference 80 was achieved by electron microprobe on two independent occasions on every wafer. These two observations were in good agreement, and therefore the uncertainty in x can be reduced to less than 0.02 at any composition. The maximum bowing at room temperature is about 70 meV around $x=0.8$. The maximum bowing in reference 81 is about 160 meV around $x=0.8$. There is a lagre deviation in maximum bowing even two sets

of data have consistent trends of variation. However the alloy composition in reference 81 was determined by Auger sputtering techniques which might introduce higher uncertainty in x. If the measured composition of the samples in reference 81 is shifted by about 0.04, the maximum bowing is reduced from 160 meV to about 100 meV for $0.7>x>0.6$. This value is more close to that in reference 80 and our result.

The theoretical curve of bandgap bowing is plotted in Figure 3-5 together with the experimental one from reference 80. The magnitudes are comparable but the asymmetry trend in experimental curve can not be explained by the present theoretical results. One reason may come from the experimental determination of bandgaps in the indirect bandgap regime from optical measurements. The second reason is that the compositional dependence of bowing has not been calculated explicitly as a function of x. If the summation in equation 3.1 is computed for some intermediate x values, we can be more certain about the theoretical trend in bandgap bowing. The spin-orbit interation is not included in our calculations. We believe its absence does not affect the theoretical curve much and can not explain the asymmetry in experimental curve either.

3.4 (HG,CD)TE ALLOY SYSTEM

The fundamental energy bandgap in (Hg,Cd)Te can vary from 1.6 eV of CdTe to -0.3 eV of HgTe. Figure 3-6 illustrates some schematic band structures of the alloy near zone center. Without spin-orbit interaction the heavy hole band is two fold degenerate and the band numbers are consistent with those in Figure 3-1. Figure 3-6a and 3-6b are of the normal band structure of zinc-blende semiconductors. State |50) is the conduction band minimum and the valence band maximum is three-fold degenerate. The nonparobolic effect is emphasized in Figure 3-6a for very small energy bandgap. Figure 3-6c represents the so-called inverted band structure in which the state |20) has the same symmetry properties as those of state |50) in normal band structure. Because the $E_0(X)$ covers two atmospheric windows around 10 um and 5 um wavelengths for x around 0.2 and 0.3 respectively, (Hg,Cd)Te is a prominant material for infrared detector.

It covers also the wavelength of the maximum of thermal radiation at room temperature and could be useful for measuring temperature gradients in the environment or in medical applications. Several reviews and Conference proceedings have been published on the alloy system in the past few years.[3,82,83,84,85] They emphasized differently on material preparation, chemical and physical preperties, defect study, transport properties, and device applications. As for energy bandgap bowing, the measured compositional dependence of fundamental bandgap have small discripancies in bowing parameter by defferent authors. The scatter of data is however not as bad as in

(Al,Ga)As. The critical x value for semiconductor-semimetal transition is around x=0.17. Reference 11 compiled all the existing data of measured bandgap and fitted them with a third-order polynomial of composition x. It will be used as a standard experimental result to be compared with our theoretical calculations.

Theoretical studies on the electronic structure of (Hg,Cd)Te were first carried out by Korringa-Kohn-Rostoker method[86] and Model Pseudopotential method[87] in 1971. Compositional dependence of bandgap was not discussed in the former and the VCA bowing in the latter was zero. Empirical pseudopotential was used to calculate the band structure and charge densities near k=0 in the VCA and a linear bandgap variation was obtained.[88] Previously published EP form factors of HgTe and CdTe[61,89,90] were considered in reference 88 and on them some modifications were made in order to improve the agreement between the experimental and theoretical reflectivities. So form factors from reference 88 are used in our model to construct the cation and anion disorders. The seven atomic-type potentials in our model is implicitly contained in the VCA in reference 88.

It is shown in Table 3-12 that the constant slope in the VCA bandgap, 1.9 eV, can not be explained by cation disorder alone which makes only 1 eV. This is another justification of our microscopic model of the one-electron alloy potential. Supportive information for different Te pseudopotential obtained in HgTe and CdTe can also be found in literative. In the calculation of band structures of parent compounds by using angular momentum dependent model pseudopoten-

tial, different depths were assumed for the potential well of Te atom which is associated with zero angular momentum l=0.[87] The purpose was to generate more realistic band structures for both HgTe and CdTe. In other band structure calculations by using the empirical tight-binding scheme, different site-diagonal parameters of Te atom has to be used in order to fit the calculated band structures well in both parent compounds.[91,92]

Figure 3-7 shows the linear approximations of cation and anion disorders for (Hg,Cd)Te. The q=0 form factor is obtained again from model pseudopotential as described in section 3.2. By the parameters listed in Table 3-13 the second the third terms in the braces of equation 3.1, which are nonlocal effects, are also less than 20% of the first term as in (Al,Ga)As. The model pseudopotential form factor $dV_C(q=0)$ is well matched with other local empirical pseudopotential form factors. The value of $dV_C(0)$ is about -0.002 Ry and the effect of small variation in it will be discussed later.

3.5 BANDGAP BOWING IN (HG,CD)TE

with the same perturbative procedure, the second-order bandgap shrinakage and energy corrections are summarized in Table 3-14 and 3-15 for x=0, 0.3, and 1.0. A 30% change in $dV_C(0)$ introduces an error in final results less than 1%. The unperturbed states are specified by their band numbers shown in Figure 3-6. Numbers in parentheses include the estimated effect of spin-orbit interaction which will be discussed later. The exclusion of spin-orbit interaction will

not affect the qualitative physics but makes the computation tractable. The factor x(1-x) in equation 3.1 is not included in Tables. The contribution from each group of energy bands to the second-order energy shift in HgTe and CdTe are listed in Table 3-16 and 3-17 respectively. The first thing to be discussed is the convergence test for the number of energy bands used in computation. Within the 15 bands the contribution from the five top most bands to the second-order energy correction is less than 10%. Their effects are less in CdTe than in HgTe because their energy denominators are larger in CdTe. Therefore, 15 bands are good enough for quantitative results and smaller number of energy bands may be used for rough approximations.

In the semi-empirical determination of the extrinsic bowing in reference 5, only the lowest conduction band and the upper three valence bands are considered. This "two-band" model has also been applied to study the compositional dependence of valence-band spin-orbit splitting and conductive-band effective mass in alloy systems.[24,93] Detailed relations between the two-band model and rigorous perturbation theory were investigated by Stroud.[94] The electronegativity difference was related to an effective matrix element in which all the matrix elements in equation 3.1 were assumed to be constant. This approach is analog to the approximation successfully used in calculating the interband absorption of semiconductors. When the matrix elements were taken out of the summation in equation 3.1, the inverse band width parameter 1/A in reference 5 was related to

the Hilbert transformation of density-of-states of conduction band and valence bands. The assumption of constant matrix elements throughout the Brillouin zone was later questioned by Altarelli in reference 93. It was shown that the constant effect could not be applied to different conduction minima which have quite different symmetry properties.

Table 3-18 shows that the "two-band" model (including bands 2, 3, 4, and 5) is very good for bandgap correction in CdTe. The accuracy is less than 1%. One possible reason may come from the cancellation between band 1 and upper conduction bands as shown in table 3-16. The model overestimates the energy correction at x=0.3 for about 8% and it underestimates the correction by 93% in HgTe. The large error in HgTe is due to the inverted band structure and small energy bandgap. In HgTe the |20) state interacts strongly with the lowest valence band. Therefore, the "two-band" model is a good approximation method for the bowing in alloy systems with direct energy bandgap 1 eV or larger.

3.6 COUPLING MATRIX ELEMENTS IN (HG,CD)TE

The effects of cation and anion disorders on the coupling matrix elements in equation 3.1 are discussed in details here in order to show their physical significance and roles in bandgap bowing. Table 3-19 shows the intraband coupling between |50) state and |5k) states in the lowest conduction band. (It is |20) and |2k) in the inverted band of HgTe.) When compared to tight-banding interpretation of

energy bands, |50) and |20) states are of the same symmtry properties of atomic S orbitals. It is noticed that the effect of cation disorder is very distinct from that of anion disorder for conduction states. $|(50|dV_C|5k)|^2$ is nearly constant throughout the Brillonin zone and at least two orders of magnitude larger than $|(50|dV_A|5k)|^2$. The constant matrix elements show that the effect of dV_C is a localized perturbation which can couple states with large difference in k values. This is another evidence that our empirical pseudopotential model is a good representation for cation disorder which is the difference between chemical natures in the core regions of two substituting atoms.

The large difference between the matrix elements of dV_C and dV_A can be explained from the charge distribution of |50) and |5k) states (or |20) and |2k) states). Figure 3-8 shows the charge densities near k=0 for |20) and |50) in HgTe and CdTe respectively. They are obtained from EP wave functions in reference 88 and the projection (110) plane is illustrated in Figure 3-9. The distribution of state |50) is centered around cation and anion atoms which are closely related to atomic S obitals. Figure 3-10 shows the total charge densities obtained from EP calculation for band 5 in ZnSe.[88]

There is no total charge densities calculated for (Hg,Cd)Te system and the charge densities obtained in ZnSe are good approximations. They may not be exactly the same as in HgTe and CdTe but the similarity should be great. The anti-bonding nature of |5k) states has large portion of charge distribution in the area where the covalent

bonding charge is nearly zero. Their interaction with dV_A is negligible because dV_A is derived from the redistribution of valence bonding charges. The larger value of $|(20|dV_C|2k)|^2$ in HgTe comes from the larger charge density of |20) state around Hg atom than that of |50) state around Cd atom as shown in Figure 3-8. This is consistent with the trend in ionicity of parent compounds.

The effects of matrix elements on energy correction are directly shown in Table 3-16 and 3-17. The |50) is always pushed downward by |5k) states or the |20) is pushed upward by |2k) states in HgTe. The interband coupling between |50) With valence bands is large under dV_C and the energy shift depends on the energy denominator in equation 3.1. With the same reason of small intraband coupling, the interband coupling of |50) with valence bands is small under dV_A expect with the lowest valence band |1k) which has strong charge distribution around the anion atom as show in Figure 3-11. Their effects are also clearly shown in Table 3-16 and 3-17. (The interband coupling of |20) state with P-like bands is similar.)

The intra-valence band coupling matrix elements are summarized in Table 3-20. The variation of $|(40|dV_A|4k)|^2$ with respect to k values is slightly larger than that of $|(50|dV_C|5k)|^2$. But both of them are always within the same order of magnitude. The spatial variation of anion disorder is centered around the anion atom but not as localized as the cation disorder. It is consistently with the physical origin because the chemical nature within the atomic core is more localized than the charge redistribution effect. The relative magni-

tude of matrix elements under dV_C and dV_A can be interpreted again by the charge distributions of |40) and |4k) states. Figure 3-12 shows the distributions of |40) state in HgTe and CdTe. The bonding nature of |40) state keeps the charge distribution oriented in between adjacent atoms. The maximum of bonding charges shifts from anion toward catron when x decreased from 1.0 to 0. This variation in charge distribution can be related to the ionicity of the alloy which varies from 0.717 of CdTe to 0.65 of HgTe. The ionicity scale of Phillips and Van Vechten[97] is used because it is in better agreement with pseudopotential calculations[96] than the ionicity scale of Pauling.[98] In CdTe the intraband matrix elements are larger for dV_A than dV_C because valence electrons are around the anion atom more. In x=0.3 and HgTe the effect of dV_C and dV_A are comparable because valence electrons move toward the cation atom for small x values. The effects of matrix elements on the energy correction have to be considered together with the energy denominator in which the band structure and bandgap are dominant factors. The |40) state is always pushed upward but the amount of energy shift varies as a function of composition.

3.7 SPIN-ORBIT INTERACTION

All the results discussed so far are obtained without considering the spin-orbit interaction. The values in the third row of Table 3-14 show a smooth variation over x. Linear interpolation is used to construct a continuous curve of bandgap bowing in which the factor x(1-x) is included. The unmarked solid curve in Figure 3-13 represents the experimental fit at 0^{o}K. The dashed curve is the calculated bowing with both cation and anion disorders but not the spin-orbit interaction. It is observed to be an overestimated one. It will be shown that the spin-Orbit effect does not change the magnitude of couping matrix element although it gives rise to different band structures. Consequently, the second-order energy correction is modified by different energy denominators but not significantly.

From the symmetry considerations, the four-fold degenerate Γ_8^v level with the spin-orbit interaction can be approximated quite accurately by pure spin states and X, Y, and Z functions. The latter are the three-fold degenerate states $|20)$, $|30)$, and $|40)$ at valence band maximum without the spin-orbit effect. According to the symmetry notatrons in reference 99, the expression of Γ_8^v states are

$$U^{8}_{\frac{3}{2}} = \frac{1}{\sqrt{2}}(X + iY)|\alpha\rangle ,$$

$$U^{8}_{\frac{1}{2}} = \frac{1}{\sqrt{6}}[-2Z|\alpha\rangle + (X + iY)|\beta\rangle] ,$$

$$U^{8}_{-\frac{1}{2}} = \frac{1}{\sqrt{6}}[(X - iY)|\alpha\rangle + 2Z|\beta\rangle] ,$$

$$u^{8}_{-\frac{3}{2}} = \frac{1}{\sqrt{2}}(X - iY)|\beta\rangle , \qquad (3.11)$$

where u is the basis function of Γ_8 state and $|\alpha\rangle$ and $|\beta\rangle$ are pure spin states.

The magnitude square of the coupling matrix element of a Γ_8 state can then be reduced to that of X function alone, provided that $(n'k'|dV|Y) = (n'k'|dV|X)$. The latter condition is satisfied in our method because the cation and anion disorders have the same T_d symmetry as the space lattice does. So the matrix elements obtained by us are the same for real cases with spin-orbit interation. The only correction needed to be done on our results is the energy denominators comimg from a different band structure. With the same equation for the coupling matrix elements, the effect of spin-orbit interaction on our results is estimated by neglected the contribution from one heavy-hole band. This is an underestimate for the contribution from the split-off band. The approximation should be good because the split-off energy is about 1 eV for all compositions in (Hg,Cd)Te. The estimated bowing is shown in Figure 3-13 by the marked solid curve. It is mentioned in Chapter 2 that the band width of upper three valence bands obtained in local empirical pseudopotential is smaller by about 40% than the real measured band width. The error of our estimated spin-orbit interaction falls within this accuracy.

3.8 CONCLUSION

The model developed in Chapter 2 is used in a perturbative approach to study the effect of alloy fluctuation potential on energy bandgap bowing in ternary alloy systems. Two important alloys (Al,Ga)As and (Hg,Cd)Te are chosen as typical examples. The intrinsic bowing parameters within the virtual crystal approximation are zero for both systems. The extrinsic bowing parameter obtained in second-order perturbation has contributions from both cation and anion disorders. Stationary non-degenerate perturbation equation is used and the effects of possible degenerate states are discussed. No numerical singularities will show up in the calculations as argued in section 3.1. The summation of coupling matrix elements is carried out over the lowest 15 bands at 88 points in the irreduable part of the Brillouiu zone. Convergence test has been examined for the number of energy bands. It is found that the contribution from the five top most conduction bands is less than 10% of the energy correction in general. Convergence test for the number of k points has not been persued because of expensive cost. From the agreement with experimental data, the choice of k points is meaningful.

The validity of using perturbation approach is justified by the criterion: $1>>(ME/BW)^2$. Where ME is the magnitude of coupling matrix elements which is at most 0.3 eV and BW is an average band width of at least 1 eV. The values of empirical pseudopotential model are chosen from previous publications. The standard is to have correct band structures for parent compounds and have disorder potential as

small as possible. Because of only a few known values for form factors obtained from band structure fitting, linear approximation is applied to construct a continuous dV(q) curve. The determination of dV(q=0) is made on the atomic Model Pseudopotentials of different cation atoms. Small variation in dV(0) does not affect the bowing parameter at all. For the shape of dV(q) curve at large q values, a monotonically decreasing tail is more meaningful than an abrupt zero tail.

From the calculated extrinsic bowing parameter in (Al,Ga)As, anion disorder plays the dominant role in it. The contribution from anion disorder makes 90% of the total bowing. The anion disorder also contributes 30% of the total bowing in (Hg,Cd)Te. Distinct effects can be noticed from the coupling matrix elements under different disorder potentials. They are related to the physical origins of disorders and the charge distributions of corresponding electronic states. Clear pictures of interactions between disorder potentials and band edge states have been given in section 3.8. The effect of spin-orbit interaction on the final bowing is discussed. It does not change the matrix elements but change the energy levels in perturbation equation. Its effect is estimated for (Hg,Cd)Te by neglection the contribution from one heavy-hole band. The error, 40% in total bowing, is within the accuracy of the band width in local empirical pseudopotential scheme.

Supportive evidence for different pseudopotentials of the same atom in different parent compounds can be found in empirical tight-

binding parameters. However, due to different choices in tight-binding parameters, the common Te atom in (Hg,Cd)Te may be set to have the same value of parameters.[36] Naturely the physical interpretations of bandgap bowing in reference 36 are quite distinct from ours. The differences are corresponded to the choice of parameters not to any deviation in basic physics. If the site-diagonal parameters of Te atom are chosen differently in two parent compounds, the interpretations in reference 36 will be modified to be more consistent with ours.

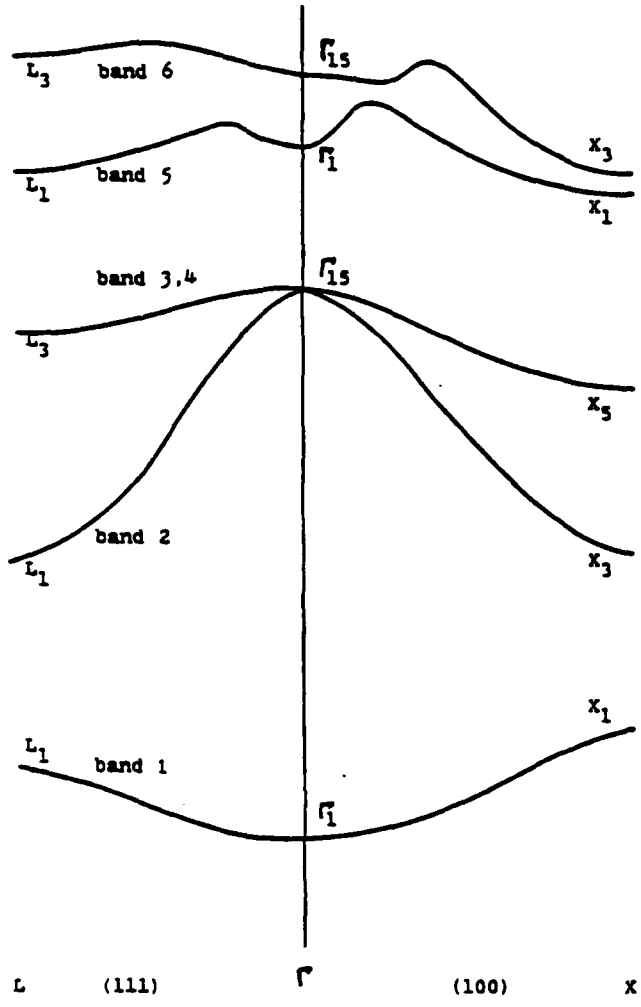

Figure 3-1. Calculated band structure of AlAs along two symmetry directions from local empirical form factors. The number of each band will be used in following calculations.

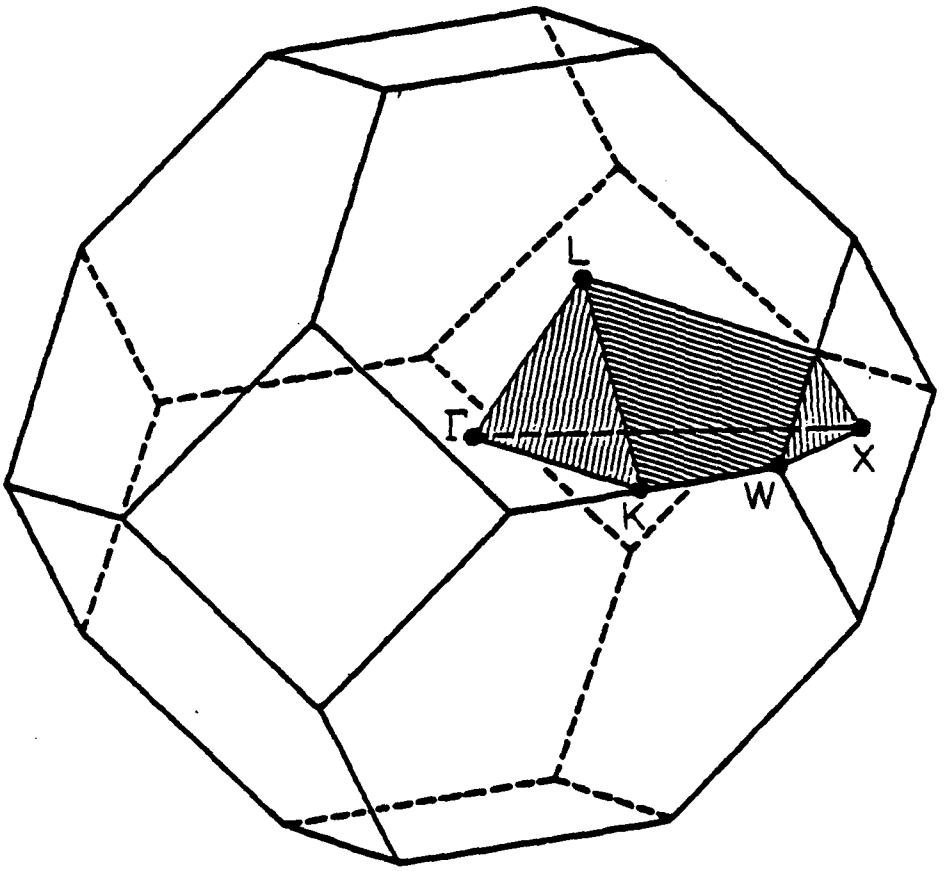

Figure 3-2. The brillouin zone of a face-center-cubic lattice. Shaded region is the irreducible 1/48 part.

Table 3-1. Empirical pseudopotential form factors of AlAs in Rydberg.

G^2	Al (reference 37)	Al (reference 65)	Al (reference 66)
3	-0.148	-0.1475	-0.15
4	0.0625	0.0625	0.07
8	0.026	0.03	0.03
11	0.0625	0.0625	0.09
	As	As	As
3	-0.292	-0.2925	-0.29
4	-0.0625	-0.0625	-0.07
8	0.026	0.03	0.03
11	0.0775	0.0775	0.05

Table 3-2. Empirical pseudopotential form factors of GaAs in Rydberg.

G^2	Ga (reference 37)	Ga (reference 67)	Ga (reference 68)
3	-0.159	-0.183	-0.16
4	0.06	0.035	0.05
8	0.0123	-0.005	0.01
11	0.07	0.078	0.07
	As	As	As
3	-0.299	-0.307	-0.30
4	-0.06	-0.035	-0.05
8	0.0123	-0.005	0.01
11	0.05	0.072	0.05

Table 3-3. Empirical pseudopotential form factors of cation and anion disorders for (Al,Ga)As in Rydberg. (reference 37)

G^2	dV cation	dV anion
3	-0.011	-0.007
4	-0.0025	0.0025
8	-0.0137	-0.0137
11	0.0075	-0.0275

Table 3-4. Site-diagonal tight-binding parameters for GaAs and AlAs determined by fitting to bulk pseudopotential calculation. (from reference 72) Unit is in eV.

	GaAs	AlAs
Ess (cation)	-2.254	-1.274
Epp (cation)	1.839	1.588
Ess (anion)	-6.593	-6.150
Epp (anion)	1.338	2.168

AD-A163 735 THEORETICAL INVESTIGATION OF POINT DEFECTS OF MERCURY CADMIUM TELLURIDE(U) CALIFORNIA UNIV LOS ANGELES SCHOOL OF ENGINEERING AND APPLIED.. D PAN 01 NOV 85 2/2

UNCLASSIFIED ARO-17684.3-EL DAAG29-81-K-0054 F/G 20/2 NL

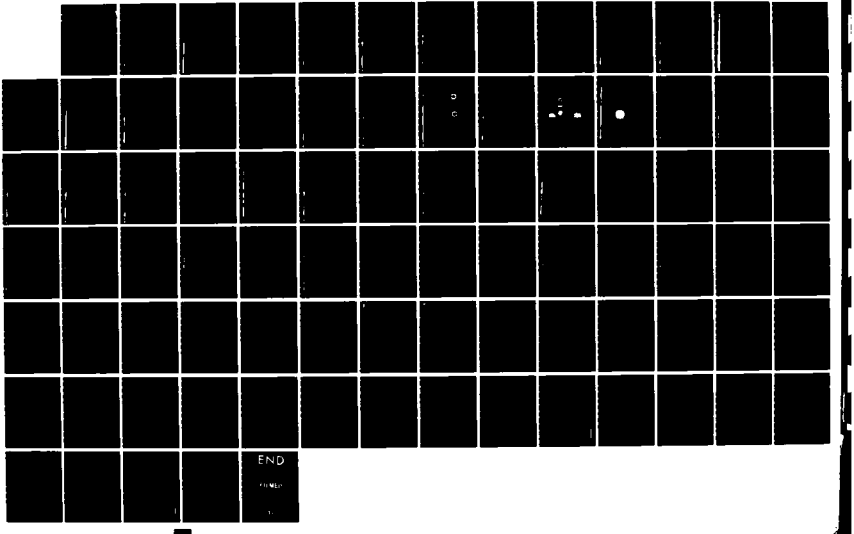

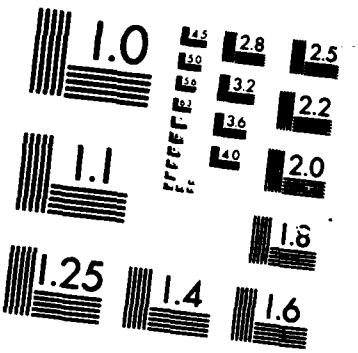

Table 3-5. Atomic model pseudopotential parameters of Al, Ga, and As atoms. Energy is in double Rydberg (27.2 eV) and length in Angstrom (A). (from reference 38)

	Ga	Al	As
A_o	1.44	1.38	2.71
A_1	1.58	1.64	(3.08)
A_2	1.41	1.92	(2.0)
R_M	2.4	2.0	2.0
k_F	0.8776	0.9276	1.0065

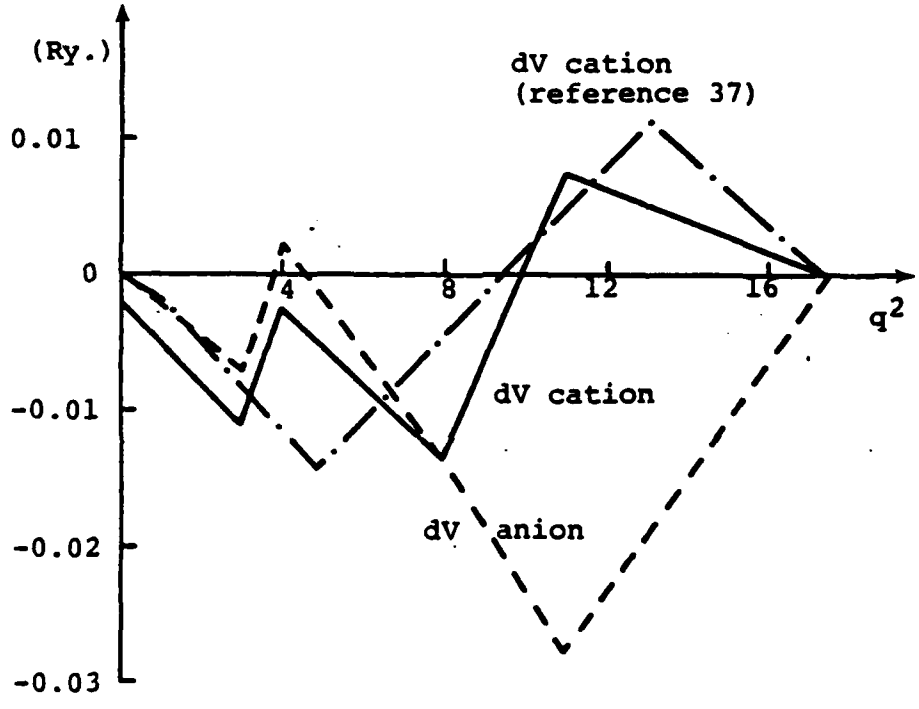

Figure 3-3. Linear approximations of disorder potentials for (Al,Ga)As.

Table 3-6. Second-order shrinkage of the lowest direct energy gap in meV. Positive sign stands for larger bandgap than the VCA value.

	dV cation	dV anion	dV cation (reference 37)
GaAs	-2	-69	+7.3
	Total:	-71	
AlAs	-17	-162	+1
	Total:	-179	
Estimated extrinsic bowing parameter	-0.01 eV	-0.115 eV	+0.004 eV
	Total:	-0.125 eV	

Table 3-7. Second-order energy correction of |40) and |50) states in meV. Arrows indicate the directions of energy shift with respect to the VCA energy levels.

		dV cation	dV anion	dV cation (reference 37)
GaAs	|50)	↓3.5	↓54	↑2.3
	|40)	↓1.6	↑15	↓5.0
AlAs	|50)	↓18	↓143	↓4.3
	|40)	↓1	↑19	↓5.3

Table 3-8 . Contributions from various energy bands on the shift of |40) state in AlAs. Unit in meV.

	Band 1	Band 2,3,4	Band 5	Band 6-10
dV cation	0	↑1	0	↓2
dV cation (reference 37)	0	0	0	↓5
dV cation (test)	0	↑20	0	↓4
on the shift of |50) state				
dV cation	0	↑5	↓36 ↑18	↓4
dV cation (reference 37)	0	↑5	↓22 ↑15	↓2
dV cation (test)	0	↑30	↓115 ↑ 43	↓18

Table 3-9. The effect of q=0 form factor in cation disorder on energy shift and bandgap bowing. Unit in meV.

		dV cation	dV cation (test)
GaAs	|50)	↓3.5	↓20
	|40)	↓1.6	↑11
AlAs	|50)	↓18	↓64
	|40)	↓1	↑15
Estimated extrinsic bowing parameter		-0.01 eV	-0.05 eV

Table 3-10. The effect of high q tail in the test cation disorder on second-order energy corrections. Unit in meV.

	Smooth tail		Abrupt tail	
	|40)	|50)	|40)	|50)
GaAs	↑11	↓20	↑12	↓25
	Total:	-31		-37
AlAs	↑15	↓64	↑13	↓69
	Total:	-79		-82

Table 3-11. The effect of high q tail in the anion disorder on energy shifts. Unit in meV.

	Smooth tail		Abrupt tail	
	|40)	|50)	|40)	|50)
GaAs	↑15	↓54	↑3	↓15
	Total:	-69		-18
AlAs	↑19	↓143	↑4	↓41
	Total:	-162		-45

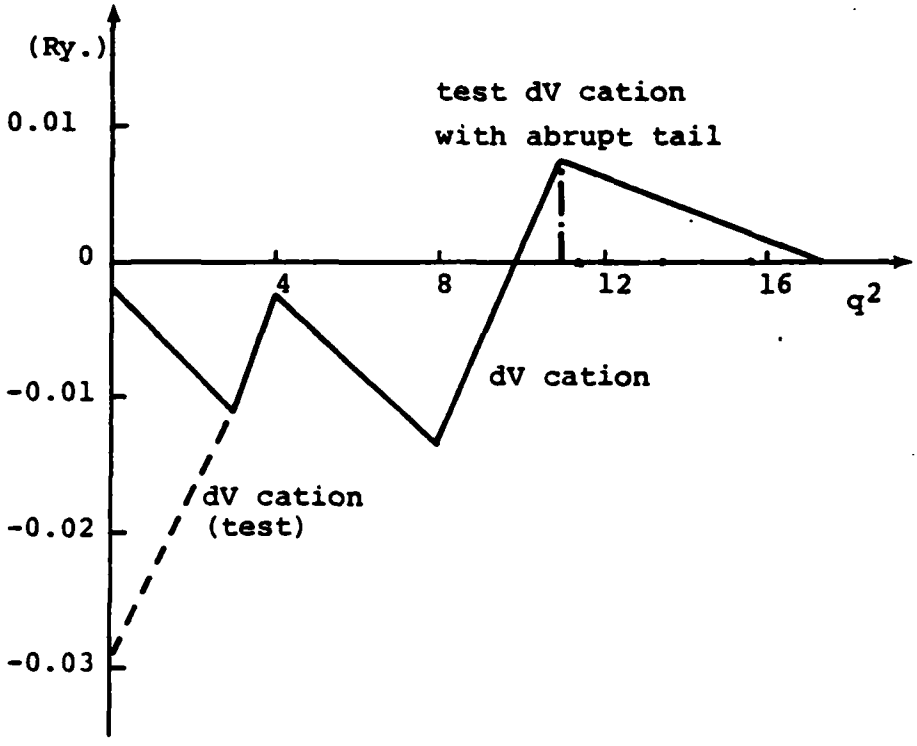

Figure 3-4. Solid curve is the cation disorder in our model. Dashed curve is the test potential which is the same as dV_C except for $0<q^2<3$. Another variation in the test potential is the abrupt high-q tail.

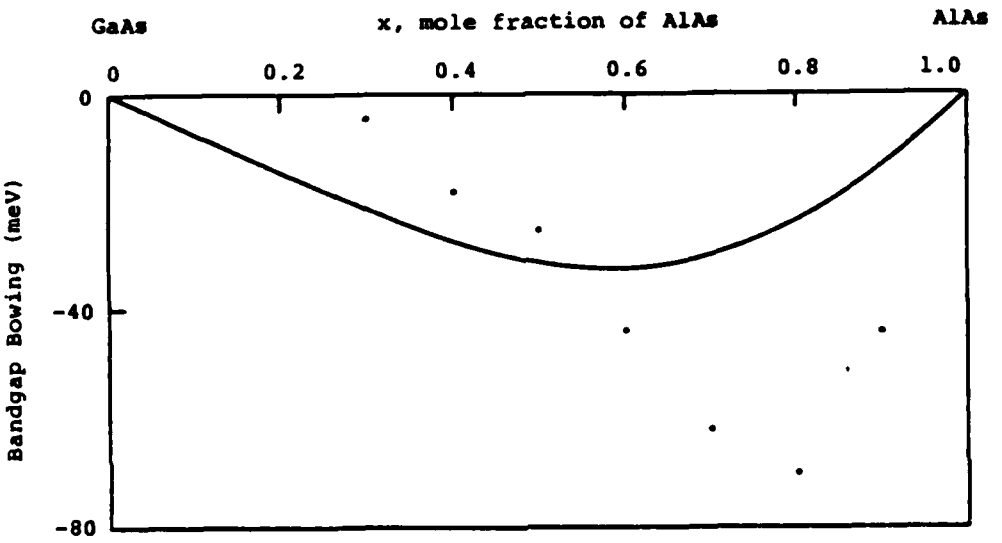

Figure 3-5. Bandgap bowing in (Al,Ga)As. Solid curve is from theoretical calculation with both disorders. The points are from measured values in reference 80.

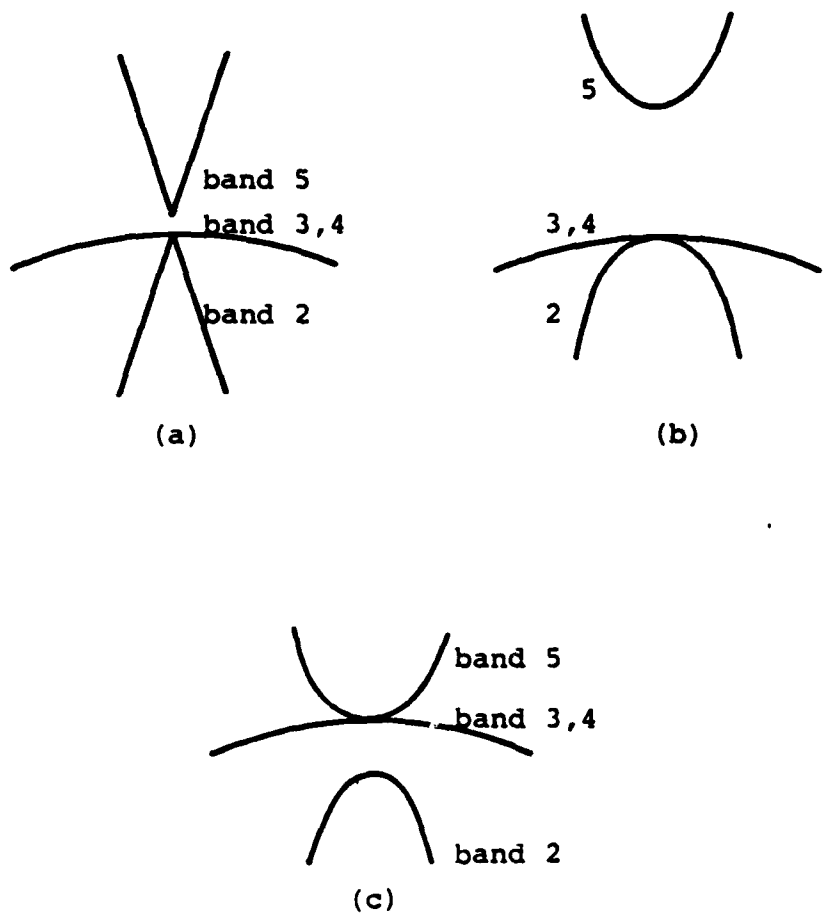

Figure 3-6. Schetch of band structures near k=0 for zinc-blend semiconductors. (a) and (b) are for normal band structure with small and large bandgaps respectively. (c) is for the inverted band structure. Band numbers are the same as in Figure 3-1.

Table 3-12. The calculated slope of VCA bandgap by a first-order perturbation calculation. The constant slope is about 1.9 eV. Contributions from cation disorder and anion disorder are listed in eV for four x values.

x	dV cation	dV anion
0.2	0.987	0.933
0.4	1.018	0.972
0.6	1.02	1.009
0.8	0.995	1.036

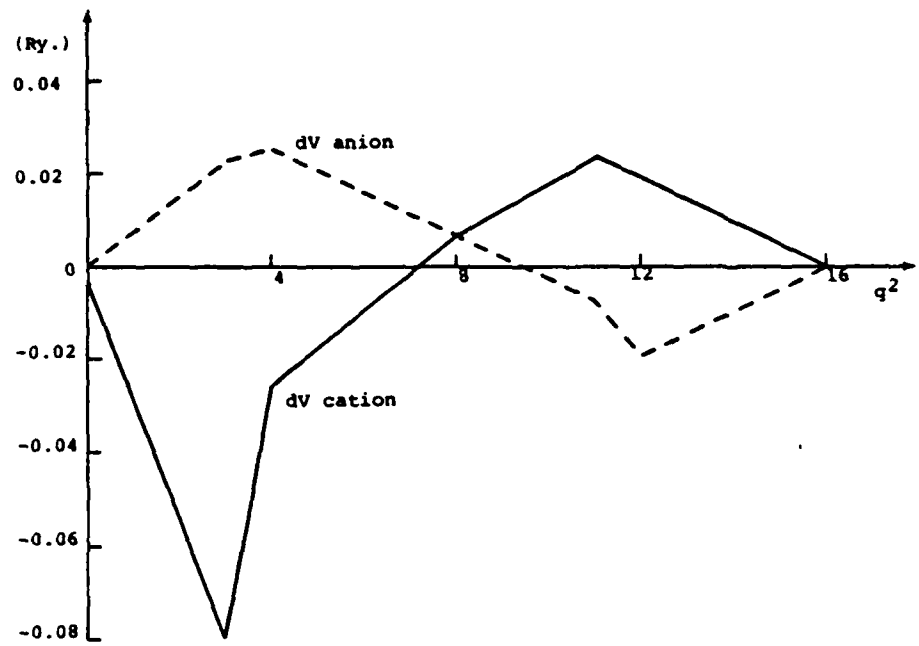

Figure 3-7. Linear approximations of disorder potentials for (Hg,Cd)Te.

Table 3-13. Atomic model pseudopotential parameters of Hg, Cd and Te atoms. Energy in double Rydberg (27.2 eV) and length in Angstron (A).

	Hg	Cd	Te
A_o	0.97	0.88	3.04
A_1	1.11	0.98	3.32
A_2	0.85	1.11	(2.80)
R_M	2.6	2.6	2.0
k_F	0.7213	0.7423	0.9209

Table 3-14. Second-order shrinkage of the lowest direct energy gap in meV. Positive sign stands for larger bandgap than the VCA value.

	dV cation	dV anion	dV cation (test)
HgTe	-65	+21	-65
	Total:	-44	
(Hg,Cd)Te x=0.3	-138	-224	-139
	Total:	-362	
Estimated extrinsic bowing parameter	-0.3 eV	-0.146 eV	-0.299 eV
	Total:	-0.446 eV	

Table 3-15. Second-order energy corrections at conduction and valence states at k=0 in meV. Arrows indicate the directions of energy shift with respect to the VCA energy levels.

	X = 0		X = 0.3		X = 1.0	
	40)	20)	50)	40)	50)	40)
ΔV_G	↑ 244	↑ 309	↑ 151	↑289	↓ 147	↑ 391
(meV.)	(↑ 88)	(↑ 268)	(↑ 130)	(↑ 118)	(↓ 155)	(↑ 198)
ΔV_A	↑ 27	↑ 6	↑ 5	↑ 229	↑ 3	↑ 316
(meV.)	(↑ 6)	(↑ 6)	(↑ 5)	(↑ 118)	(↑ 3)	(↑ 159)

Table 3-16. The convergence test of the energy shifts of band edge states in HgTe. Unit in meV. The numbers in last column represent their percentage in total energy shifts.

		Band 1	Band 2	Band 3,4,5	Band 6-10	Band 11-15
dV_C	|40)	↑1	↑30	↑283	↓54	6%
		Total: ↑244				
	|20)	↑28	↑406	↓53	↓55	5%
		Total: ↑309				
dV_A	|40)	0	↑11	↑26	↓8	7%
		Total: ↑27				
	|20)	↑6	↑0.2	↓0.1	↓0.2	2%
		Total: ↑6				

Table 3-17. The convergence test of the energy shifts of band edge states in CdTe. Unit in meV. The numbers in last column represent their percentage in total energy shifts.

		Band 1	Band 2,3,4	Band 5	Band 6-10	Band 11-15
dV_C	|50)	↑9	↑138	↓240	↓49	3%
		Total: ↓147				
	|40)	↑2	↑420	↓5	↓21	1%
		Total: ↑391				
dV_A	|50)	↑3	0	0	0	0%
		Total: ↑3				
	|40)	0	↑330	↓2	↓5	2%
		Total: ↑316				

Table 3-18. The validity of two-band model is checked by the energy shifts of band edge states.

x		Two band	Whole	Error
HgTe	|40)	↑350	↑271	
	|20)	↑353	↑315	
	Total	-3	-44	underestimate 93%
x=0.3	|50)	↑176	↑156	
	|40)	↑568	↑518	
	Total	-392	-362	overestimate 8%
CdTe	|50)	↓102	↓144	
	|40)	↑743	↑707	
	Total	-845	-851	less than 1%

Table 3-19. Magnitude square of the intra-conduction band coupling matrix elements.

	$\lvert(20\lvert dV_C\rvert 2k)\rvert^2$		$\lvert(20\lvert dV_A\rvert 2k)\rvert^2$
HgTe	5×10^{-3} - 7×10^{-3}	$\gg$	5×10^{-7} - 1×10^{-5}
	$\lvert(50\lvert dV_C\rvert 5k)\rvert^2$		$\lvert(50\lvert dV_A\rvert 5k)\rvert^2$
(Hg,Cd)Te x=0.3	1.5×10^{-3} - 3×10^{-3}	$\gg$	2×10^{-6} - 2×10^{-5}
CdTe	1.5×10^{-3} - 3×10^{-3}	$\gg$	2×10^{-6} - 2×10^{-5}

Table 3-20. Magnitude square of the intra-valence band coupling matrix elements.

	$\lvert(40\lvert dV_C\rvert 4k)\rvert^2$		$\lvert(40\lvert dV_A\rvert 4k)\rvert^2$
HgTe	1×10^{-5} - 4×10^{-4}	$\lesssim$	1×10^{-5} - 1×10^{-4}
(Hg,Cd)Te x=0.3	1×10^{-5} - 1×10^{-3}	$\lesssim$	1×10^{-4} - 3×10^{-4}
CdTe	1×10^{-5} - 4×10^{-4}	$<$	1×10^{-4} - 4×10^{-4}

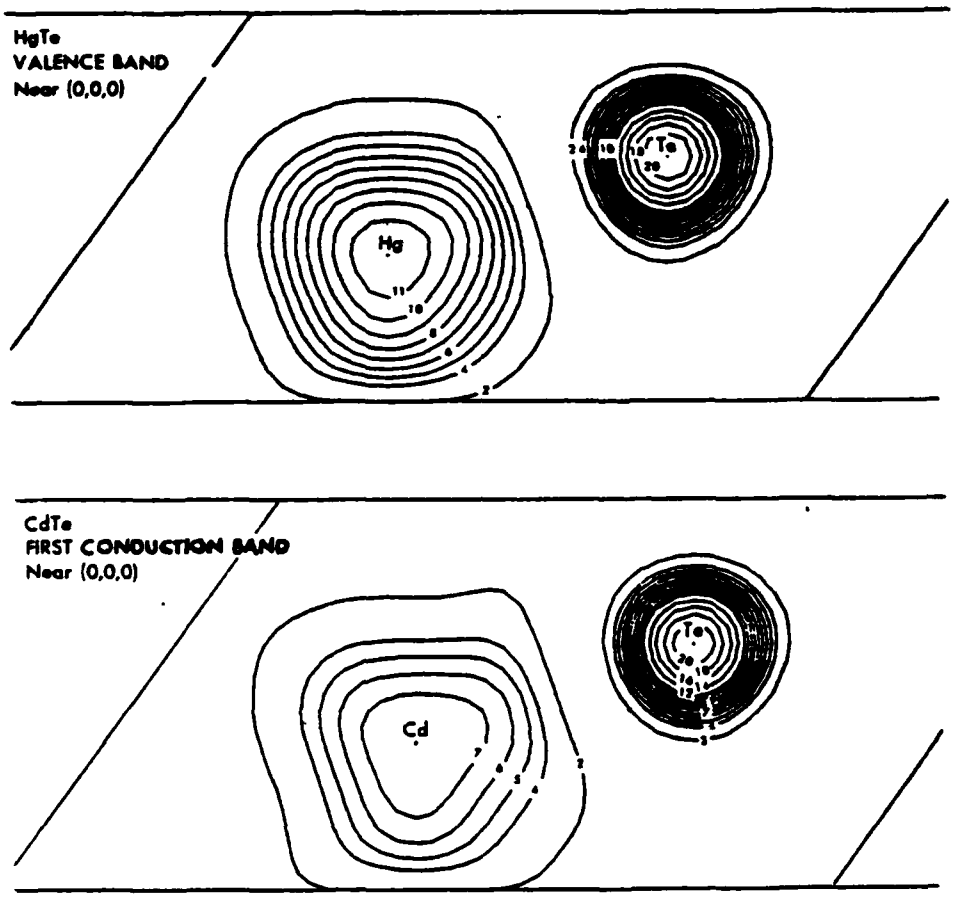

Figure 3-8. Charge densities near k=0 for |20) state in HgTe and |50) state in CdTe (from reference 88).

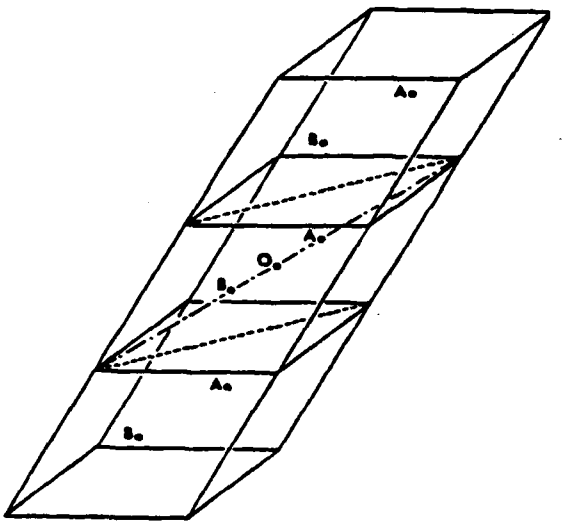

Figure 3-9. Location of atoms in the primitive cells. A section of $(1\bar{1}0)$ plane is shown bounded by dashed lines. This bounded plane passes through both atoms A and B. The extended plane passes through all of the atoms shown in the diagram. Each atom has four nearest neighbors bonded tetrahedrally (from reference 96).

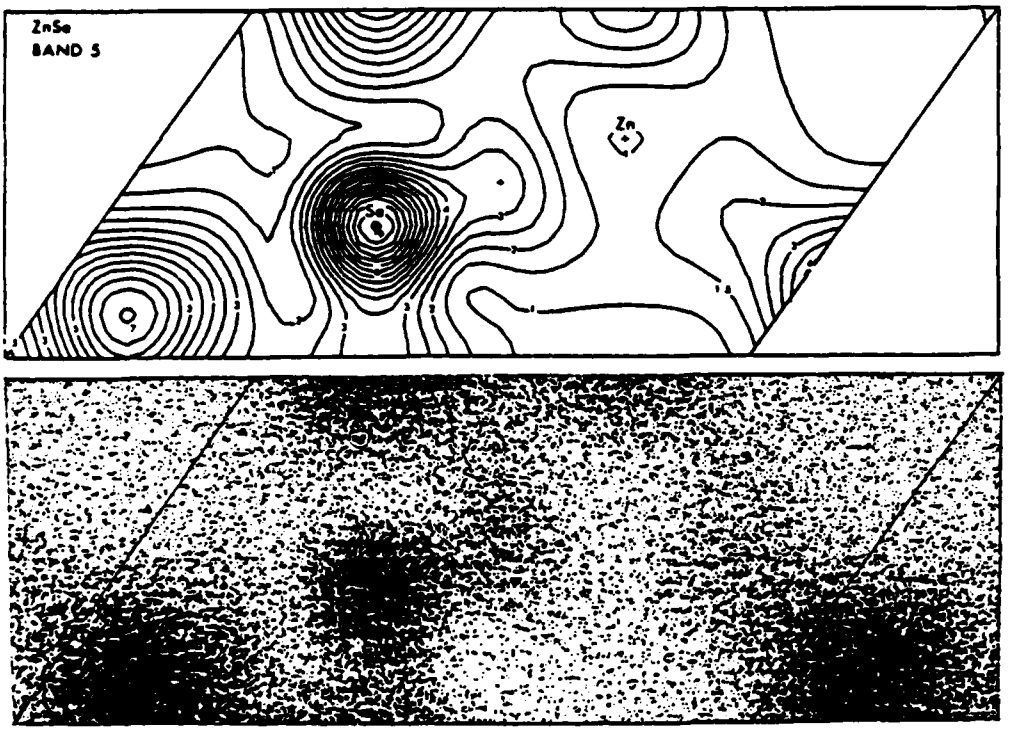

Figure 3-10. Hypothetical charge density for the first conduction band (band 5) of ZnSe (from reference 96).

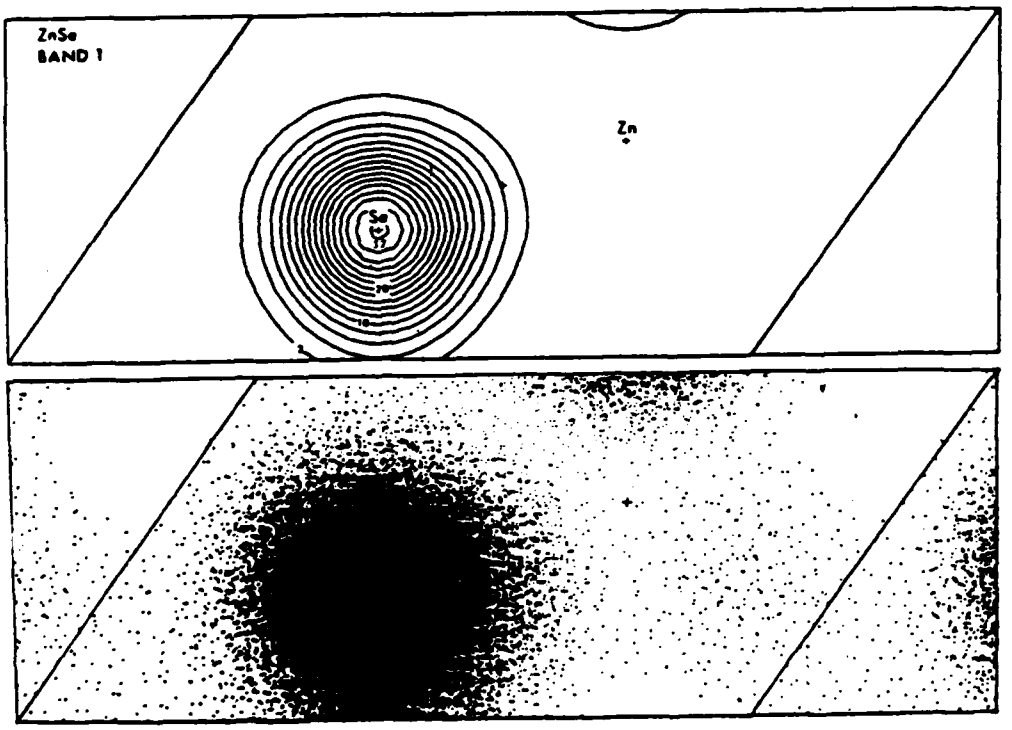

Figure 3-11. Charge density of the lowest valence band (band 1) of ZnSe (from reference 96).

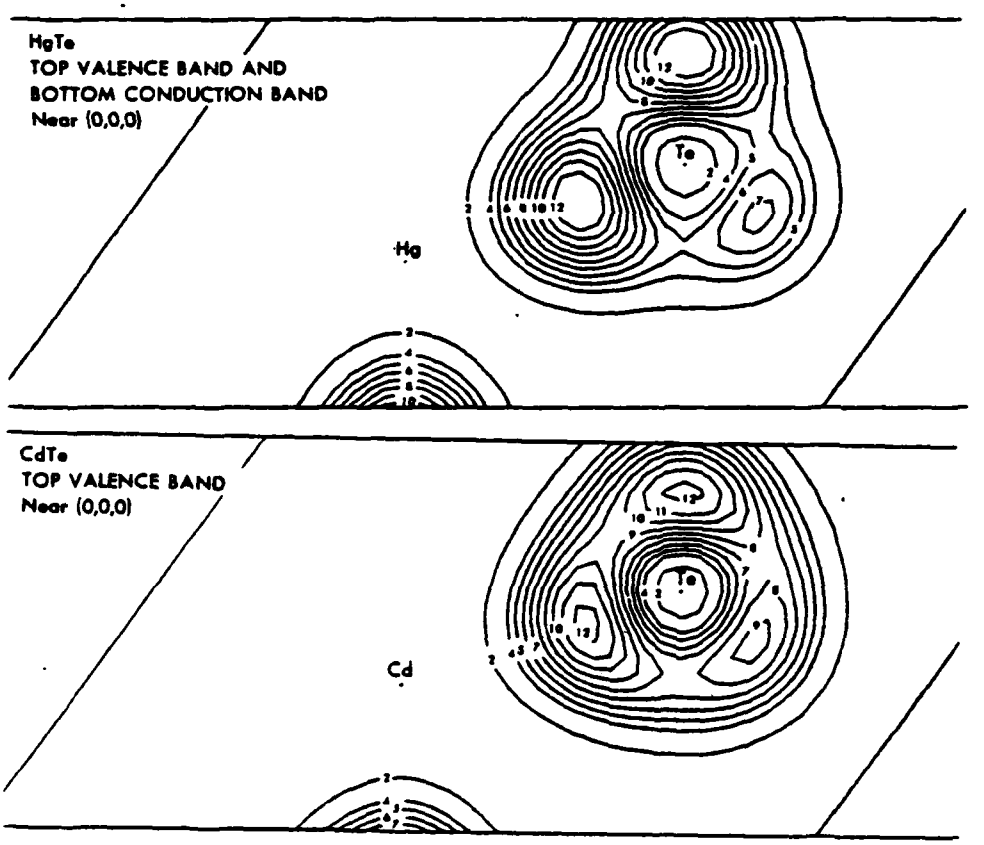

Figure 3-12. Charge densities near k=0 for |40) state in HgTe and CdTe respectively (from reference 88).

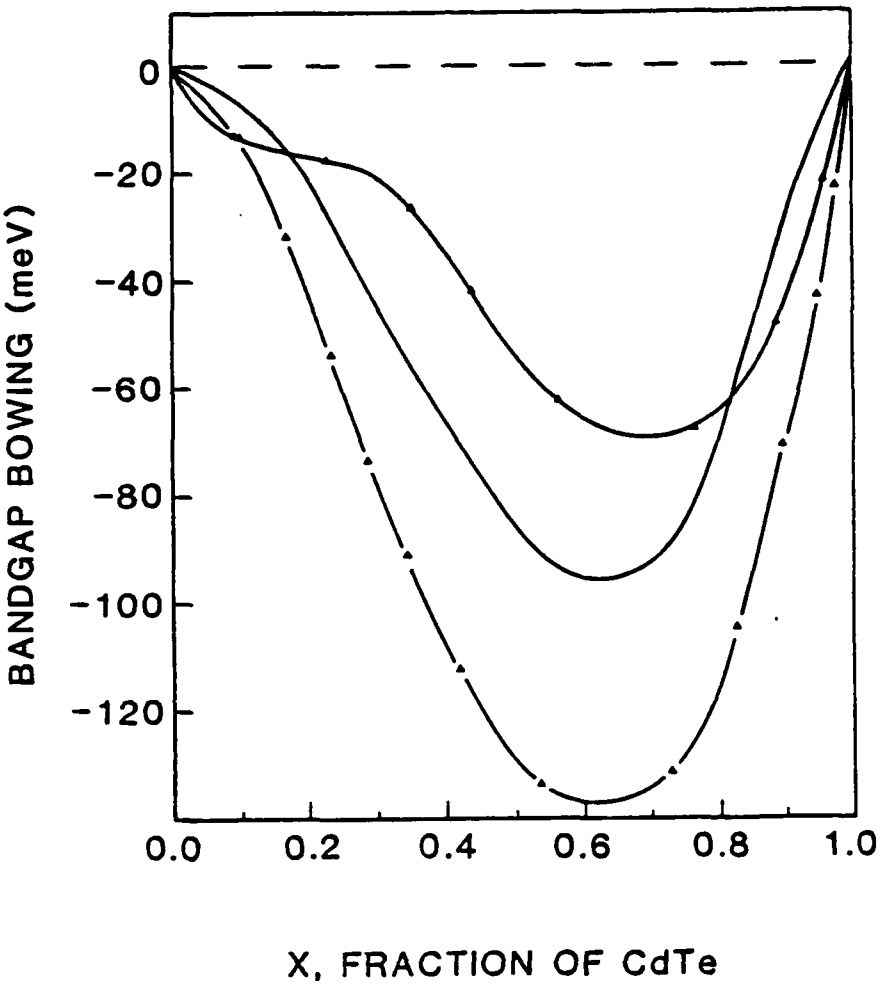

Figure 3-13. Bandgap shrinkage in (Hg,Cd)Te. Solid curve ——— is experimental fit at 0°K. Marked dash curve -▲- is the calculated result without spin-orbit interaction. Marked solid curve —▲— includes the estimated spin-orbit effect. Both cation and anion disorders are included in two theoretical curves.

APPENDIX C

Chapter IV

ALLOY BROADENING

4.1 ENERGY LEVELS INSIDE THE BANDGAP

The energy level and origin of point defects in alloy systems is a mystry by itself. We will concentrate in this chapter on the broadening of defect levels in the presence of the alloy fluctuation potentral. And a background review of the energy levels inside the bandgap is first introduced. There is no allowed electronic state within the forbidden energy gap in a perfect crystal. Real crystals are never perfect and almost all applications of semiconductors are based on impurity effects rather than on the properties of the ideal crystal alone. Deliberately added foreign atoms in small concentrations (1-100 ppm), so-called dopants, can alter the physical properties of the material tremendously in a desired fashion. They may increase (or decrease) the conductivity by many orders of magintude or increase the luminescence efficiency. Unintentional trace impurities and other lattice imperfections in extremely tiny concentrations (less than 1 ppm) can also affect the material quality considerablly - often uncontrollably and in an undesired manner. All the imperfections can introduce energy levels within the band continumm and within the bandgaps. We shall focus our disscussion only on the discrete energy levels caused by point defects within the bandgaps.

In dealing with semiconductors it is useful to classify the defect levels as shallow and deep. In the following we consider those defect levels shallow which have values not significantly larger than those of the conventional shallow acceptors and donors. Effective-Mass theory provides an adequate description for their ionization energies and wave functions.[39] All other defects, having energy levels between those of the shallow donors and accptors, are referred to as deep. In contrast to the shallow levels, the deep levels can have ionization energies comparable with half the bandgap energy, $E_g/2$. Theoretical understanding of them is not as complete as of shallow levels. Special papers and detailed reviews describing the complexity of the subject and various mathematical approaches to its solution are available.[117,188]

Experimental methods in defect study is breifly summarized here: (i) The standard semiconductor assesment techniques, resistivity and Hall-effect measurements, are indispensable tools to establish the electrical properties of shallow donors and acceptors. Their application to deep level defects is considerably more difficult. (ii) Optical spectroscopy is one of the most powerful techniques for the identification of shallow level defects. For two reasons luminescence has been less successful in deep-level research; the first one is the strong electron-phonon interaction and the second one is the lack of good photodetectors in certain wavelengths. (iii) Although its usefulness for defect identification is limited, deep-level transient spectroscopy (DLTS) technique yields information about all important electrical par-

ameters of a deep trapping center. Other magnetic and nuclear type measurements are also available in defect study. It is obvious there is no single method that is capable of detecting all the desriable information about both shallow and deep defect levels in a perfect crystal.

In alloy semiconductions previously described theories and experimental techniques have been applied for defect assessment. Besides the difficulties in crystal growth, an additional complication of defect problem in alloy systems is the non-periodic one-election potential at any fixed composition. Any discrete energy level obtained in the VCA may be broadened statistically in the alloy due to the influence of the alloy fluctuation potential. The experimentally observed alloy broadening has been mostly deduced from optical measurements. This effect on simple acceptors and donors will be studied by a first-order perturbation calculation in the framework of Effective-Mass theory. The effect on acceptor bound-exciton will be discussed later in details.

4.2 BROADENING OF SIMPLE LEVELS

By simple level we mean that an electron or a hole is bound to a single defect center. (Al,Ga)As and (Hg,Cd)Te are used again as typical systems for illustration. The study on shallow levels in (Al,Ga)As and (Hg,Cd)Te has been extensive in the past. The ionization energies of dopants and residual defects are usually deduced from electrical measurements or luminescence data.[101,102,103] When

the theoretical formula were fitted to experimental data in order to extract the ionization energy, the shallow levels were always assumed to be discrete ones with their broadenings neglected. Although accurate experimental information about the broadining of shallow levels is difficult to obtain, we believe that the uncertainties, _ 2 meV and _ 3 meV, associated with measured acceptor ionization engergies in (Al,Ga)As[102] and (Hg,Cd)Te[103] can be related to the V_f. A quantitative method of calculating the alloy broadening of shallow levels is developed and tested in this section.

Because of the random nature of V_f, the shape of broadening is assumed to be a Gaussian distribution. We shall calculate the root mean square values of the statistical broadening by the correlation function of V_f in equation 1.2 and first-order perturbation theory. The impurity wave function in the VCA is expressed as the product of an envelope function and the Bloch function at the corresponding band edge.

$$\Psi_{imp}(\bar{r}) = f(\bar{r})\ \chi_{n\bar{k}}(\bar{r}) \qquad (4.1)$$

where the total impurity wave function is normalized to unity in the whole volume, the Bloch function is normalized to unity in a primitive cell (this normalization of Bloch state is differant from that given in bandgap bowing in Chapter 3) and the envelope function is normalized to the volume of a premitive cell. The Bloch function is obtained from the local empirical pseudopotention band structure calculation in

the VCA and the envelope function is obtained in the Hydrogenic-like Effective-Mass theory.

The root mean square of broadening can be obtained from

$$\Delta E^2_{alloy} = \overline{\langle \psi_{imp} \mid V_f \mid \psi_{imp} \rangle}^2$$

$$\doteq [x(1-x)] \left[\frac{1}{\Omega} \int f^4(\bar{r})\, d^3r\right]$$

$$\left[|\langle \chi | dV_c | \chi \rangle|^2 + \frac{1}{4} |\langle \chi | dV_A | \chi \rangle|^2\right], \quad (4.2)$$

where Ω is the volume of the primitive cell; V_f, dV_C, and dV_A are defined as before.

Within the scheme of Hydrogenic Effective-Mass theory, the ground state radius of a shallow level is obtained by

$$a_{imp} = 0.53\, \epsilon_0\, m_0 / m^*, \quad (4.3)$$

where 0.53 is the Bohr radius in Angstrom, ϵ_0 is the static dielectric constant of the semiconductor, and m^* is the effective mass at corresponding band edge. Equation 4.2 then becomes

$$\Delta E^2_{alloy} = \left[\frac{\Omega}{8\pi a^3_{imp}}\right][x(1-x)]$$

$$\left[|\langle \chi | dV_c | \chi \rangle|^2 + \frac{1}{4} |\langle \chi | dV_A | \chi \rangle|^2\right]. \quad (4.4)$$

The first factor in equation 4.4 gives the average probability of finding an election or a hold in a primitive cell. The factor x(1-x) represents the variation of the average strength of v_f due to compositional changes. The last factor in equation 4.4 is the microscopic contribution of dV to the alloy broadening from one premitive cell. With clear physical meaning for each term in equation 4.4, the broadenings of shallow levels in (Hg,Cd)Te are calculated as an illustrative example.

Table 4-1 and 4-2 summarize the parameters for shallow acceptor and donor levels in (Hg,Cd)Te respectively. The static dielectric constant as a function of composition is obtained from the curve in reference 3. A constant spherically averaged heavy-hole effective mass 0.45 m_0 is used for all compositions. The measured effective mass of heavy-hole are 0.40 m_0 for (100) direction, 0.49 m_0 for (110) direction, and 0.53 m_0 for (111) direction in reference 82. The m_0 stands for the free-electron mass. Their mathematical average 0.473 m_0 is closed to the calculated spherical mass obtained from the Luttinger parameters in the same reference. The effective mass for electron as a function of composition is adapted from the k.p theory.[184] Different energy band parameters used in the k.p calculation may introduce variations in the root mean square value of donor states by about 8% at x=0.48 and 11% at x=0.8. These uncertainties are not important because the broadening is too small for donor levels to be determined experimentally.

Table 4-3 and 4-4 list numerical values of the third term in equation 4.4. The matrix elements of dV_C and dV_A at band edges are carried out by using 65 plane waves for the expansion of the EP Bloch functions. The spin-orbit is neglected in this calculation. The compositional dependence of matrix elements can be understood from the arguments in section 3.6.

Figure 4-1 shows the calculated half width as a function of composition. Two solid curves are the broadenings of shallow acceptor and donor states. Small numerical values for shallow donor states come from the large donor radius which corresponds to the small probability of finding an electron in a unit cell. The broadening of acceptor states has a maximum of about 6 meV as shown by the solid curve in Figure 4-1. It results from the oversimpled solution of the hydrogenic-type effective-mass equation. In a more accurate equation, the impurity potential is screened by a position dependent dielectric function and not by a single dielectric constant.[118] The asymptotic value of the dielectric function at large distance is that of the static dielectric constant but its value for small distance approaches to unity. With the more accurate treatment in impurity potential, the acceptor ionization energy is about half value of the one obtained in the hydrogenic-type approximation. Consequently the hole radius is larger and the broadening is small. The maximum broadening of acceptor states in the dashed line in Figure 4-1 is about 3 meV. It is close to the experimental uncertainty in measured acceptor ionization energies.[103] The validity of the single-band ap-

proximation in Effective-Mass theoty is checked by the following criterion.[117]

$$\left[\frac{a}{a_{imp}}\right]^4 \frac{E_{imp}}{E_g} \ll 1 , \qquad (4.5)$$

where a is the lattice constant, E_{imp} is the ground state ionization energy of the shallow impurity, and E_g is the bandgap of host crystal. The value of equation 4.5 is less than 1% for x changing from 0.2 to 1.0.

To justify the neglect of spin-orbit interaction, a detailed calculation including the spin-orbit (SO) interaction is carried out for x=0.48. The procedure is quite different from the 65 plane-wave method used for the band calculation without the SO effect. Within the total 113 plane waves used as expansion basis, 59 plane waves are treated exactly and the rest 54 are taken into account through the modified Lowdin perturbation scheme.[41,185,186] There are two effects from the spin-orbit interaction. The first one is in the VCA. The spin-orbit interaction will modify the charge distribution of |40) and |50) states and consequently change the matrix elements of disorder potentials at band edges. The resulting changes of alloy broadening due to these modifications of Bloch functions are less than 5%. The second effect is in the fluctuation potential derived from the difference of the spin-orbit parameters of Hg and Cd atoms. This effect was found to be negligible. Since it is very expensive to include these small effects, they are neglected in the calculation.

Besides shallow levels, deep levels may also be broadening in the alloy. The impurity wave function and ionization energy of a very localized deep level is a complicated problem. If the wave function is assumed to be given in the form of equation 4.1 and the envelope function has the shape of hydrogenic 1S orbital, the half width of alloy broadening can be estimated as a function of ground state radius. The dashed lines in Figure 4-2 are obtained by using conduction band Bloch functions, while the solid lines are from valence band Bloch functions. The intention of this figure is to estimate the alloy broadening of deep levels in (Hg,Cd)Te. Because the wave functions are probably oversimplified, the results in Figure 4-2 should be interpreted with great caution. We feel that the results indicate an upper bound of about 0.1 eV for the alloy broadening of deep levels in all alloy systems.

4.3 EXCITONS IN ALLOY SEMICONDUCTORS

In many non-metallic solids, an electron and a hole may be bound together by their attractive electrostatic interactions, just as an electron is bound to a proton. The bound electron-hole pair is called an exciton. It can move through the crystal transporting excitation energy but it is electrically neutral. The internal structure of intrinsic excitons has been studied in detail with much quantitative accuracy. Precise knowledge of them is important not only by itself, but also as the firm basis for further developments. The behavior of excitons in the presence of other entities such as neutral impurities, trapping

potentials, meterial boundary, photons, phonons, excitons or carriers, etc. has also been under intensive investigation.[167,168,169]

In the photoluminescence study of point defects in semiconductors, exciton may bound to varies impurities, defects, and complexes. The subsequent decay from the bound state, recombination of the electron with a hole, yields information concerning the center to which the exciton was bound. Early photoluminescence investigations were primarily centered on free-to-bound and bound-to-bound transitions such as the so-called "edge emission" studies which gave rise to relatively board emission. In the 1960s the effort shifted to more intensive studies of the sharp-line emission, aimed at identifying the bound-exciton impurity transitrons and at achieving a better understanding of the residual impurity and defect structure of semiconductors, which have applications in the electronic industry. The magnetic field splittings of these sharp-line transitions make it possible to differentiate between neutral and ionized donor and acceptor impurities. In conjunction with systematic impurity-doping experiments, specific donor and acceptor impurities may be identified.

Transitions involving both free and bound excitons are observed in alloy semiconductors in spite of the random crystal potential. Narrow free-exciton peaks have been observed in the absorption spectra of direct bandgap Ga(As.P).[110] As of the same reason discussed for shallow level broadening, the large Bohr radius of excitons in direct bandgap alloy may cause the effect of alloy fluctuation potential small. Bound as well as indirect excitons, on the other hand, may have a

much smaller radius and stronger broadening may be expected. Because of the complicated nature of bound-excitons in alloys, different anthors attributed different broadened lineshapes to exciton-phonon interaction[111] or the alloy fluctuation potential.[27,28,112,113,114]

Quantitative calculations of the broadening due to the V_f are few. Results from theoretical calculation of the alloy broadening in reference 43 by using the coherent-potential approximation were 10-20 times smaller than experimental data. A much better agreement between theoretical and experimental values was obtained by using the coherent-potential approximation in reference 28. In Ga(As,P):N alloys (1>x>0.6) the luminescence due to the radiative recombination of nitrogen-bound-excitons is shifted toward lower energies with respect to excitation spectra. This shift is attributed to the band broadining generated by local disorder potential around nitrogen atoms. The magnitude of half width of broadening has a maximun value about 35 meV which is consistent with the simple upper bound obtained in section 4.2. The application of our model to the alloy broadening of bound-exciton spectral line will be discussed in the next section.

4.4 BOUND-EXCITON RECOMBINATION LINE IN (HG,CD)TE

Recent photoluminescence experiment on (Hg,Cd)Te with x=0.48 reported an observation of acceptor bound-exciton recombination line with a width of 6 meV.[27] Because of the very accurate experimental measurement, it is taken as a quantitative test ground for the model of the alloy fluctuation potential. The theoretical accuracy now de-

pends mainly on the correctness of impurity wave functions. The acceptor bound-exciton is a complicated four-body problem. There are two holes and an electron surrounding a positive charge center. A self-consistent scheme based upon the spherical model of shallow acceptor[40] has been developed for acceptor bound-exciton.[41] We shall not repeat the derivations here but use directly the formulations in reference 41.

There are initial and final states for the bound-exciton recombination line. The root-mean-square of alloy broadening of the recombination line is defined as

$$\Delta E^2_{alloy} = \overline{\left[(E_I - E_F) - \overline{(E_I - E_F)} \right]^2} \qquad (4.6)$$

where the bar represents an ensemble average, E_I is the initial state containing a neutral acceptor and a neutral exciton, and E_F is the final state which is a simple acceptor state. If only the first order correction is considered, E_I and E_F can be approximated as

$$E_I = E^{(o)}_{BE} + \langle \Psi_{BE} | V_{f,BE} | \Psi_{BE} \rangle , \qquad (4.7)$$

$$E_F = E^{(o)}_{A} + \langle \Psi_{A} | V_{f} | \Psi_{A} \rangle , \qquad (4.8)$$

$$\Psi_{BE} = \Psi_{e,BE}(\bar{r}_1) \mathcal{A} \Psi_{h,BE}(\bar{r}_2) \Psi_{h,BE}(\bar{r}_3) , \qquad (4.9)$$

$$V_{f,BE} = V_f(\bar{r}_1) - V_f(\bar{r}_2) - V_f(\bar{r}_3), \qquad (4.10)$$

where A denotes the antisymmetrization operator for the two holes, $\Psi_{e,BE}$ and $\Psi_{h,BE}$ are the self-consistent electron and hole wave functions of acceptor bound-exciton, and Ψ_A is the hole wave fuction of the neutral acceptor. The alloy fluctaution potential V_f is originally defined for a valence electron in the one-electron approximation. If must bear an additional minus sign for the positively charged holes. Equation 4.6 is then approximated as

$$\Delta E^2_{alloy} \doteq \overline{[\langle \Psi_{e,BE} | V_f | \Psi_{e,BE} \rangle + 2\langle \Psi_{h,BE} | -V_f | \Psi_{h,BE} \rangle - \langle \Psi_A | -V_f | \Psi_A \rangle]^2}$$

$$\doteq \overline{\langle \Psi_{e,BE} | V_f | \Psi_{e,BE} \rangle^2} + \overline{\langle \Psi_A | V_f | \Psi_A \rangle^2} + 4\overline{\langle \Psi_{h,BE} | V_f | \Psi_{h,BE} \rangle^2} - 4\overline{\langle \Psi_{h,BE} | V_f | \Psi_{h,BE} \rangle \langle \Psi_A | V_f | \Psi_A \rangle}. \qquad (4.11)$$

Because of the large radius of electron wave function, the small interactions between $\Psi_{e,BE}$, $\Psi_{h,BE}$, and Ψ_A are neglected.

Each term in equation 4.11 is derived explicitly in Appendix A. The input parameters needed for the self-consistent calculation of the

envelope functions are listed in Table 4-5. The use of the spherical model is justified by the values of parameters. The results of the spatial integration of envelope functions are listed in Table 4-6. The length is normalized to the acceptor Bohr radius which is about 104 angstrom. The upper bound of integration is chosen as seven or ten acceptor Bohr radius around where the magnitude of envelope function is nearly zero. The matrix elements of cation and anion disorder potentials at band edges are summarized in Table 4-7. They are obtained from the empirical-pseudopotential calculation in the VCA with and without the spin-orbit interaction. The disorders are the same as defined by Figure 3.6. The discripancy in matrix elements with and without spin-orbit interaction has an effect less than 10% in the final root-mean-square of broadening. From the values in Table 4-8 the calculated root-mean-squre of broadening is 0.95 meV without the spin-orbit interaction and 0.9 meV with the interaction. If only the catron disorder pontential is included, the root-mean-square is about 0.37 meV. The anion disorder pontential contributes only 30% in the bandgap bowing but is 60% in the alloy broadening. The reason is that there are two holes in the acceptor bound exciton. They interact more strongly with the anion disorder pontential which is derived from the valence change redistribution. However, the calculated full-width-half-maximum of 2 meV is only one third of the experimentally measured 6 meV. There must be other mechanisms which may also cause broadening to the bound-exciton recombination line.

4.5 J-J COUPLING AND CONCENTRATION BROADENING

The multiplets of acceptor bound-exciton in perfect crystal have been extensively studied theoretically and experimentally.[115] The hole-hole coupling is believed to be important for the multiplet structures. In the so-called "j-j coupling scheme", two holes of angular momentum j=3/2 are combined antisymmetrically to form J=0 and J=2 states. (Small j here is the total angular momentum operator which is written as F in Appendix A. Capital J here is not the effective spin operator appeared in appendix A). According to atomic theory, in which the j=3/2 states are formed by the spin-orbit interaction between a P electron and its spin, the energies of the J=2 donblet should be lower than the J=0 singlet. The existence of the doublet J=2 states is due to the breakdown of sphrical symmetry in the srystal. For the shallow acceptor bound-exciton in the VCA, the J=2 states are indeed lower in energy than the J=0 state as the same in atomic case.

To investigate quantitatively the j-j coupling of the two holes in the bound-exciton, the effect of bound electron is neglected for simplicity. By using the techniques of multiplet theory for atoms, it can be shown that the J=2 states are the ground state of the model Hamiltonian and the energy separation from the J=0 state is given by

$$\Delta = \frac{64}{25} \iint \left[f_{oh,BE}(r_1)\, g_{oh,BE}(r_1) \right] \left[f_{oh,BE}(r_2)\, g_{oh,BE}(r_2) \right] \frac{r_a^2}{r_b^3}\, r_1^2 r_2^2\, dr_1\, dr_2 \quad , \qquad (4.12)$$

where f_{0h} and g_{0h} are defined as before and r_a (r_b) is the smaller (larger) of r_1 and r_2. The reason of this splitting is due to the mutual scattering of the two holes between S-like and D-like orbitals. It is interesting to note that the mutual scattering between D-like orbitals makes no contribution to the j-j splitting in this case.

The calculated value of j-j splitting in the VCA by using the self-consistent f_0 and g_0 functions is about 1 meV. The full-width-half-maximum of the bound-exciton recombination line is then estimated by an addition of two Gaussian distributions with ΔE=0.9 meV respectively, separated by 1 meV. The calculated full width is 2.8 meV which is about half of the experimental data. Experimental results of Ga(As.P):N case demonstrated the possibility of detecting the combination of two Gaussian distributions separated by j-j splitting in optical spectrum.[114] Although the j-j splitting in this case resulted from the interaction between an election and a hole, the situation of two holes should be in principle the same. From the experience of calculating the j-j splitting in compound semiconductors, however, the theoretical value is always an overestimate to the experimentally measured splitting.[115] Therefore, the 3 meV alloy broadening including the effect of j-j splitting should also be an upper bound of theoretical prediction.

Because of the small electron effective-mass, the radius of $\Psi_{e,BE}$ is very large. The interaction of a neutral bound-exciton complex with nearest neutral acceptors due to the overlap of impurity wave functions may cause the recombination line to be further broadened.

The theory of this "concentration broadening" derived in reference 42 is briefly summarized in Appendix B. A quantitative calculation is carried out for $N_A=1\times10^{16}$ cm^{-3} of (Hg,Cd)Te ; x=0.48. The most important contribution from the envelope functions in concentration broadening is the decaying tails at large distance which may have nonzero overlap. In order to have simple equations, the tail of $f_0(r)$ is approximated by an decaying exponential function with proper normalization constant. The D-like $g_0(r)$ is neglected in the calculation. The parameters describing the decaying tails are $\alpha=2.32$, $\beta=0.5$, $\gamma=3.47$ in one over length for $\Psi_{h,BE}$, $\Psi_{e,BE}$, and Ψ_A respectively. The length is in acceptor Bohr radius which is 104.25 A. The variations of $I_0(R)$, $I_1(R)$, and $J_0(R)$ as functions of distance R are plotted in Figure 4-3. $J_1(R)$ is neglected because it is so small. The transition energy E(R) is plotted in Figure 4-4 and the full-width-half-maximum of concentration broadening for $N_A=1\times10^{16}$ shown in Figure 4-5 is 0.73 meV. The full width for $N_A=5\times10^{15}$ and 2.5×10^{16} cm^{-3} are 0.3 and 2 meV respectively. Concentration broadening alone can not explain the observed width in the (Hg,Cd)Te samples.

With the correlated alloy and concentration broadenings the root-mean-square value of a Gaussian distribution is 0.97 meV which is determined by

$$\Delta E^2_{total} = \Delta E^2_{alloy} + \Delta E^2_{concentration} . \qquad (4.13)$$

The total calculated full width of bound-exciton recombination line is only 3 meV taking into all possible considerations. Carefully worded in the original paper was there also a macroscopic broadening effect due to the inhomogenuity of the sample. The possible macroscopic broadening in the bound-exciton measurement due to the size of exciting laser spot is about 2 meV. The upper bound of the theoretical broadening is then 5 mev which is in good agreement with the experimental value.

4.6 CONCLUSION

The roles of simple defect levels and bound-exciton states in alloy semiconductors are briefly described together with the experimental assesment techniques for defect levels. The problem of determining energy levels and physical origins of various point defects in perfect crystals is by itself intricate. It becomes even more complicated in alloys because of the existence of the aperiodic alloy fluctuation potential. When the effect of V_f is added to the VCA results, a discrete level in the virtual crystal bandgap may be broadened into a continuously distributed energy band. The reason of this statistical broadening comes from the sampling of local fluctuations in potential by the bound carrier around the defect center. Carefully measured values of the broadening can serve as good probes for the existence of the V_f.

If the defect level is deep within the energy bandgap, the bound carrier will be strongly localized around the defect center. The sam-

pling of V_f is emphasized by the large probability of finding the carrier in a unit cell and correspondingly the alloy broadening is significant. However the ground state wave function of a deep center is difficult to obtain quantitatively. Instead our investigation on alloy broadening starts from the shallow impurity level of which the broadening is considerably small. The reason of relative value of alloy broaneding of shallow and deep levels can be given by simple arguements. The impurity wave function obtained in the VCA is approximated by an effective-mass type solution. It is expressed as a product of an envelope function and a Bloch state at the corresponding band edge. The Coulombic impurity potential is screened by the static dielectric constant of the host alloy. The Bloch states at band edges are used to compute the matrix elements of the disorder potential in a unit cell. The envelope function is used to calculate the probability of finding the bound carrier of the center in a unit cell. The root-mean-square of broadening in first-order is related to the combined effects of the matrix element of V_f and the probability at any fixed composition. The more localized a level is, the larger the alloy broadening it has. And it is found that the accuracy in impurity wave function is the most important factor in determining the broadening.

The calculated half-widths of alloy broadening in (Hg,Cd)Te with x between 0.2 and 1 are shown in Figure 4-1. The trends in matrix elements of dV_C and dV_A at band edges are similar as discussed in section 3.6. They can be interpreted by the physical definitions of

disorder potentials and charge distributions of Bloch states. The maximum broadening of shallow acceptor level obtained in the Hydrogenic Effective-Mass theory is about 6 meV. But with the more accurate wave functions obtained in the spherical model of shallow acceptor, the maximum broadening reduces to about 3 meV which is close to the uncertainty in measured acceptor binding energies.[182,183] The root-mean-square of broadening of deep levels is roughly estimated by an oversimplified effective-mass type envelope function. We believe that the upper bound of alloy broadening for a very localized level is 0.1 eV. When compared with the 0.03 eV broadening of the deep isoelectronic N center in Ga(As,P), the simple prediction is a good one.[28]

Accurate measurements on bound-exciton photoluminescence spectra suggested a 6 meV full-width broadening in (Hg,Cd)Te with x=0.48. The experimental uncertainty due to the macroscopic inhomogenuity in samples is about 4 meV. The remaining with of 4 meV should be the intrinsic property of the sample. The calculated full-width due to the fluctuation potential with very accurate impurity wave functions is about 2 meV. The wave functions are obtained in a self-consistent scheme in which the realistic valence band structure is included.[41] Besides the effect of V_f, other possible mechanisms are all considered. Due to the very small electron effective-mass in (Hg,Cd)Te, there may be interaction between a neutral acceptor bound-exciton complex and nearby neutral acceptor. This so-called "concentration broadening" is calculated by the dominant binary interaction of over-

lapping impurity wave functions. It is only 0.8 meV for the sample doping. The half-width of broadening of the two correlated mechanisms is still 1 mev.

Another mechanism which can cause fine structures in the acceptor bound-exciton ground state configuration is also investigated. The interaction of the two holes in the acceptor bound-exciton may introduce a split in ground state energy which is similar to the "j-j splitting" in atomic theory. Two holes of total angular momentum j=3/2 can form J=0 and J=2 states in the ground state configuration within the VCA. The energy separation between these two states in (Hg,Cd)Te with x=0.48 has an upper bound of 1 meV. If each level of the fine structure is broadened independently, the recombination line-shape will be a superposition of two broadened distributions. There is experimental evidence for this type of broadening in luminescence spectrum.[114] The theoretical value of broadening with all the considerations is about 75% of the experimental value. It is a good indication for the correction of our model of the fluctuation potential.

Table 4-1. Parameters of shallow acceptor levels in (Hg,Cd)Te. The hole effective mass is 0.45 m_o and not a function of x.

x	Dielectric constant	Acceptor radius (A)
0.2	17.3	20.4
0.32	15.9	18.7
0.4	15.4	18.1
0.48	14.2	16.7
0.6	13.2	15.5
0.7	12.3	14.5
0.8	11.8	13.9
0.9	11.0	12.9

Table 4-2. Parameters of shallow donor levels in (Hg,Cd)Te. All equations are from reference 104 in which the static dielectric constant was wrong.

$$\frac{m_e}{m_e^*} = 1 + \frac{P^2}{3}\left(\frac{2}{E_g} + \frac{1}{E_g+\Delta}\right)$$

$P^2 = 18 + 3x$ (eV)

$E_g = 1.79x - 0.26$ (eV)

$\Delta = 1.00 - 0.24x$ (eV)

Table 4-3. Magnitude square of matrix elements at valence band edge in (Hg,Cd)Te. Unit in eV.

x	dV cation	dV anion
0.2	7.784×10^{-2}	0.2228
0.32	5.76×10^{-2}	0.2318
0.4	4.121×10^{-2}	0.2372
0.48	2.856×10^{-2}	0.2425
0.6	1.44×10^{-2}	0.2495
0.7	6.561×10^{-3}	0.255
0.8	1.936×10^{-3}	0.2601
0.9	8.1×10^{-5}	0.2652

Table 4-4. Magnitude square of matrix elements at conduction band edge in (Hg,Cd)Te. Unit in eV.

x	Cation disorder	Anion disorder
0.2	1.649	3.025×10^{-5}
0.32	1.56	2.25×10^{-6}
0.4	1.491	1×10^{-6}
0.48	1.421	9×10^{-6}
0.6	1.30	2.5×10^{-5}
0.7	1.192	4.9×10^{-5}
0.8	1.08	6.4×10^{-5}
0.9	0.964	8.1×10^{-5}

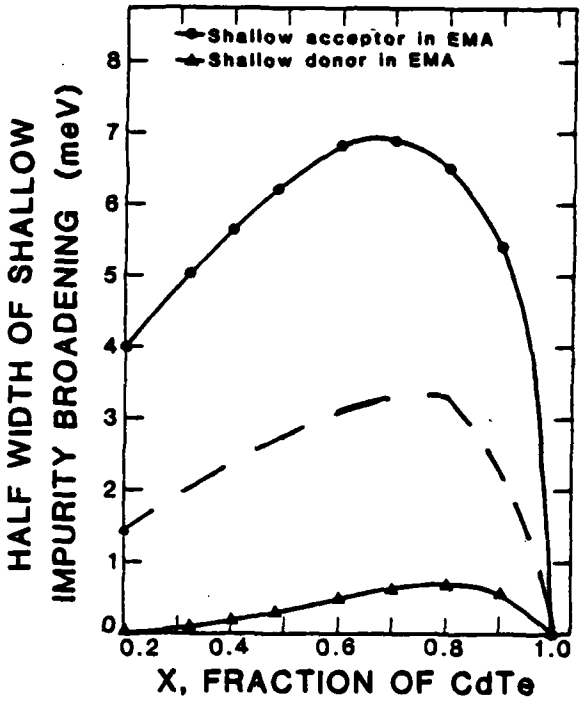

Figure 4-1. The alloy broadening of the shallow donor and acceptor states in (Hg,Cd)Te. Dashed curve is shallow acceptor in more accurate Spherical model.

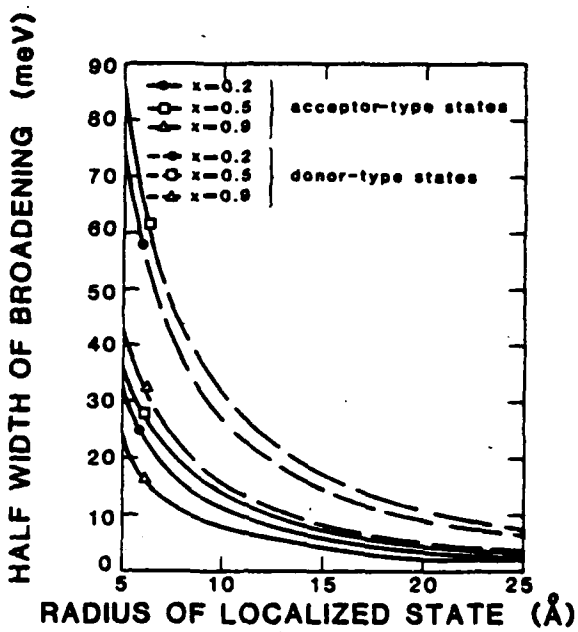

Figure 4-2. The alloy broadening versus the radius of localized states.

Table 4-5. Material parameters of (Hg,Cd)Te; x=0.48 for the spherical model (from reference 82).

bandgap = 600 meV

Luttinger parameters of valence band

r_1^L = 13.85

r_2^L = 5.37

r_3^L = 6.17

u = 0.845

static dielectric constant = 14.2

acceptor Bohr radius = 104.25 A

acceptor Rydberg = 4.865 meV

Table 4-6. Spatial integration of envelope function for bound-exciton recombination line in (Hg,Cd)Te; x=0.48.

$$\frac{1}{4\pi}\int_0^7 |f_{oh}|^4 r^2 dr = 0.609$$

$$\frac{1}{4\pi}\int_0^7 |g_{oh}|^4 r^2 dr = 0.0117$$

$$\frac{1}{4\pi}\int_0^7 |f_{oh}|^2 |g_{oh}|^2 r^2 dr = 0.042$$

$$\frac{1}{4\pi}\int_0^7 |f_{oA}|^4 r^2 dr = 1.458$$

$$\frac{1}{4\pi}\int_0^7 |g_{oA}|^4 r^2 dr = 0.0251$$

$$\frac{1}{4\pi}\int_0^7 |f_{oA}|^2 |g_{oA}|^2 r^2 dr = 0.0941$$

$$\frac{1}{4\pi}\int_0^{10} |f_{oe},BE|^2 r^2 dr = 3.062 \times 10^{-3}$$

$$\frac{1}{4\pi}\int_0^7 |f_{oh}|^2 |f_{oA}|^2 r^2 dr = 0.931$$

$$\frac{1}{4\pi}\int_0^7 |g_{oh}|^2 |g_{oA}|^2 r^2 dr = 0.0162$$

$$\frac{1}{4\pi}\int_0^7 |f_{oh}|^2 |g_{oA}|^2 r^2 dr = 0.076$$

Table 4-6. (continued)

$$\frac{1}{4\pi} \int_0^7 |g_{oh}|^2 |f_{oA}|^2 r^2 dr = 0.05$$

$$\frac{1}{4\pi} \int_0^7 |f_{oh} g_{oh} f_{oA} g_{oA}| r^2 dr = 0.06$$

Table 4-7. Matrix elements of cation and anion disorders at conduction and valence band edges in (Hg,Cd)Te; x=0.48. Numbers in parenthesis are the value for the microscopic contributions of dV at band edges.

	$(\phi_V\|dV_C\|\phi_V)$	$(\phi_V\|dV_A\|\phi_V)$	$(\phi_C\|dV_C\|\phi_C)$	$(\phi_C\|dV_A\|\phi_C)$
Without spin-orbit interaction	-0.153	0.985	-1.175	-0.006
	(0.266)		(1.381)	
With spin-orbit interaction	-0.224	0.857	-1.194	-0.031
	(0.234)		(1.426)	

Table 4-8. Numerical values of each term in equation 4.12. Unit in eV.

Term	Without spin-orbit interaction	With spin-orbit interaction
first	6.292×10^{-8}	6.496×10^{-8}
	(6.292×10^{-8})	
second	1.166×10^{-5}	1.028×10^{-5}
	(1.029×10^{-6})	
third	6.918×10^{-6}	6.079×10^{-6}
	(6.081×10^{-7})	
fourth	-1.773×10^{-5}	-1.561×10^{-5}
	(-1.562×10^{-6})	
broadening	0.95 meV	0.9 meV
	(0.37 meV)	

(Numbers in parenthesis are with only dV cation.)

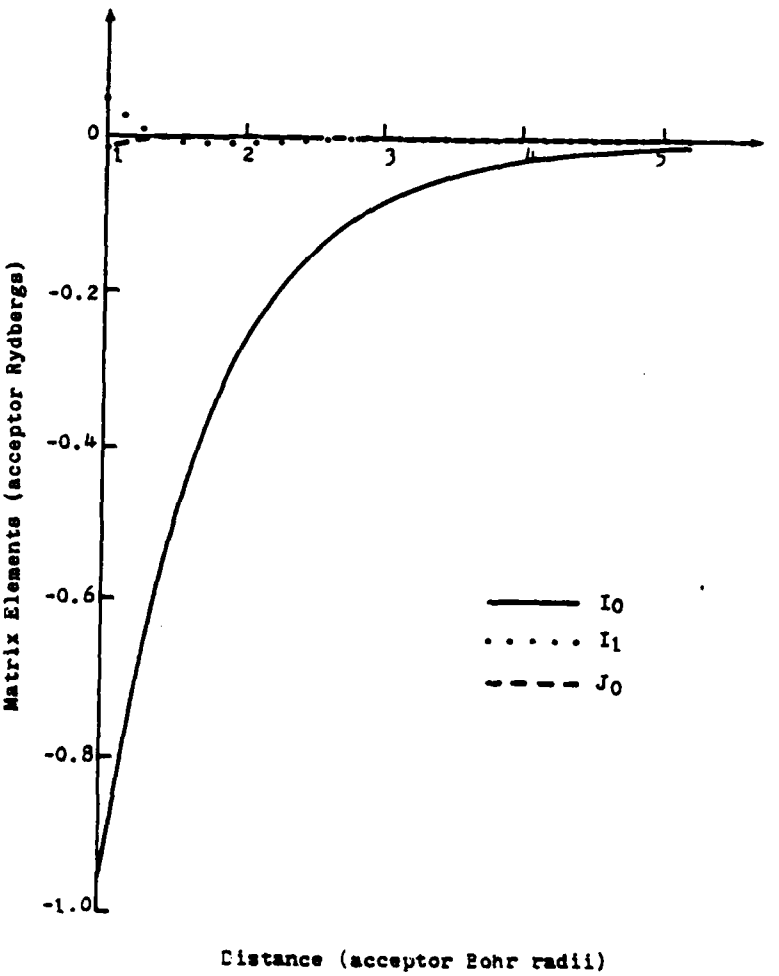

Figure 4-3. The binary interaction matrix elements for shallow acceptors in (Hg,Cd)Te; x=0.48 versus seperation between the two acceptors.

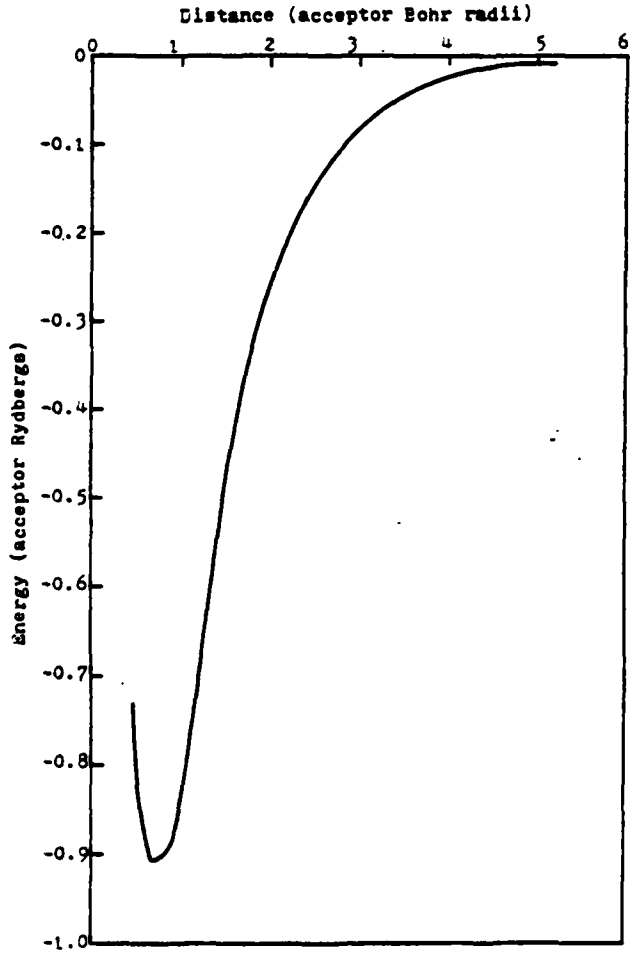

Figure 4-4. Transition energy versus the separation between two acceptors in (Hg,Cd)Te; x=0.48.

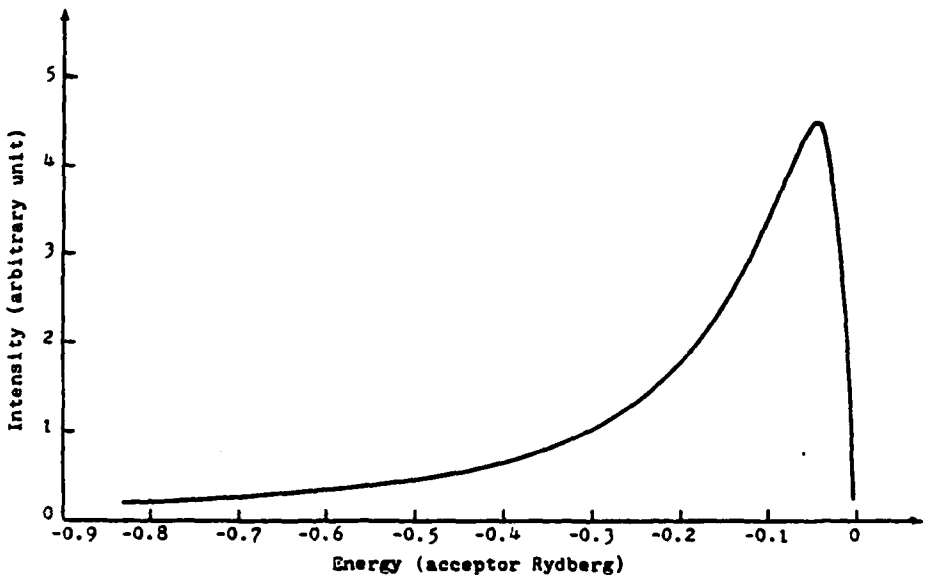

Figure 4-5. The calculated acceptor bound-exciton spectral intensity versus energy for (Hg,Cd)Te; x=0.48.

APPENDIX D

Chapter IV

MOBILITY OF $HG_{1-X}CD_XTE$ NEAR ZERO BAND GAP

4.1 INTRODUCTION

The two zinc-blende compounds HgTe and CdTe form a continuous series of alloys $Hg_{1-x}Cd_xTe$, where x is the mole fraction of CdTe in the alloy. The alloy system has been of great interest in recent years because of the wide range of its physical properties. The alloy system is a mixture of a semimetal (HgTe) with a semiconductor (CdTe); the energy gap Eg in this alloy system varies continuously from -0.3 eV in HgTe to 1.6 eV in CdTe. The zero gap alloy is occured at x = 0.164 at 4.2K.

The continuous variation of band parameters with composition x has caused a great deal of interest in its electrical and optical properties. Recently there have been many workers investigating the properties of $Hg_{1-x}Cd_xTe$ or its applications. One of the most important applications of $Hg_{1-x}Cd_xTe$ materials is for infrared dectors[1,2]. The alloy can make photodiodes. W.W. Anderson[3] has investigated the band-to-band tunneling and impurity-to-band tunneling ion-implanted n^+ on p $Hg_{1-x}Cd_xTe$ photodiodes. Also this alloy has been used in tunable lasers[4]. In the next section, some structural and optical properties of this material are briefly introduced.

$Hg_{1-x}Cd_xTe$ has shown unusually high electron mobilities[5] ($\mu \approx 10^7$ $cm^2/V \cdot s$). Recently, J. Bajaj, S.H. Shin, G. Bostrup and D.T. Cheung of Rockwell International Science Center[34] have observed the maximum electron mobility occured near 40K for near zero band gap $Hg_{1-x}Cd_xTe$ ($x \approx 0.16$). In this chapter we will mainly discuss the mechanisms for these observations. It is also shown in Figs. 3, 6 and 7, theoretically and experimentally, that the maximum mobilities occured in $Hg_{1-x}Cd_xTe$ at the composition of zero band at fixed temperature and electron concentration (n), especially for low temperature and low n. In general, one would expect the mobility to reach a maximum near the cross point, because the density of states at the Fermi level exhibits a minimum.

Since the alloy, $Hg_{1-x}Cd_xTe$, has so many different features and we are so interested in the transport properties, in this chapter we will discuss the properties of $Hg_{1-x}Cd_xTe$ and its mobility phenomena at near zero band gap.

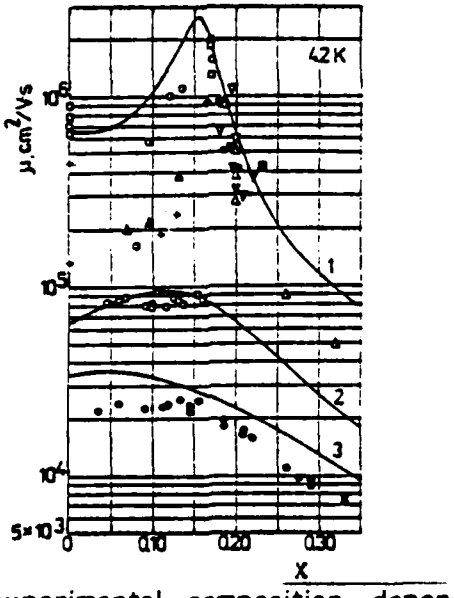

Figure 6: Theoretical and experimental composition dependences of electron mobility in $Hg_{1-x}Cd_xTe$ mixed crystals with the following electron concentrations: $n=2\times10^{15}$ cm^{-3}, $n=2\times10^{17}$ cm^{-3} and $n=9\times10^{17}$ cm^{-3} at 4.2K, (curves 1-3, respectively), reported in Ref.(31).

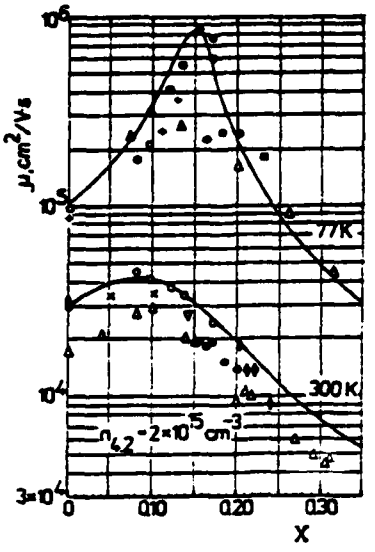

Figure 7: Experimental and theoretical dependences of electron mobility in $Hg_{1-x}Cd_xTe$ at 77 and 300K for samples with the following electron concentrations: 6×10^{14} cm^{-3} and 2×10^{15} cm^{-3}, reported in Ref.(31).

4.2 GENERAL FEATURES AND PARAMETERS

As mentioned in the previous section, $Hg_{1-x}Cd_xTe$ has an energy gap , Eg, which varies from -0.3 eV to 1.6 eV. The Eg is the energy difference (Eg > 0 for normal semiconductor structure, Eg<0 for inverted band structure). The band structure, whose dispersion relation was given in chapter III Eq.(45), for different x are shown in Fig. 8. We can see from the curves in Fig. 8 that if Eg is very close to zero the conduction band is a V-shaped non-parabolic band, which is different from the cases of large |Eg|. Also when Eg ≈ 0, from

Eq.(46) we can see the non-parabolic parameter is very large, and from Eqs.(47) and (48) we can see the effective mass at the conduction band edge m^*_e is very small as shown in Fig. 9.

What is the relation between Eg and x? There are many researchers working on this problem. Five different representations which are describing the Eg in terms of x and T are listed below :

(1). Ref.(35)

$$Eg = -0.304 + 5\times10^{-4}T + |1850-T| \times 10^{-3}\,x. \qquad (132)$$

(2). Ref.(36)

$$Eg = -0.302 + 1.93\,x + 5.35\,(10^{-4})T\,(1-2x) - 0.81x^2 + 0.832x^3 \qquad (133)$$

(3). Ref.(37)

$$Eg = -0.30 + 5.0\times10^{-4}T + (1.91 - 10^{-3}T)\,x \qquad (134)$$

(4). Ref.(38)

$$Eg = -0.303 + 1.73\,x + 5.6\times10^{-4}(1-2x)T + 0.25\,x^4 \qquad (135)$$

(5). Ref.(39)

$$Eg = -0.25 + 1.59 + 5.233\times10^{-4}(1-2.08\,x)T + 0.327\,x^3 \qquad (136)$$

Fig. 10(a) shows the five different Eg versus x curves at 4.2K. Fig. 10(b) shows the temperature and composition dependences of the energy

gap and the long-wavelength limit λ_c of $Hg_{1-x}Cd_xTe$ from Ref.(39). The left-hand ordinate is the forbidden energy gap expressed in electron volts, whereas the right-hand one is the corresponding absorption edge wavelength or photodetector long-wavelength limit. The data illustrate that the composition $Hg_{0.795}Cd_{0.205}Te$ is the proper choice for an infrared detector operating at 77K having an energy gap of 0.1 eV (long-wavelength limit of 12.4 μm). The temperature dependences of the intrinsic carrier concentration with composition as an independent parameter is illustrated in Fig. 11[40]. The non-parabolic conduction band was used in the calculation. It is shown that the smaller the x, the higher the intrinsic carrier concentration at fixed temperature. Fig. 12 depicts longitudinal and transverse phonon frequencies as functions of composition at 77 and 300K[7]. The LO and TO frequencies were deduced by Kramers-Krong analysis of reflectivity measurements.

The method to calculate the transport properties of non-parabolic band $Hg_{1-x}Cd_xTe$ has been described very clearly in chapter III by using the variational technique. There are some parameters used in the calculation of $Hg_{1-x}Cd_xTe$, listed in Table 2 of Ref.(31), which have been worked out quite accurately from many workers (refer to Ref.(31)).

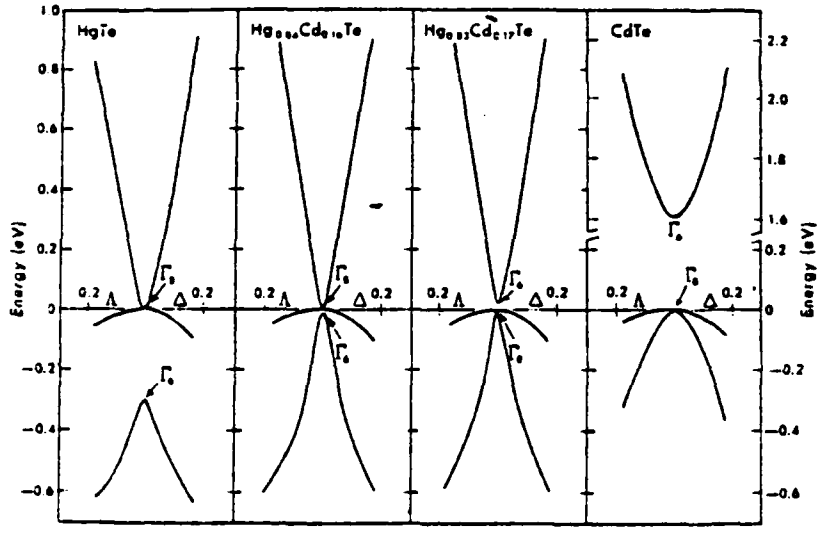

Figure 8: Band structures near Γ for HgTe, CdTe, and two alloys near the semimetal-semiconductor transition region. The band structures extend from Γ to $|k|=0.18(2\pi/a)$ in the Λ and Δ directions.

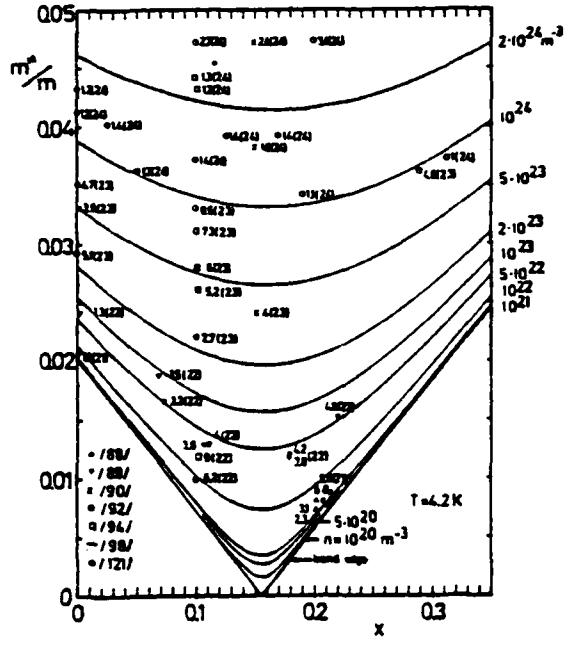

Figure 9: Conduction-band effective masses as a function of x at liquid helium temperatures for various carrier concentration n.

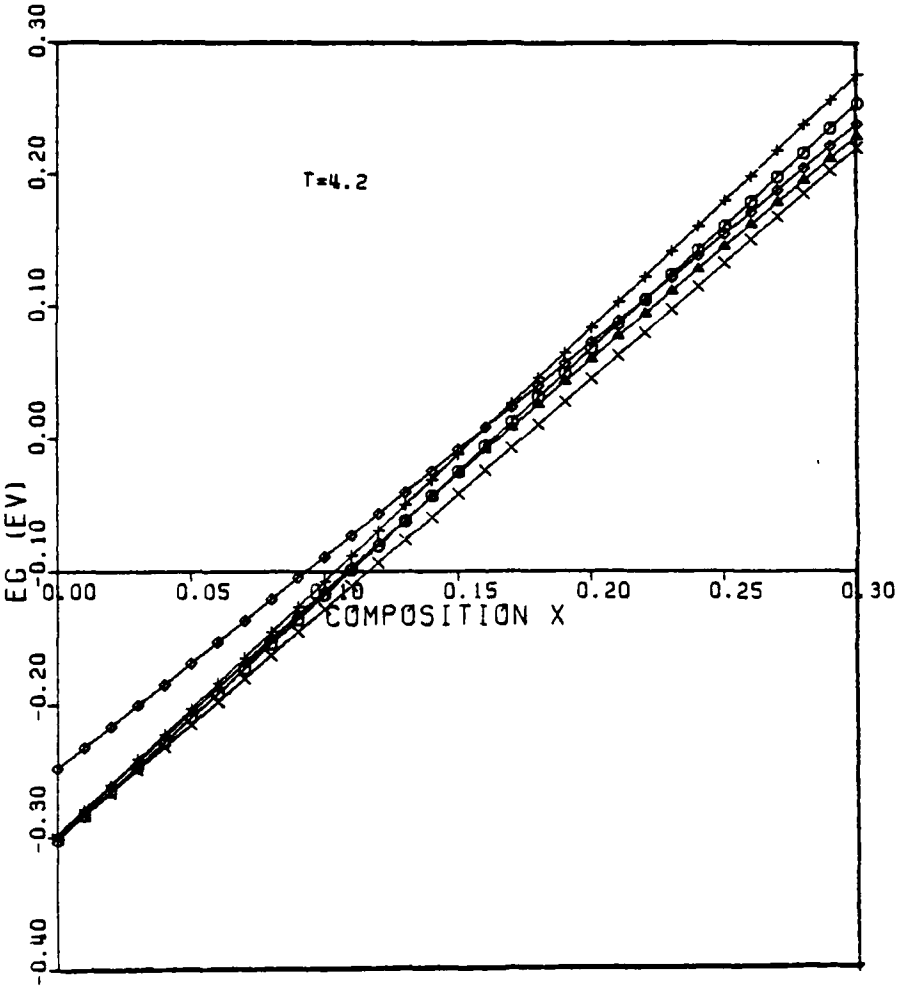

Figure 10a: Five different relationships betweem energy, Eg, and composition, x, in $Hg_{1-x}Cd_xTe$ at 4.2K as refered to Ref. (35-39).

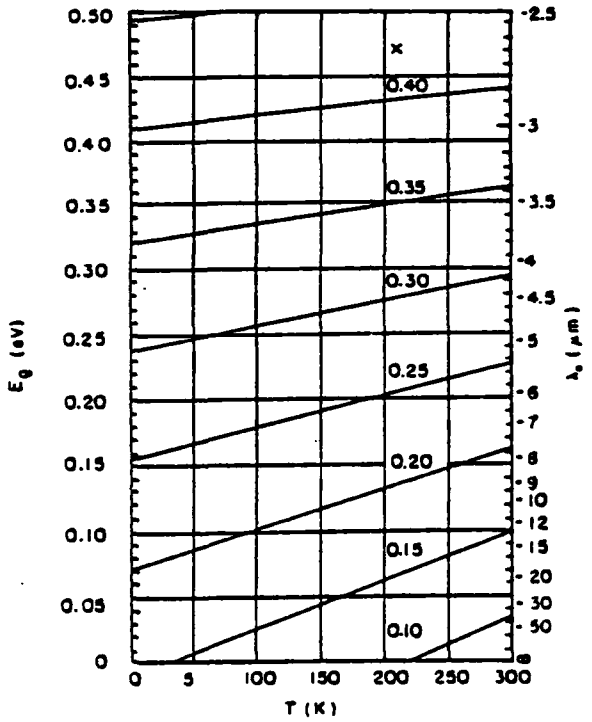

Figure 10(b): The temperature and composition dependences of the energy gap and the long-wavelength limit λ_c of $Hg_{1-x}Cd_xTe$.

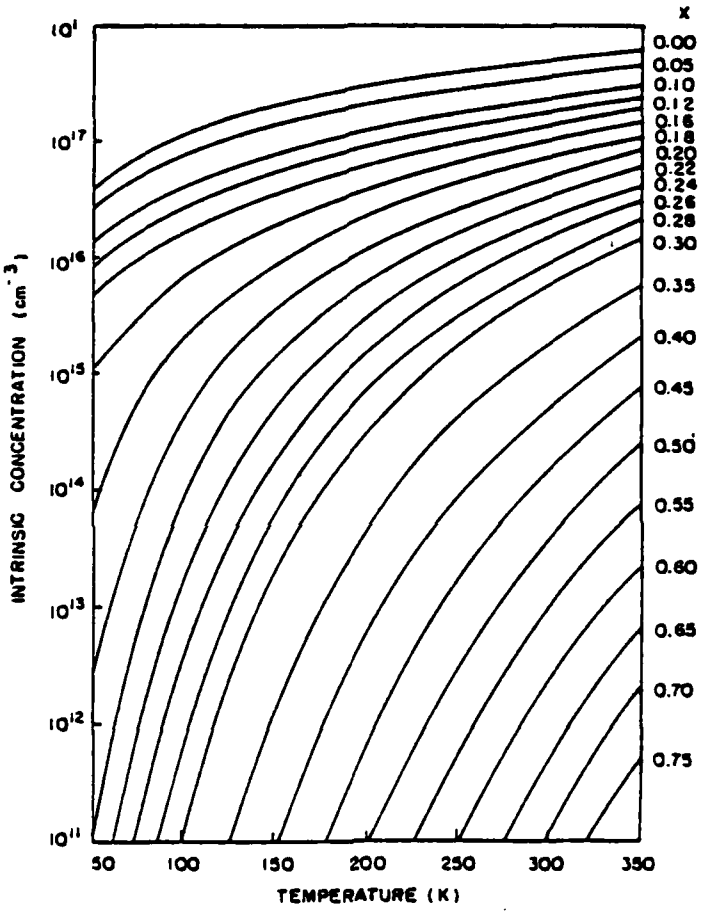

Figure 11: Temperature dependence of the intrinsic carrier concentration in $Hg_{1-x}Cd_xTe$. Composition x is as an independent parameter.

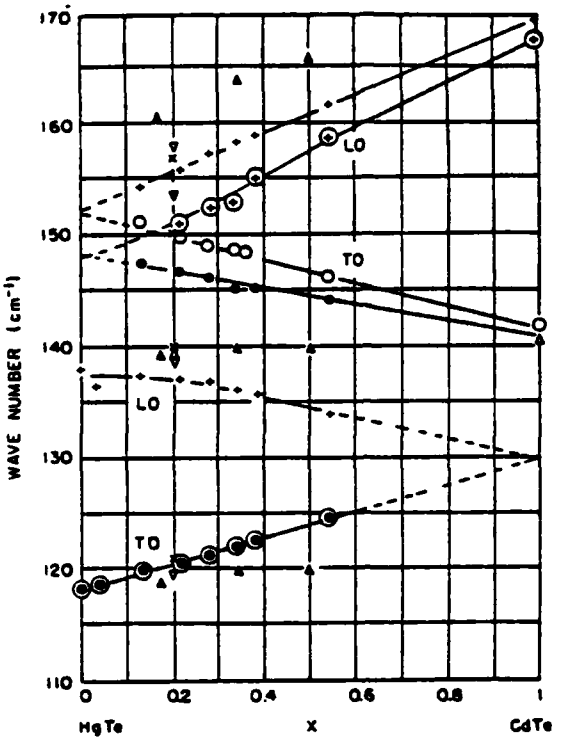

Figure 12: Longitudinal and transverse phonon frequencies in $Hg_{1-x}Cd_xTe$ at 77(+,O) and 300K(⊕,●).

4.3 RESULTS AND DISCUSSION

In this section we will discuss the results of mobility from Rockwell International Science Center[24], It was shown that the maximum mobility occured near 40K for $Hg_{0.84}Cd_{0.16}Te$ near cross point as shown in Figs. 13, 14. To calculate the mobility and temperature relation, we started by finding the Eg, M^*_e and α , which are functions of T. Once we have those data, we can calculate the Fermi level, which is found from the charge neutrality equation

$$\eta + N_A^- = P + N_D^+ \qquad (137)$$

where n and p are the electron and hole concentration respectively, and N_A, N_D are acceptor and donor concentrations. N_D^+ has been assumed to be temperature independent, because donor states are not virtual bound states, so that electrons in donor states are unlocalized. In other words, these electrons are always in conduction band states, leading to a total ionization of the donors at zero temperature. So we set $N_D^+ = n$ at 4.2K. After we had solved the Fermi levels, we used the variational principle formulated in chapter III to solve the mobilities for temperature from 4.2K to 300K. To explain the experimental data in Ref.(40), we would like to make some corrections on it. At very high temperature, such as 300K, samples are already intrinsic. According to our calculations from the charge neutrality equation, we found out the compositions of $Hg_{1-x}Cd_xTe$ for sample #81 was about 0.165, and for sample #82 and #83 were about 0.17. The following calculations were based on the compositions we found.

For low electron concentration $n \approx 10^{14}$ cm^{-3}, we found the most important scattering mechanisms are impurity scattering and polar optical phonon scattering. Therefore, we found the mobility vs temperature, shown in Fig. 15, which was pretty close to the experimental data in Fig. 13 for temperature higher than 50K. For very low temperature, mobility drops as temperature cools down in experiments. From our calculations we found the results can not be explained by impurity scattering. Up to now from a survey of other works, all of them have observed the same low temperature phenomena but no one has provided a satisfactory explanation so far. Therefore, we believe the low tempera-

ture mobility properties must be a consequence of some other scattering mechanism.

We investigated the neutral impurity scattering contribution. We found, for near zero gap material, at very low temperature, temperature variation causes the effective mass to change abruptly, due to non-parabolicity effect, and offsets the increase due to neutral impurity scattering shown in Fig. 13 as temperature varies in the 4.2K - 40K range.

We believe the low temperature phenomena is due to resonance scattering effect. It is believed that a number of Hg vacancies remains after annealing $Hg_{1-x}Cd_xTe$. And the experimental evidences of resonant acceptor states were reported in HgTe and $Hg_{1-x}Cd_xTe$[41,42]. Ref.(41) gives the activation energies of E_{A1} of the resonance A1 as a function of the energy gap Eg as shown in Fig. 16, which can be plotted as Fig. 17 by setting the zero energy at conduction band edge to express the location of resonance level. Because no E_{A1} data available to us for energy gap greater than 10 meV, in our calculations, we use E_{A1} by interpolating from Fig. 17. The relation can be expressed approximately by the following linear equation:

$$E_{A1} = \begin{cases} 15.35 - 0.594 \cdot Eg & Eg \geq 0 \\ 15.35 + 0.162 \cdot Eg & Eg < 0 \end{cases} \qquad (138)$$

We believe the acceptors are double acceptor mercury vacancies[62]. From helium spectrum[18] as shown in Fig. 18, we believe the resonance energy, defined by E_r, is the energy between ground state 1s and higher levels. The most important resonance occurs between 1s and 2s states. E_r is shown in Figs. 16, 17 as a function of energy gap Eg; the ionization energy for helium is about $1.25 \cdot E_r$. In our model, we assume the energy of acceptor level E_A is about $1.25 \cdot E_r$ or $1.50 \cdot E_r$, which give pretty good agreement of electron concentrations with experiments.

Assume the acceptor concentration is 1.0×10^{16} cm^{-3}. From charge neutrality equation we solved the Fermi energy. Ef, E_A and E_r are shown in Figs. 19 and 20 for $E_A = 1.25 \cdot E_r$ and $E_A = 1.50 \cdot E_r$, respectively. It is very interesting to see the energy difference betwen Ef and E_r. We believe if the energy difference $|Ef - E_r|$ is less than about 1 meV the resonance scattering occurs. What does the 1 meV difference energy come from? We believe it comes from the thermal energy. Since the resonance level is a function of energy gap and there is no existing data of E_r for energy gap greater than 10 meV, and as there are at least five different expressions of energy gap as we mentioned earlier in this chapter, we think 1 meV is only approximated. One way to look at the resonance scattering, which we believe might be valid, is that resonance scattering occurs whenever the energy difference between Ef and E_r is less than the thermal energy. It is also very interesting to see the fact that resonance scattering occurs below 45K for all the samples. Therefore, we believe resonance scattering

dominates at low temperature 4.2K - 45K and which causes the mobility to drop as the temperature is lowered.

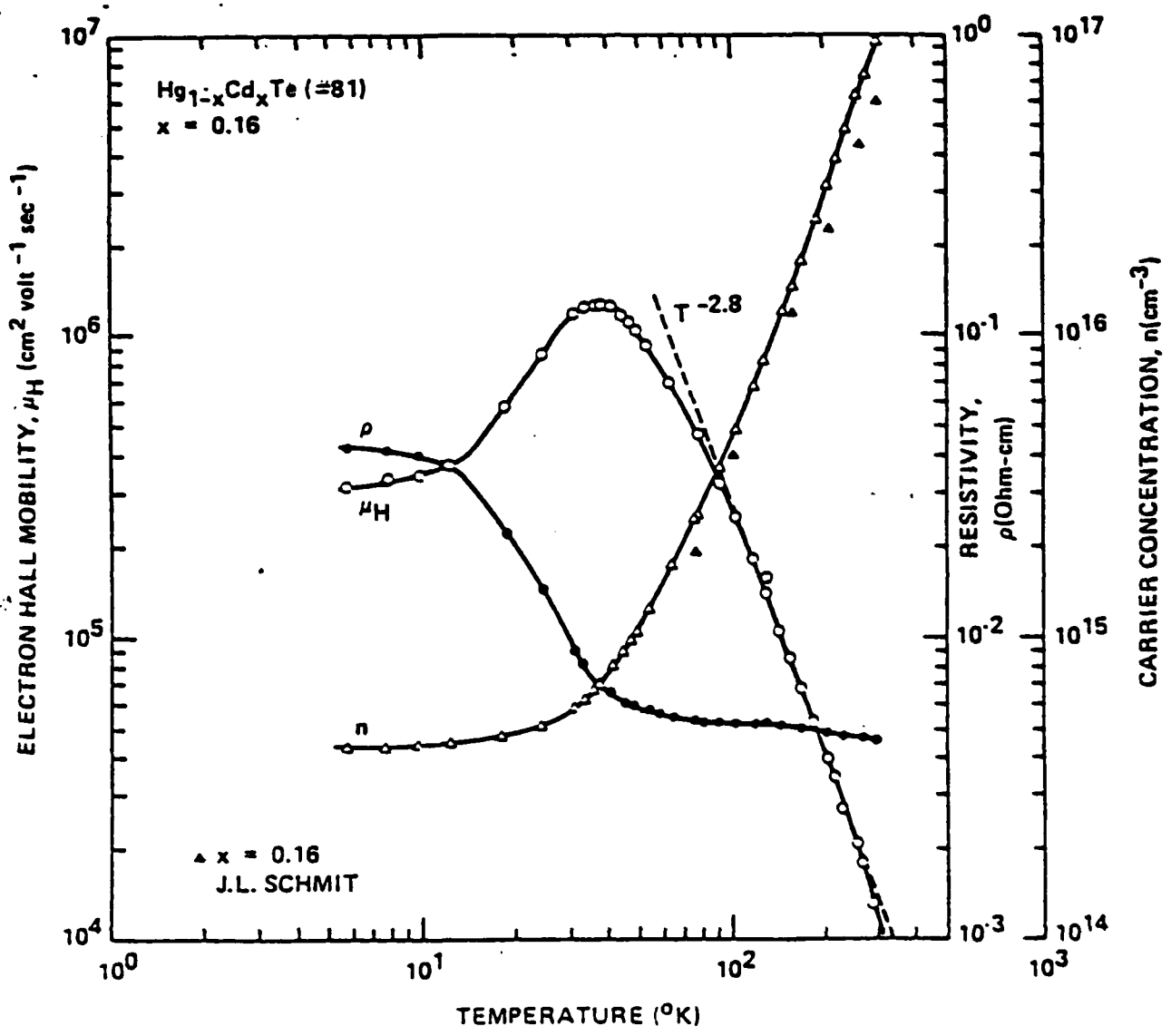

Figure 13: Electron Hall mobility, carrier concentration and resistivity as a function of temperature in $Hg_{0.84}Cd_{0.16}Te$.

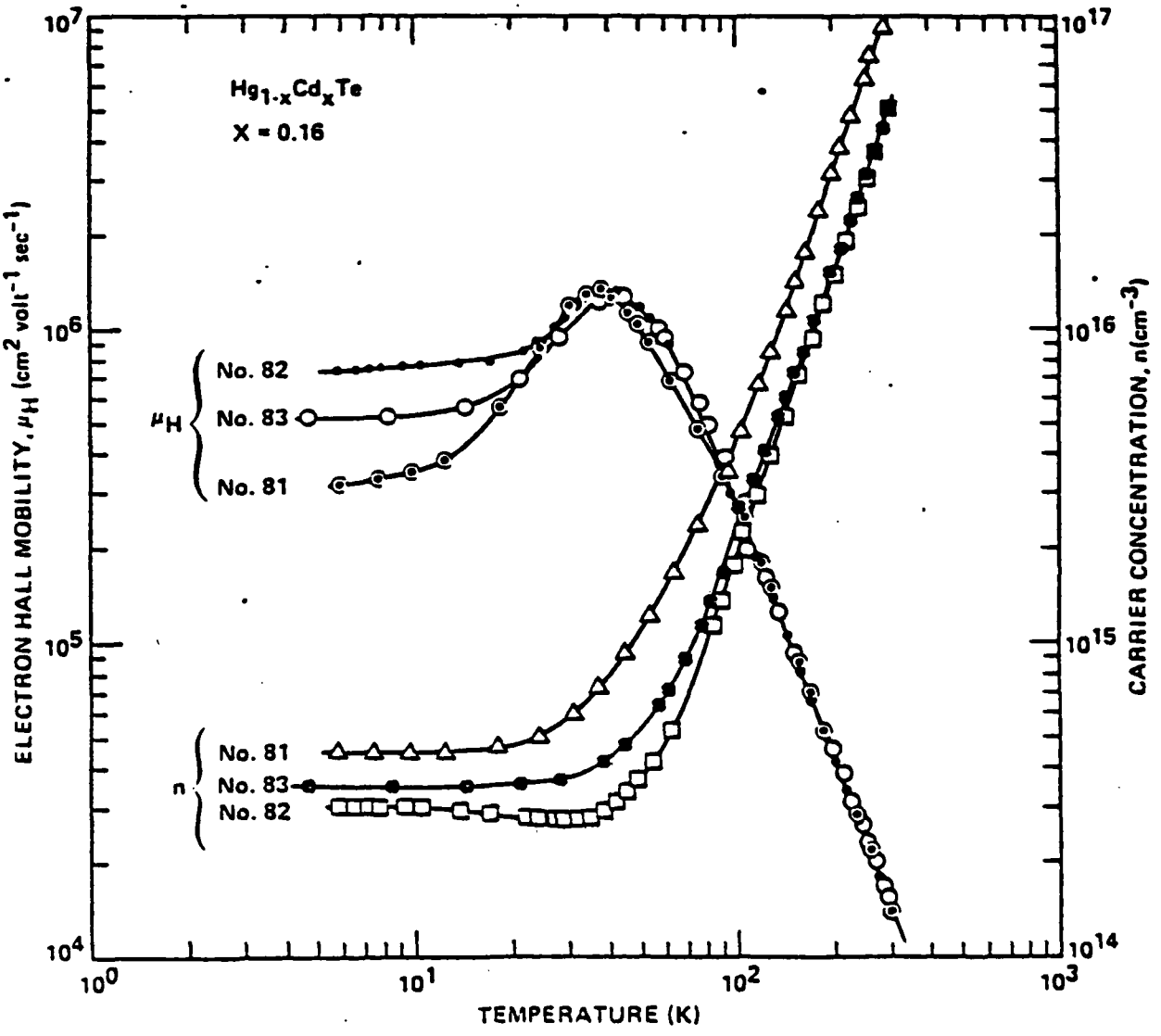

Figure 14: Electron Hall mobility and carrier concentration as a function of temperature for three different $Hg_{1-x}Cd_xTe$ samples with $x \approx 0.16$.

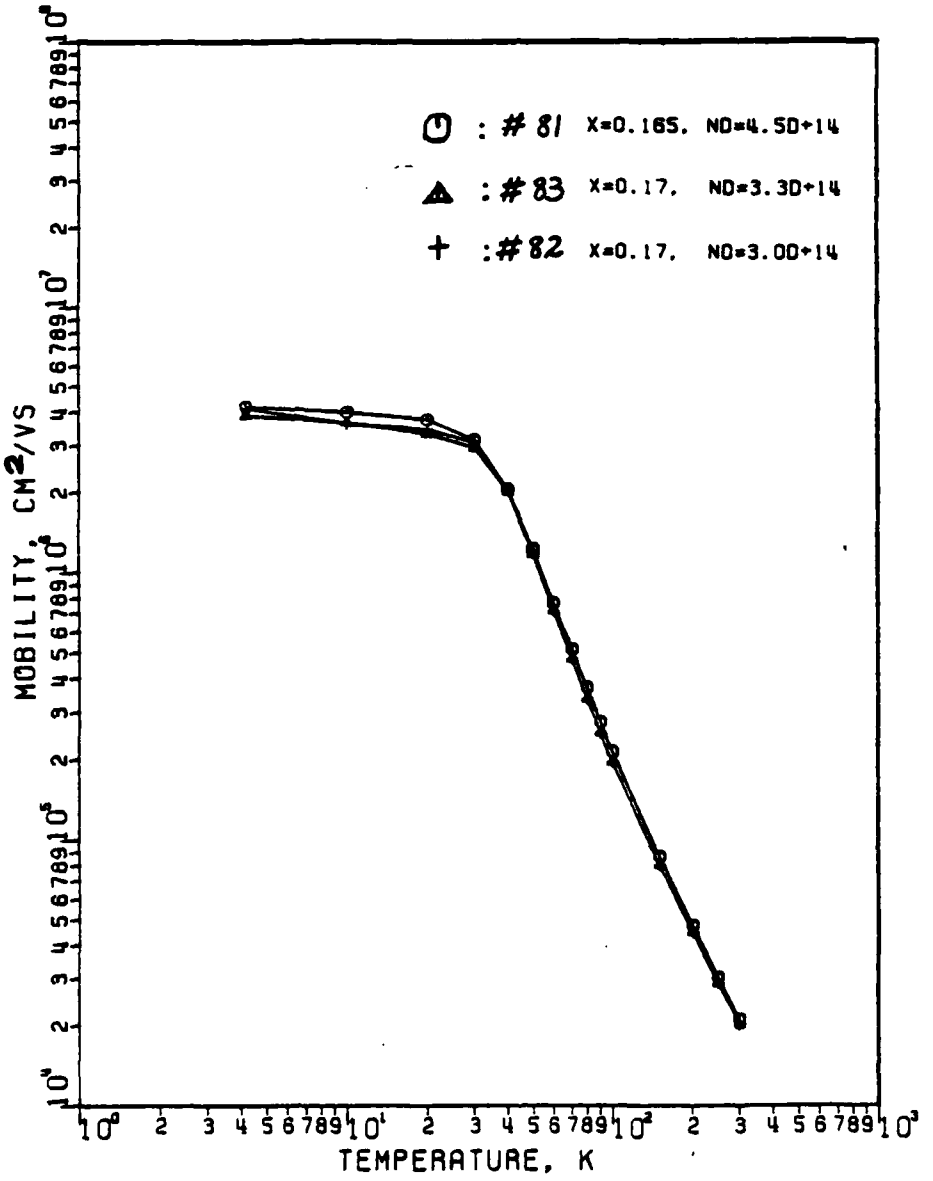

Figure 15: Theoretical results of electron mobility as a function of temperature for three different $Hg_{1-x}Cd_xTe$ samples in Fig. 14. Sample #81 is x=0.165; #82 & #83 are x=0.17.

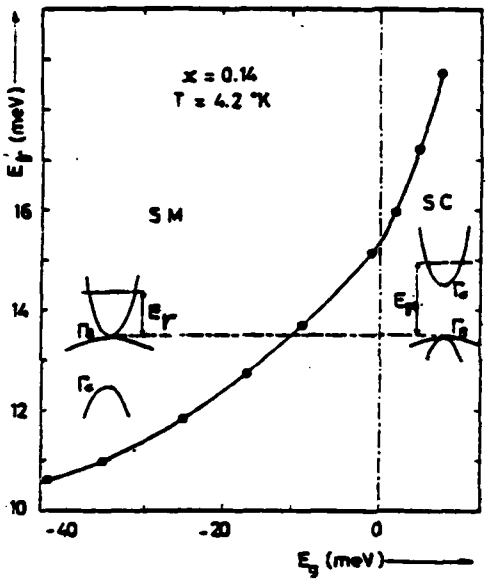

Figure 16: Experimental variations of the resonance energy E_Γ as a function of the energy gap Eg. The zero energy is defined as the top of the valence band.

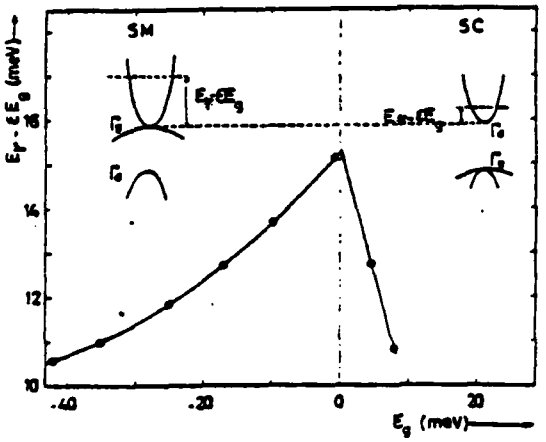

Figure 17: Energy difference between the resonance level and the bottom of the conduction band as a function of the energy gap Eg for $Hg_{1-x}Cd_xTe$ alloys according to the results reported in Fig. 16.

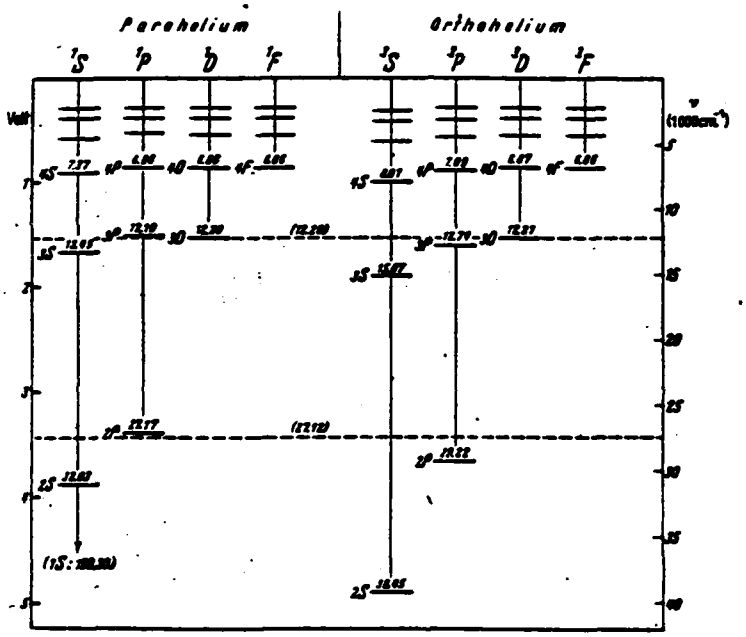

Figure 18: The experimental energy levels of helium. The scale on the left represents ionization potential in electron volts. The numbers next to the levels are the wave number corresponding to the ionization potential, expressed in units of 10^3 cm^{-1}. The dotted lines represent the energy levels of hydrogen (nuclear charge = Z-1 = 1).

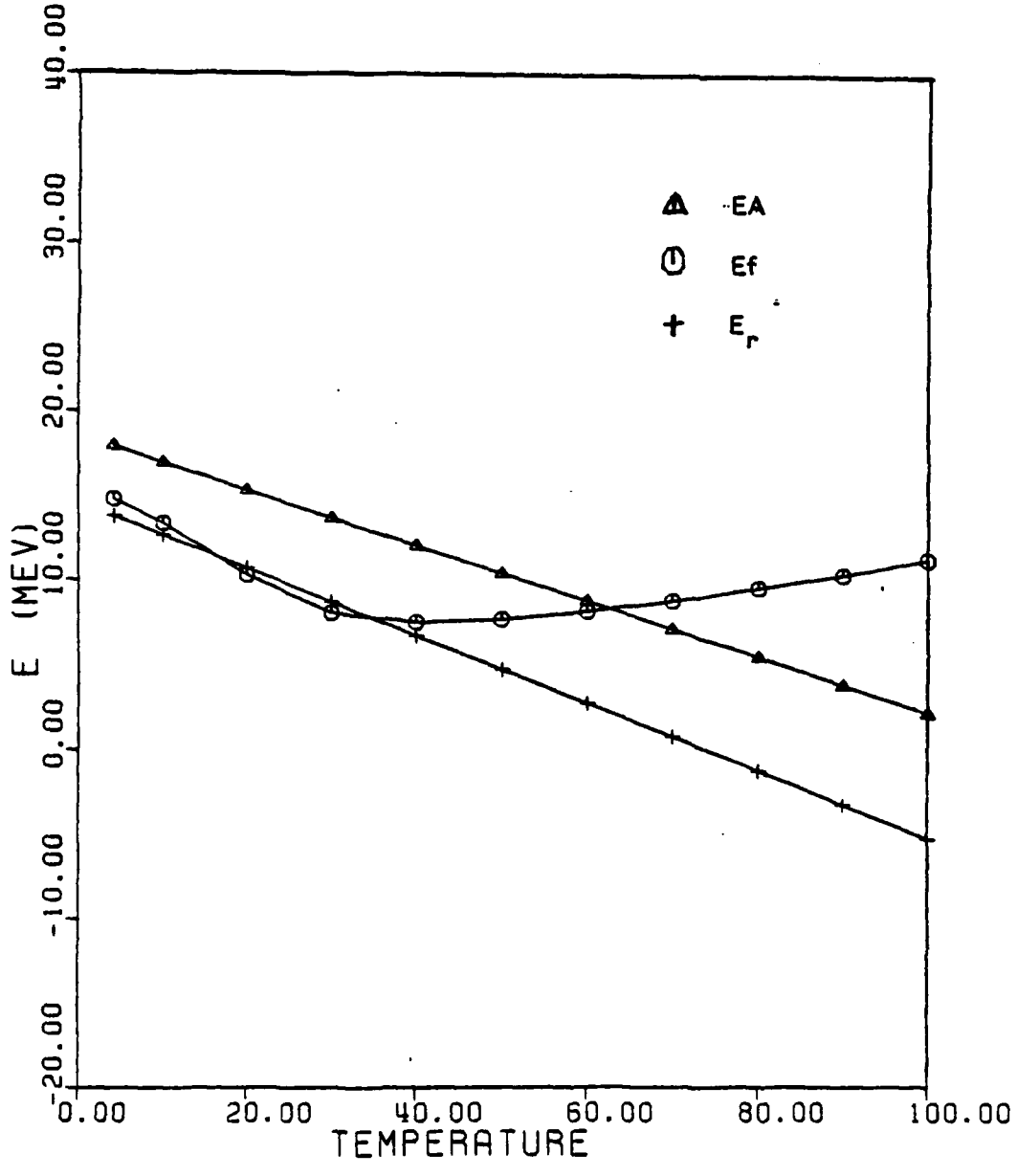

Figure 19(a): The temperature dependences of EA, Ef and E_r on EA=1.25*E_r. The sample is #81 in Fig.14.

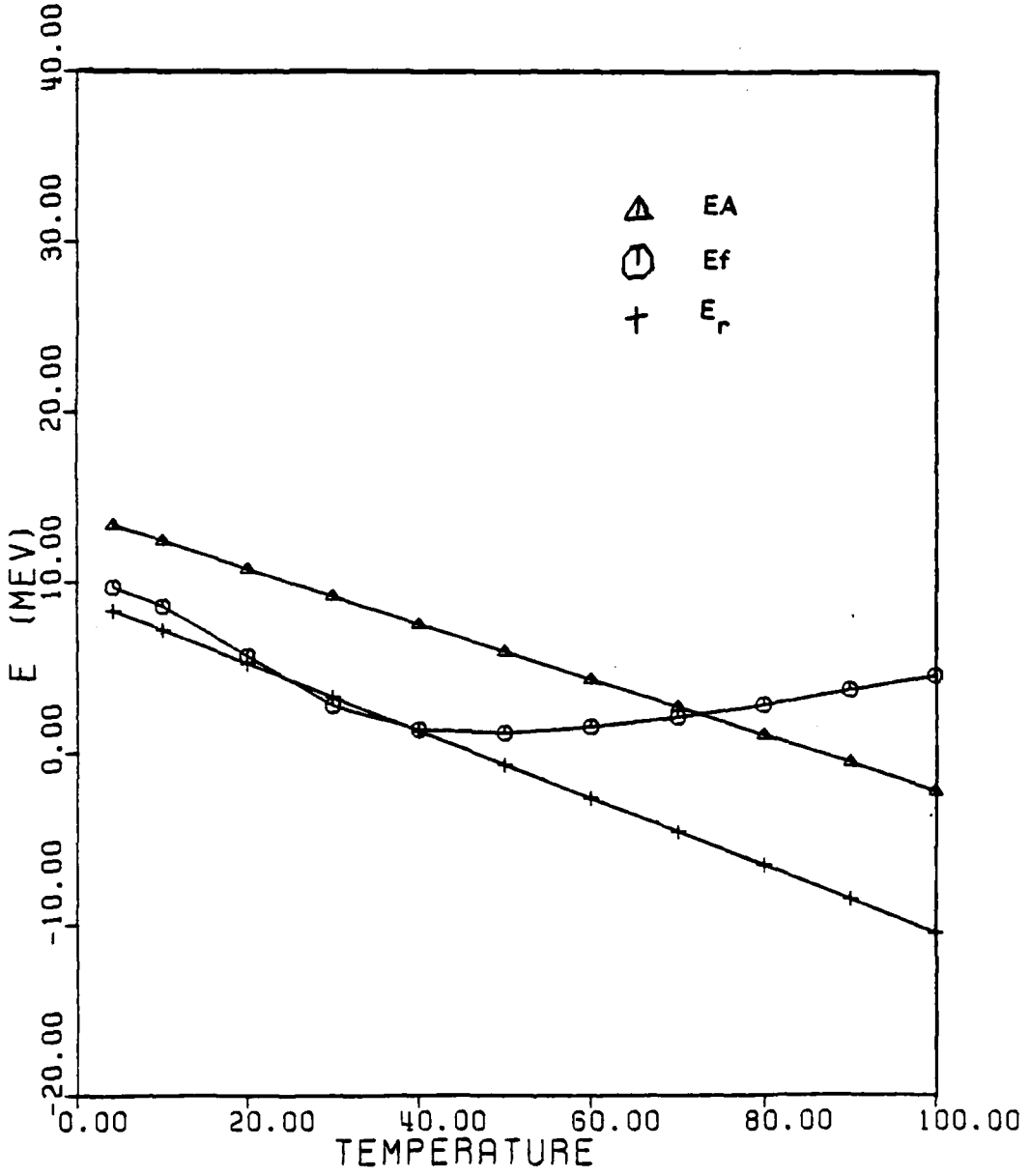

Figure 19(b): The temperature dependences of EA, Ef and E_r on EA=1.25*E_r. The sample is #83 in Fig.14.

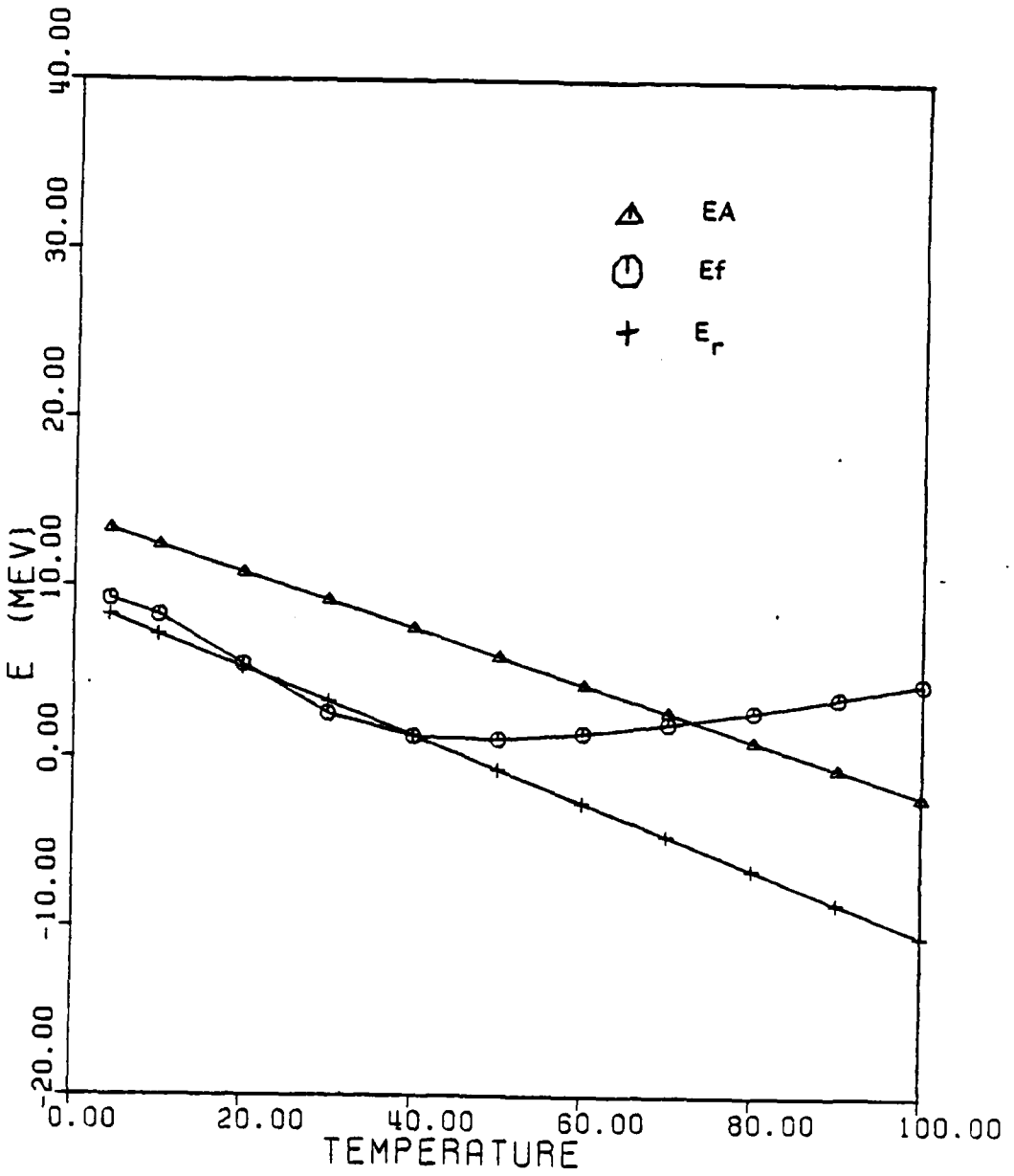

Figure 19(c): The temperature dependences of EA, Ef and E_r on EA=1.25*E_r. The sample is #82 in Fig.14.

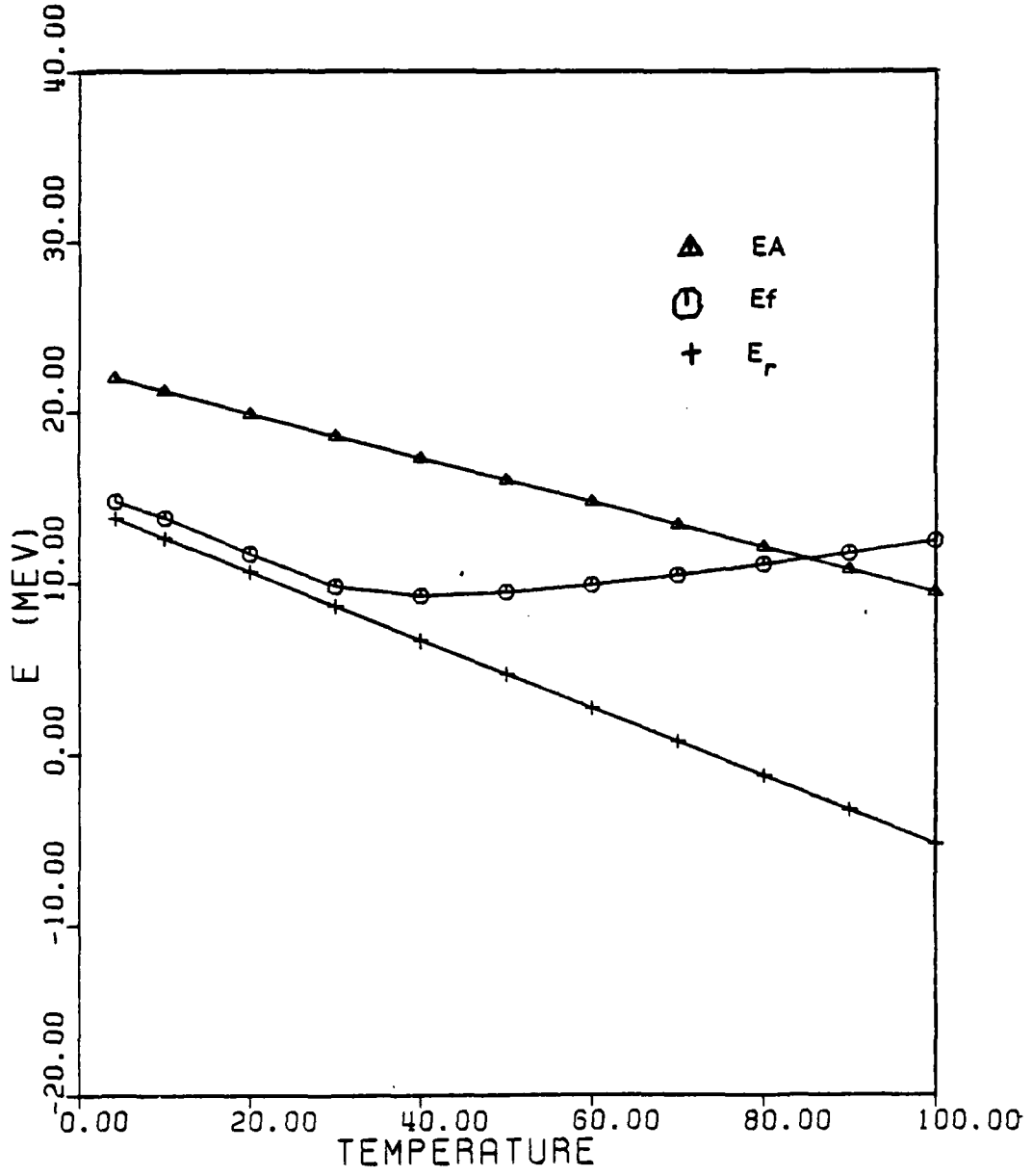

Figure 20(a): The temperature dependences of EA, Ef and E_r on EA=1.5*E_r. The sample is #81 in Fig.14.

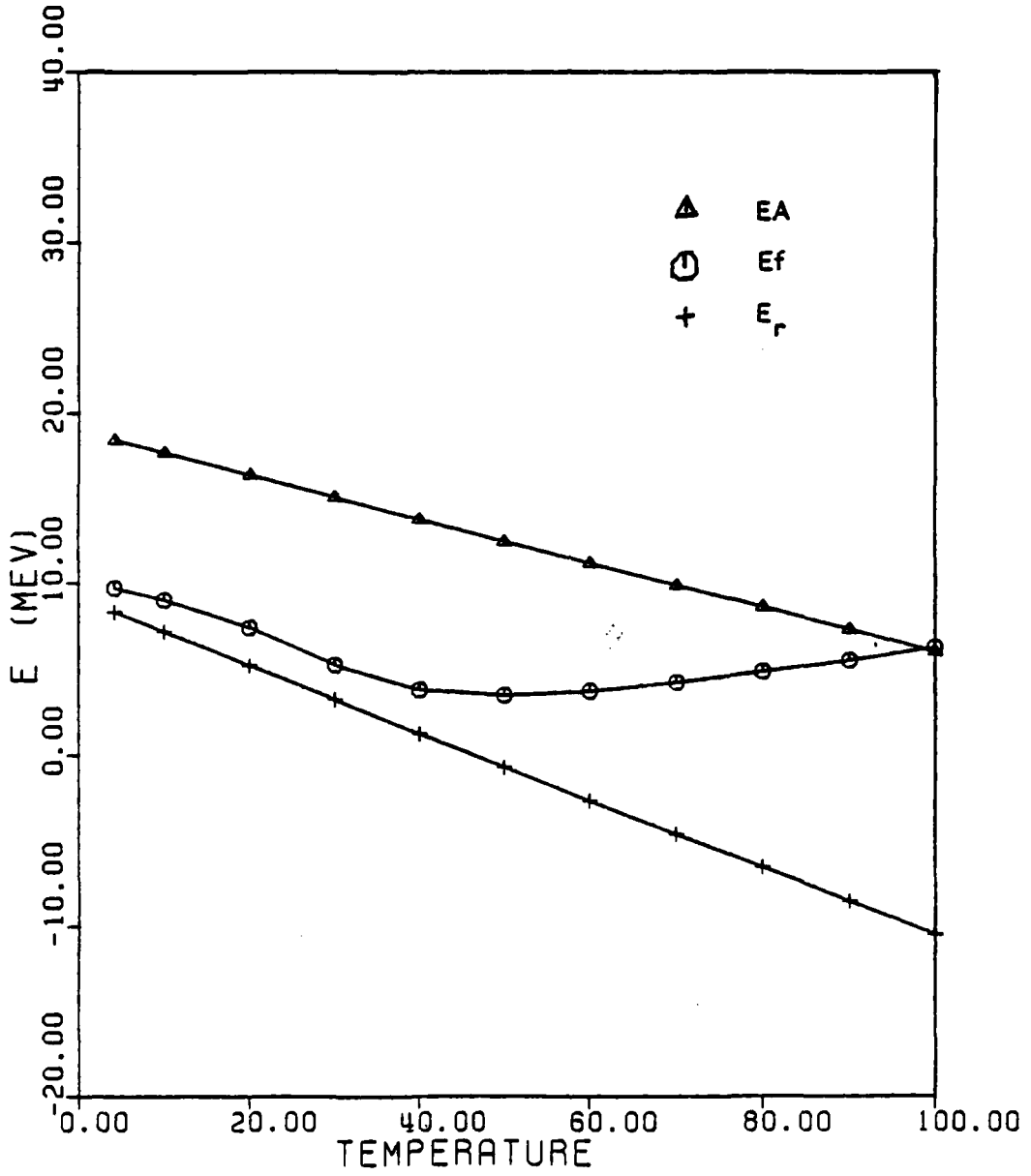

Figure 20(b): The temperature dependences of EA, Ef and E_r on EA=1.5*E_r. The sample is #83 in Fig.14.

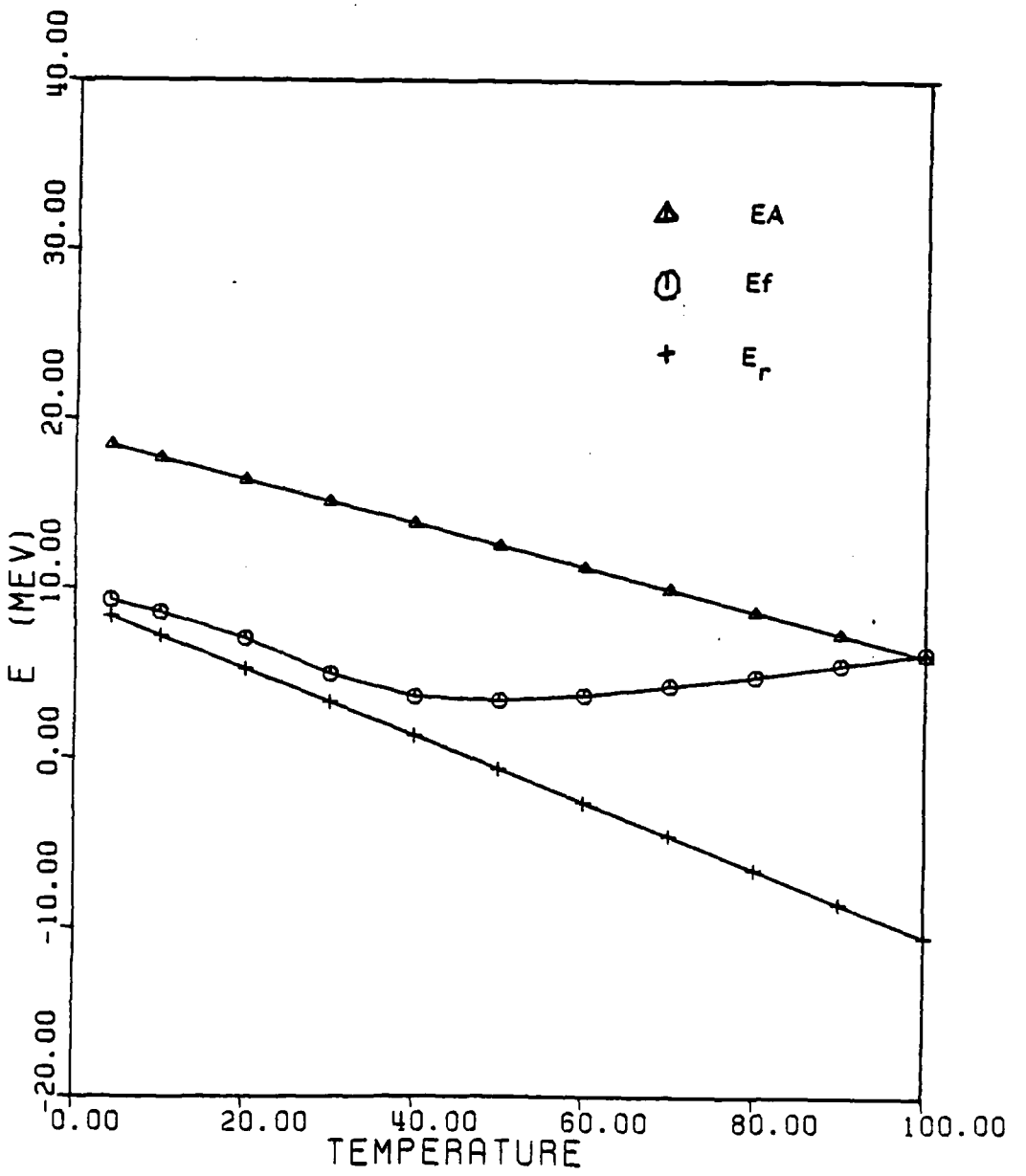

Figure 20(c): The temperature dependences of EA, Ef and E_r on EA=1.5*E_r. The sample is #82 in Fig.14.

4.4 CONCLUSION

Impurity scattering and polar optical phonon scattering are the two most important scattering mechanisms in $Hg_{1-x}Cd_xTe$. For low electron concentration and narrow band gap $Hg_{1-x}Cd_xTe$ at very low temperature, resonance scattering may play a significant role in the mobility-decrease phenomena.

We found that if the energy difference between Fermi level and resonance level is less than 1 meV, resonance scattering occurs which lowers the mobility value. It can also be noticed that resonance scattering is important at low temperature only. Most people think of the mobility as reaching a maximum value near the cross point, zero band gap, because the density of states at the Fermi level exhibits a minimum. But from our investigation we conclude that it is not always true. We believe the maximum mobility is due to the starting point of resonance scattering, which lowers the mobility value. Once resonance scattering is reduced, the mobility will be dominated by impurity scattering again even at very low temperature. This phenomena was observed by C. Finck, etc., in Ref.(42). They have seen a dip in mobility at low temperature T1 of $Hg_{1-x}Cd_xTe$ shown in Fig. 2 of Ref.(42). But away from T1, even higher or lower temperature range, the mobility is higher than the mobility at T1. That is because the resonance scattering dominates at temperature close to T1 and impurity scattering dominates at other temperature ranges.

END

FILMED

3-86

DTIC